Materials and Nanotechnology

Introduction

The focus of the Materials and Nanotechnology Program is technology development related to processing, analysis, testing and characterization of materials in general. These are achieved through execution of R&D projects in engineering and materials science, cooperative projects with private and public sector companies, universities and other research institutes. Besides technology development, this Program also fosters training and human resource development in association with the University of São Paulo and many industrial sectors. This Program is divided into sub-programs in broad areas such as ceramics, composite and metallic materials as well as characterization of physical and chemical properties of materials. The sub-programs are further divided into general topics and within each topic, R&D projects. A brief description of progress in each topic during the last three years follows.

Biomaterials

CaO-MgO-SiO_2 ceramic glass system

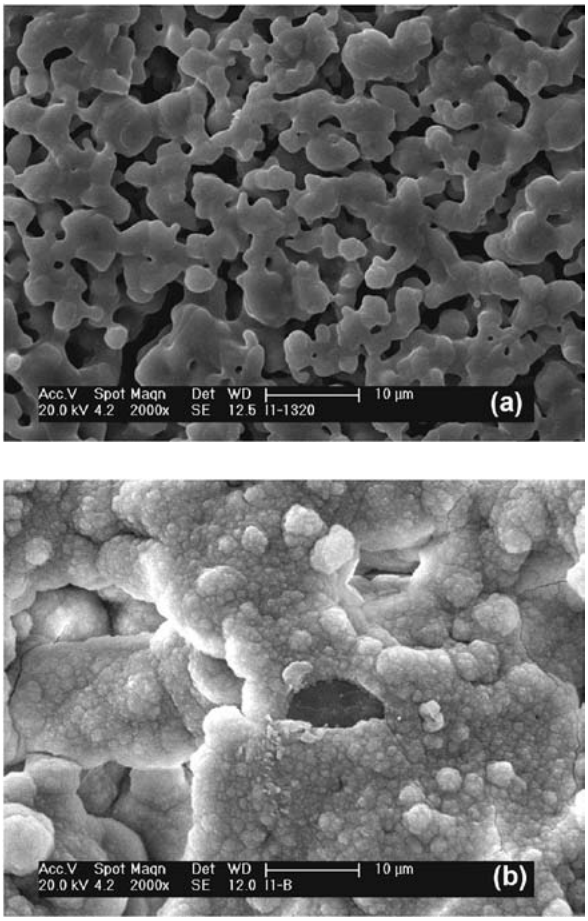

Figure 1: SEM micrographs of sintered glass-ceramic body surface: before (a) and after (b) 14 days soaking in SBF.

Bioactive glasses and glass-ceramics have been extensity studied in the biomedical field due to their interaction with the physiological environment when implanted. This interaction stimulates a response from the body, bonding to host tissue. Since 1969, when Hench introduced the first bio-glass (Na_2O-CaO-SiO_2-P_2O_5), many other variations on bioactive glasses and glass-ceramic materials, such as synthetic hydroxyapatite (HA) and other calcium phosphates have been studied. Some of ternary CaO-MgO-SiO_2 system ceramics have high capacity of bio-reparation and bioactivity on bone tissue surface by HA formation. In this work, CaO-MgO-SiO_2 bioactive glass-ceramic powder was synthesized by a modified sol-gel method. Non-aggregated SiO_2 particles were initially prepared by surfactant template sol-gel technique, via acid-catalyzed hydrolysis from Na_2SiO_3. Ca and Mg ions were embedded on the silica particles. The glass-ceramic body sintered at 1320 °C, from synthesized powder, confirmed the presence of bioactive phases, such as, $CaSiO_3$ and $Ca_2MgSi_2O_7$. Immersion studies in simulated body fluid (SBF) for different time intervals were carried out to study the bioactivity of the material. The evolution of bioactivity revealed, after 7 days soaking of the glass-ceramic body in SBF, apatite particles were formed on the surface, confirmed by FTIR spectra. Figure 1 shows SEM micrographs of the glass-ceramic before (a) and after 14 days (b) soaking in SBF. In figure 1(a) continuously connected crystalline grains with open pores microstructure of sintered body are observed. In figure 1(b), particles with nano microspheres morphology uniformly deposited on the surface are seen.

As confirmed in figure 2, the prepared glass-ceramic did not show cytotoxicity. According to ISO 10993-5, when the cell viability of the non-diluted extract in the indirect method is higher than 70%, the sample can be considered non cytotoxic. The cell viability of the

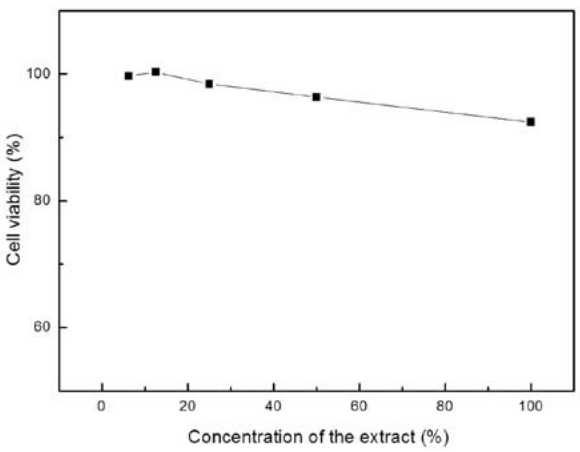

Figure 2: Cytotoxicity test with CHO: Cell viability as a function of extracts dilutions from 100 to 6.25%.

non-diluted extract was 97.5%, by reason of this, the samples were considered non cytotoxic. No toxic effect of the prepared material was found in the cytotoxicity test with CHO (Chinese hamster ovary) cells.

A new modified sol gel method to preparing CaO-MgO-SiO_2 ceramic powder was presented. Use of low-cost Na_2SiO_3 is attractive to substitute the usual high-cost TEOS as Si source. According to ISO 10993-5, the obtained material can be considered non cytotoxic.

Silicon Nitride Ceramics for Bone Compatibility

In view of the growing demand to perform different procedures for bone regeneration, silicon nitride based ceramics are increasingly being considered for applications in biomedicine. This interest is justified by the propitious mechanical properties, osseointegration, bactericidal capacity and adequate image characteristics - which allow implant visualization through techniques such as X-rays, computed tomography and magnetic resonance imaging.

On the other hand, the bioinert characteristics of the silicon nitride ceramics, whose biological response does not lead to chemical bonds with the host tissue, have motivated us to develop dense and bioactive composites with great mechanical properties.

As it is known, the production of dense silicon nitride ceramics by the conventional sintering method requires using additives, in order to promote the liquid phase sintering, which remains in the silicon nitride grain boundaries as an amorphous or partially crystalline secondary phase. Thus, the production of dense and bioactive silicon nitride ceramics is based on the proper selection of the sintering aids. The selected additives must promote densification and a microstructure formed by elongated β-Si_3N_4 grains dispersed in a bioactive phase formed by the solidification of the liquid phase during the cooling step of the sintering process.

In this study, silicon and calcium oxides were used as sintering aids as well as to obtain a secondary phase containing P_2O_5 free bioactive glasses, so that the contact with the physiological fluids favors the apatite deposition on the final material surface due to formation of Si-OH groups. Samples with 80 or 90 wt.% silicon nitride and different contents of additives were obtained by pressureless sintering and characterized in regard to apparent density by the Archimedes method. The crystalline phases formed in the grain boundaries and the α×β-Si_3N_4 transformation were evaluated by the X-ray powder diffraction. The morphology, grain size and phases distribution were analyzed by scanning electron microscopy. Also, The Young modulus was determined by a non-destructive dynamic method, while the hardness and fracture toughness were determined using the Vickers indentation method.

In vitro, cytotoxicity tests were performed by the indirect method as suggested in ISO 10993-5, using fibroblast cell line (Balb/c). Bioactivity studies in SBF (Simulated Body Fluid) and osteoblast adhesion tests with MG63 line cells were carried out on the samples.

The results showed that samples reached high densification, microstructure formed by β-Si3N4 grains dispersed in an intergranular secondary phase, as well as non citotoxicity. The materials also presented relatively high values of fracture toughness and lower values of Young modulus than those found for these ceramics with conventional compositions.

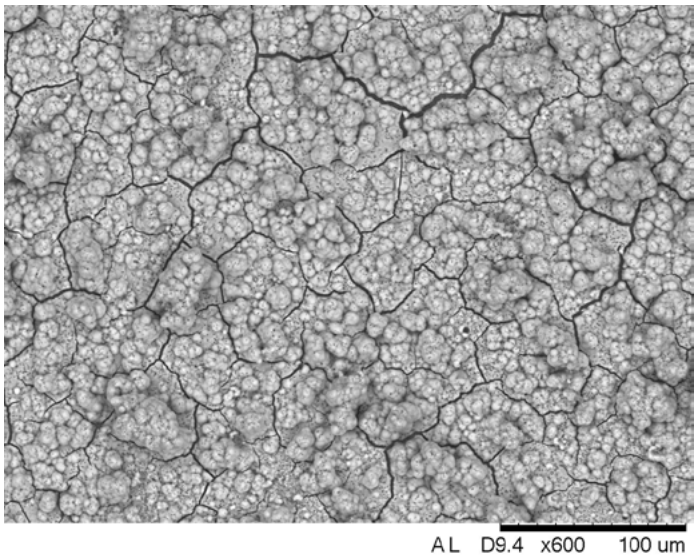

Figure 3: Image of a silicon nitride sample submitted to bioactivity test in SBF after 16 days of immersion

Backscattered scanning electron micrographs of the samples surfaces submitted to SBF tests indicate the formation of a superficial layer with globular structures (Figure 3), typical of the apatite, indicating the bioactivity of the studied composites.

The osteoblast adhesion tests with MG63 line cells showed the positive effect of the vitreous phase on the bioactivity, since the number of cells increased as the culture time for all studied samples. The bone formation ability of the samples can also be verified by the large areas of calcified matrix shown in the image of the surface stained with alizarin after 14 days of cell culture (Figure 4).

Hence, considering the results of densification, microstructure, mechanical properties and in vitro biological behavior, the obtained silicon nitride composites is a promising for applications in biomedical devices, mainly in intervertebral disc spacers, artificial l disc replacement and acetabular components in total hip prostheses.

Figure 4: Light microscopy image of alizarin red S staining for mineralization in MG-63 cells for a silicon nitride sample after 14 days of culture.

Laser bean marking applied to orthopedic implant

Laser beam marking is used to ensure the identification and traceability of biomaterials. The texturing imparts greater adhesion to the surfaces of implantable medical devices. The treatments performed altered the roughness of the biomaterials as a function of the increase of the pulse frequency (Figure 5)

The microstructure and chemical composition of the surfaces underwent changes that directly affected the passive layer of the stainless steels, favoring the triggering of the corrosion process. This effect was evidenced by SVET, XPS and the characterization of electronic properties of the passive film. The parameters used for the marking did not induce a decrease in the cellular viability of the samples, as no cytotoxicity was showed even after prolonged incubation. The studied biomaterial was adequate on the biomechanical tests, since the laser treatments, under the conditions used, did not induce the formation of surface tensions of magnitude capable of leading the fatigue fracture, indicating infinite fatigue life; the region of fracture by tension could not be related to the laser marking (Figure 6c). The wear volume decreased as a function of the increase in micro hardness produced by the increase of the pulse frequency in the texturing. The visual character of the markings and texturing was assured after the majority of the tests performed.

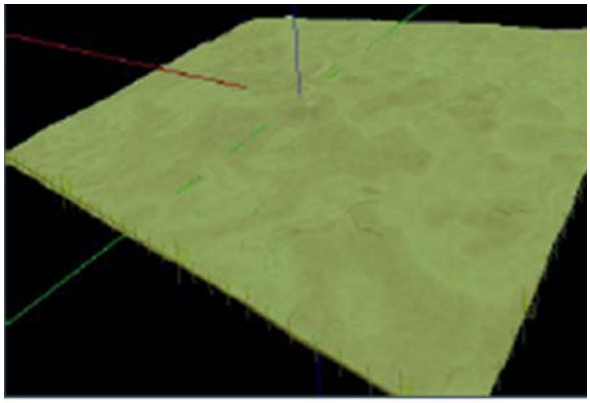

(a)

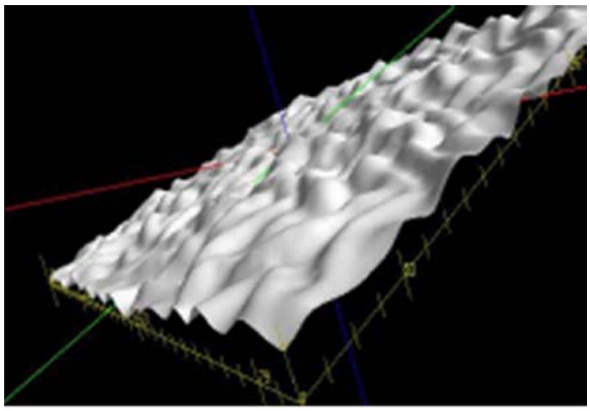

(b)

Figure 5: Topography of (a) untreated and (b) textured laser biomaterials

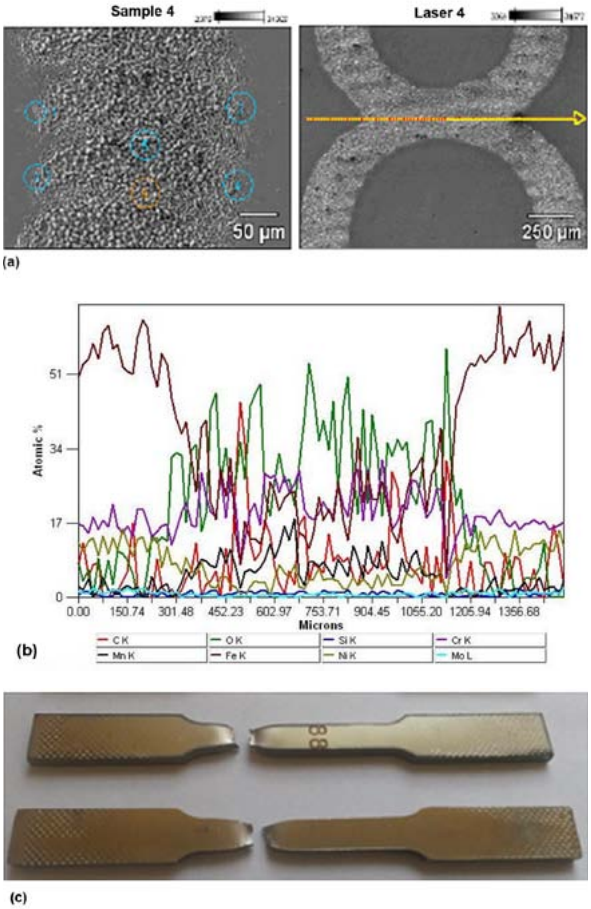

Figure 6: (a) Regions of the sample-4 analyzed by points and by line, respectively. The arrow indicates the direction adopted for the analysis by "line scan"- No attack, (b) On-line mapping of the distribution of the chemical elements present on the sample surface-4, (c) Marked and standard fractured tensile specimens.

Determinants of corrosion resistance of Ti-6Al-4V alloy dental implants in an in vitro model of peri-implant

Titanium (Ti) and its alloys are widely used for manufacturing dental implants and orthopedic prostheses owing to their high biocompatibility and corrosion resistance. These favorable properties for in vivo implantation are due to Ti ability to form a passive oxide film, i.e. TiO_2, immediately after contact with oxygen. This passive layer is very stable and adherent to the Ti surface during function in the oral cavity. However, up to 20% of individuals with dental implants develop peri-implantitis; a chronic inflammatory disease causing loss of jawbone and eventually implant failure and removal. The etiology of peri-implantitis has not been fully unraveled, but has been traditionally considered to be associated to microbial infection. Recent results from our group, however, have found that Ti corrosion products are vastly increased around diseased implants as compared to healthy ones. This observation indicates that the micro-environment to which the implant is exposed during peri-implant inflammation is highly aggressive leading to TiO_2 passive layer attack. The aim of this work is to simulate peri-implant inflammatory conditions in vitro to determine which factors affect corrosion susceptibility of Ti-6Al-4V dental implants in phosphate solution. The effect of hydrogen peroxide (surrogate for reactive oxygen species, ROS, found during inflammation), albumin (a protein typical of physiological fluids), deaeration (to simulate reduced pO2 conditions during inflammation), and pH (3, 4.5 and 7) were investigated. The corrosion resistance of Ti-6Al-4V was performed by electrochemical techniques and surface characterization after exposure to corrosion immersion test. The results showed that the most aggressive conditions to the Al-6Al-4V alloy were these typical of occluded cells, i.e. oxidizing conditions (H_2O_2), high acidity (pH=3), presence of protein and deaeration of the physiological medium. Our results provide evidence that titanium corrosion can be triggered by intense inflammatory conditions.

Zirconia dental ceramics

Yttria tetragonal zirconia polycrystals (Y-TZP) have been used in dentistry for metal free prosthesis due to esthetics associated with a high mechanical performance. However, the presence of humid environment can cause an accelerated tetragonal to monoclinic (t-m) phase transformation and consequent catastrophic failure of this material. This process, known as low temperature degradation (LTD) or aging, has been evaluated in vitro in our laboratory in a hydrothermal pressurized reactor at 150°C in order to accelerate the crystallite phase transformation kinetics. The degradation studies have been performed in commercial and laboratory synthesized dental ceramics.

The aim of commercial dental Y-TZP studies was the determination of speed of the front of phase transformation zone growth during hydrothermal aging, and to correlate with the biaxial flexural strength. The effect of the asso-

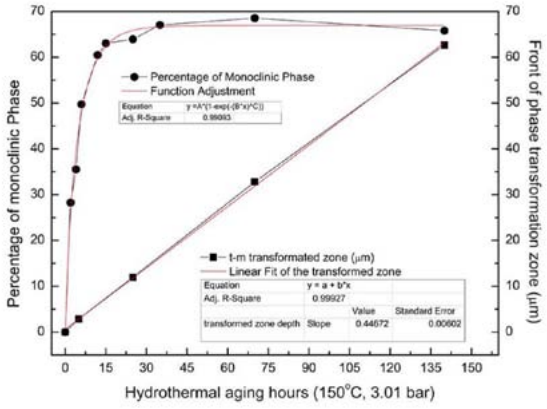

Figure 7: Comparison of t-m phase transformation data: XRD (sigmoidal curve) and SEM (linear fit).

ciation of hydrothermal aging and fatigue with biaxial flexural strength was also evaluated.

The results indicate that the sigmoidal behavior of phase transformation during hydrothermal aging, described in the literature, was a consequence of the limitation of X-ray depth penetration during X-ray diffraction analysis (Figure 7). It has been proven by scanning electron microscopy (Figure 8) and optical coherence tomography (OCT) that Y-TZP submitted to hydrothermal aging present a linear front of phase transformation as a function of aging time with decrease of the biaxial flexural strength after 140 h of aging at 150°C, 3,01 bar. Additionally, it was determined by kinetics studies that the phase transformation speed rate at the body temperature (37°C) is very low and will not cause deleterious effect on Y-TZP ceramics even overestimating the life of a human being in a hundred years.

Y-TZP composites are also promising dental materials that have been studied in our laboratory. Alumina, for example, can form a physical barrier against low temperature degradation, with hardness increasing, despite the reduction in fracture toughness (Figure 9). On the other hand, titania addition can enhance ceramic bioactivity as the presence of TiOH groups on ceramic surface induce apatite nucleation when in contact with blood fluids (Figure 10). In both cases, coprecipitation route has been employed for powder synthesis, allowing the study of additive composition effect. The ceramic processing includes powder forming by uniaxial pressing followed by sintering using different techniques such as conven-

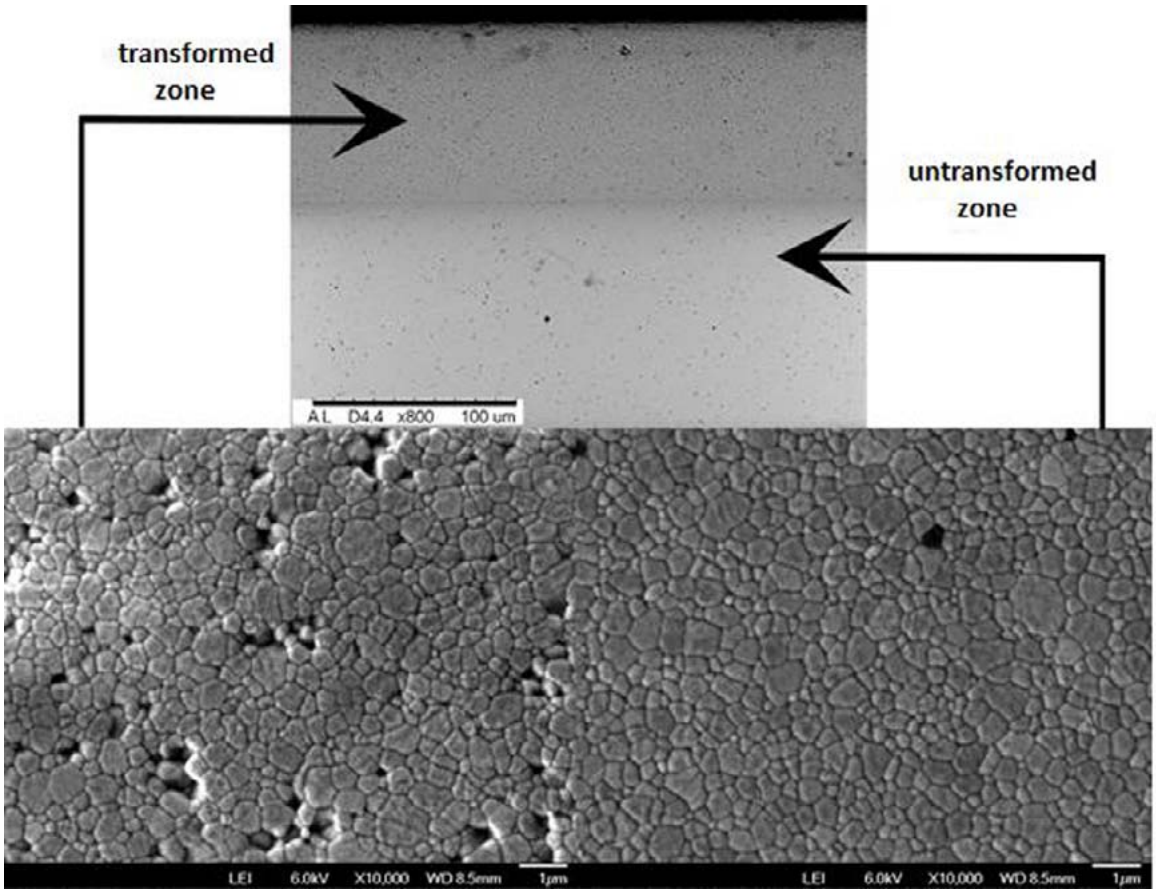

Figure 8: SEM and FEG-SEM images comparing the transformed zone microstructure and the untransformed zone of Y-TZP hydrothermally aged for 140h at 150°C.

tional resistive heating, microwave energy and two-step sintering. Promising results have been observed with the addition of 10-20wt% of alumina and 10-30wt% of titania.

Biomedical metals

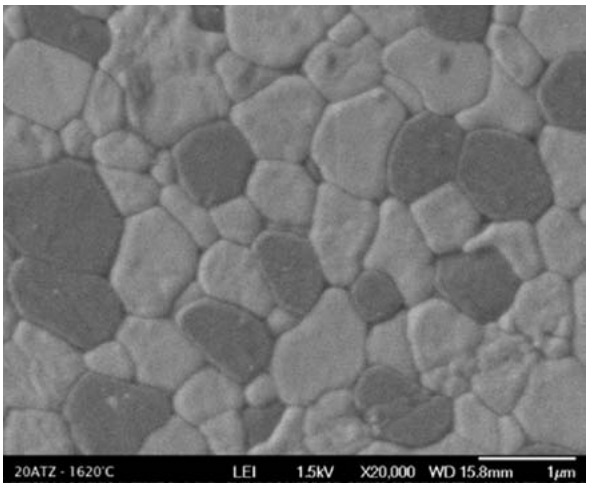

Figure 9: FEG-SEM image of Y-TZP-20 wt% Al_2O_3 composite.

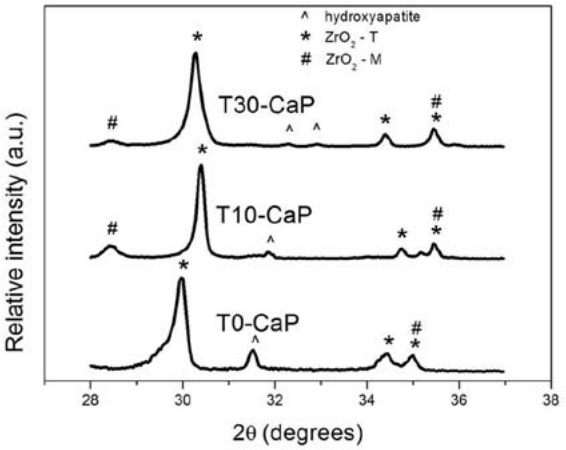

Figure 10: X-ray diffraction patterns of Y-TZP/TiO_2 samples after coating.

The topography of metallic implants is one of the factors that influence the bone healing and the osseointegration process. Machined implants have been used for many years, but some studies have shown that the increase in surface roughness tends to enhance, not only the interface between the bone and the implant, but also the bond strength at this interface Therefore, in order to improve the biological, chemical, and mechanical properties of the implants, material scientists have tried several surface modifications including mechanical treatment, thermal spraying, sol–gel coatings, chemical and electrochemical treatment, ion implantation, and so on.

When a biomaterial has the first contact with the body, its surface adsorbs proteins from blood and interstitial fluids. The inflammatory response depends on this formed layer of proteins, which will determine the activation of coagulation cascade, complement system, platelets and immune cells. Depending on the cellular and immune responses at the implantation site of biomaterials, rejection or degradation of the implant may take place. The key to the improved implant performance is to develop materials capable of avoiding detrimental immune responses.

Titanium is the main metal studied for implant application due to its biocompatibility and desirable mechanical properties. To improve the biological interaction of the implant with bone, different processes using surface modification have been performed; with the same goal to improved biological interaction, a new concept of structure modification is being applied. In that way, metallic porous structure can provide good mechanical properties and enhanced biological interactions, by the phenomenon of tissue invasion also referred as bone-ingrowth. The porous implants must have interconnected porosity that give the support required for vascular continuous nourishing allowing mineralization of bone tissue. Thus, pore channels must allow the infiltration of cells responsible for formation of the tissue matrix within the material, in order to meet the requirements for a lasting healing rehabilitation.

Production methods of porous metallic materials for implants are mainly based on powder metallurgy (PM), because it allows the manu-

facturing of parts with complex shapes and dimensions close to those of the end products (near-net shape process). The production of porous parts by space-holder technique using organics comprises several steps, which are: (1) mixing organic compounds with metal powder; (2) removal of the organic binder by heat treatment, generating the porous green body; (3) controlled sintering, in order to obtain porous structures with desirable mechanical properties. In this study, we aimed to produce porous implants of commercially pure titanium (cp-Ti) and Ti-13Nb-13Zr alloy by space-holder and suspension technique, using albumin as binder and natural polymers (corn starch, rice starch, potato starch and gelatin). The structure and surface features of the produced parts were analyzed by X-ray diffraction microscopy techniques. Special attention is given to understand the effect of surface nanoroughness on the interaction between the implant surface and bone cells.

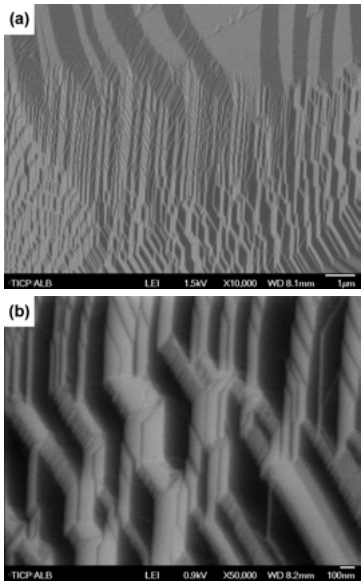

Figure 11: FEG-SEM images of the surfaces of pore walls with (a) lower and (b) higher magnification.

Porous Ti samples (40% of porosity) and Ti-13Nb-13Zr alloy samples (60% of porosity) with interconnected pores and high surface roughness in nanoscale presented good response in biocompatibility tests. The morphology of faceted pore walls with polygonal - like morphology is attributed to the preferential growth of some crystallographic planes, probably the basal plane, during the sintering process due to the lower surface energy of this compact plane (Figure 11). The obtaining of porous, with addition of albumin or natural polymers by powder metallurgy, results in an outstanding structure for osseointegration. In macroscale, the bone ingrowth is favored by the high porosity and, on the nanoscale, the nanoroughness propitiated a suitable surface for cell attachment, improving the bone implant contact area (Figure 12).

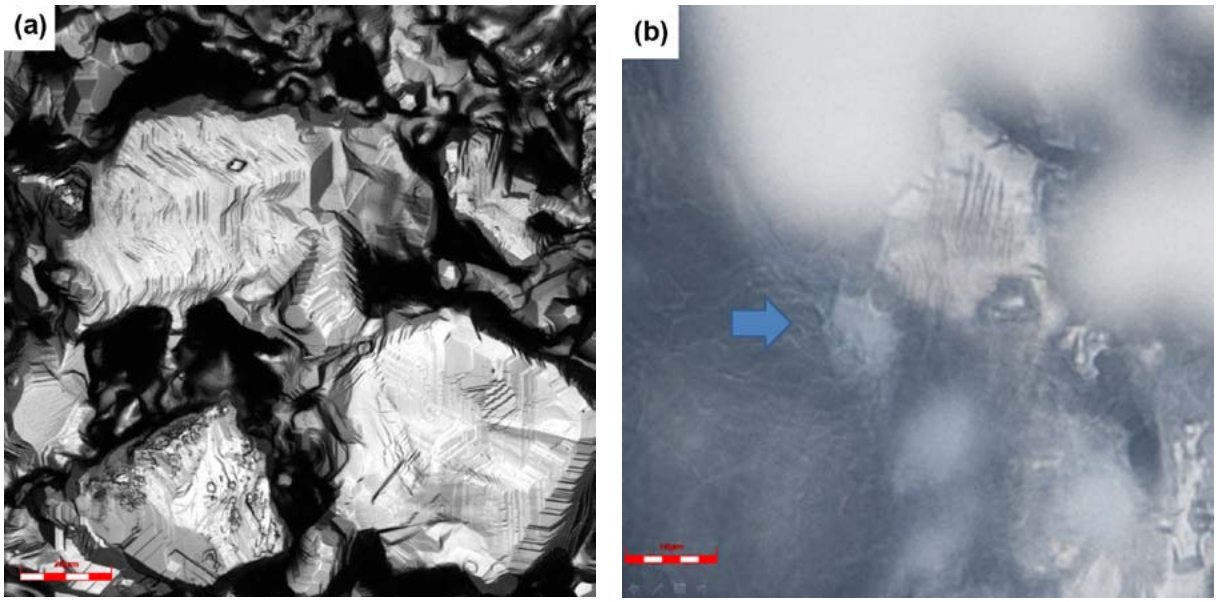

Figure 12: Confocal microscopy of the porous Ti implant: (a) surface of the implant before in vivo study; and (b) after in vivo study. Arrow indicates a cell attached on a surface.

Chemical Synthesis and Processing of Ceramic Powders

Graphene synthesis for energy and biomedical applications

Graphene is an allotropic form of carbon packed in two-dimension layer (2D) with honeycomb lattice structure that can be isolated from graphite (Figure 13). Its remarkable technological importance is due to the outstanding physical and chemical properties such as electrical and thermal conductivity, elastic modulus, fracture strength, flexibility, surface area, adsorption and desorption capacity of gases and biocompatibility. Experimental and theoretical studies on the synthesis and properties of graphene have been carried out since the nineteenth century, but its popularity was motivated from the paper of Nobel Laureates Geim and Novoselov, published in 2004, in which the physical effects predicted in theoretical studies were confirmed experimentally. Using a simple method of mechanical exfoliation of graphite sheets by adhesive tapes, it was produced a material with high mobility of charge carriers at room temperature. As the scale-up of this procedure is very difficult, other methods have been proposed for synthesis of graphene layers. CVD has been proposed for production of large area films and wet-chemical treatment of graphite has been indicated for preparation of small graphene-based platelets. The latter is suitable for applications in energy conversion and storage systems and ceramic biocomposites, which is the focus of the researches developed at Ceramic Raw Materials Laboratory of IPEN. Besides the experimental facilities concerning the use of homogeneous colloidal suspensions, the low-cost production makes this method an attractive choice.

The graphene synthesis procedure employed by Ceramic Raw Materials group was adapted from the method developed by Hummers and Offeman in 1958 and improved by Marcano et al in 2010 in order to enhance safety. Typically, graphite flakes (G) is oxidized with a mixture of concentrated sulphuric and phosphoric acids followed by addition of potassium permanganate and hydrogen peroxide under specific conditions of stirring and heating. The mixture is centrifuged and the remaining solid material is sonicated with deionized water. This material, denominated graphene oxide (GO), is further reduced with acid ascorbic solution. The obtained black suspension is centrifuged and the resultant reduced graphene oxide (rGO) is treated with hydrochloric acid solution, deionized water and methanol. After

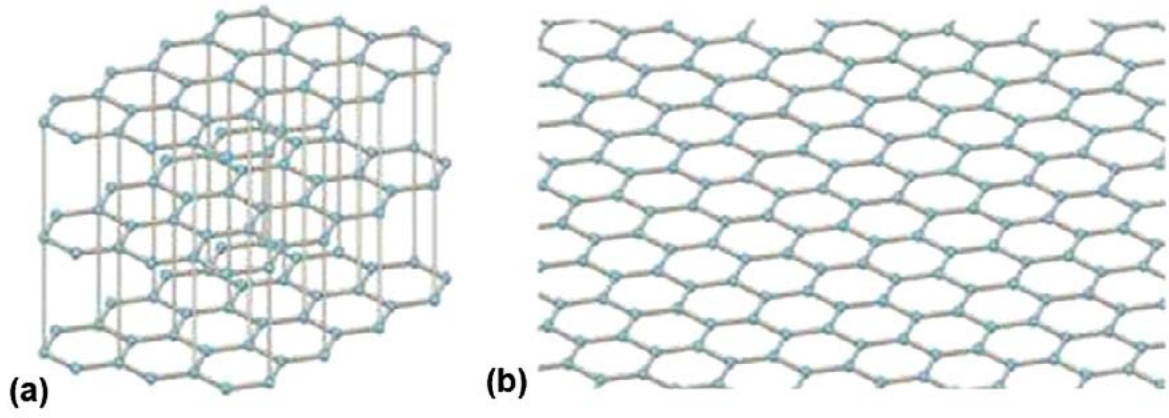

Figure 13: Schematic representations of graphite (a) and graphene (b) structures. Adapted from https://br.pinterest.com/nonikatz/graphene/

sonication and centrifugation, rGO powders are oven-dried and deagglomerated. The applicability of these powders has been evaluated for electrocatalyst support for polymeric fuel cell, supercapacitor electrodes and zirconia bioceramics reinforcement.

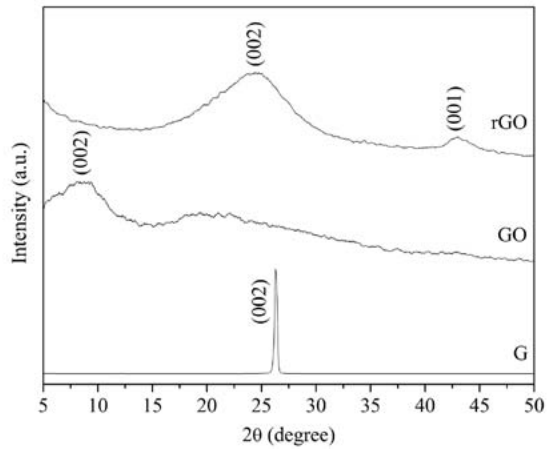

Figure 14: Normalized X-ray diffraction patterns of the starting graphite (G), synthesized graphene oxide (GO) and reduced graphene oxide (rGO).

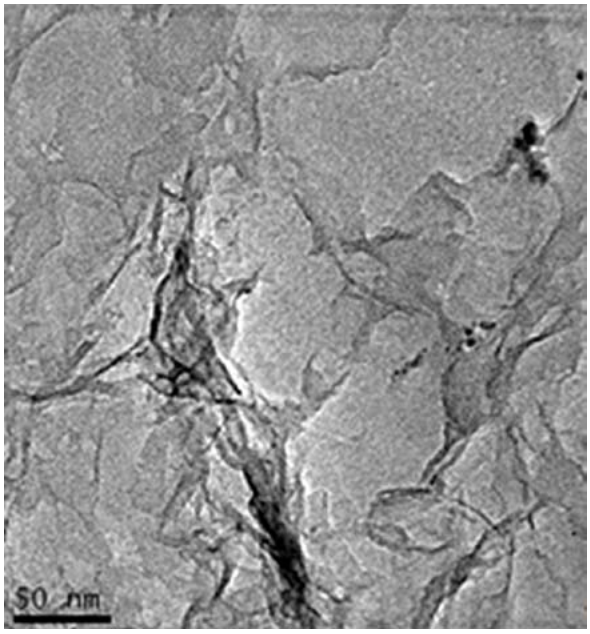

Figure 15: Transmission electron microscopy (TEM) images of reduced graphene oxide (rGO)

X-ray diffraction patterns of the starting graphite (G), synthesized graphene oxide (GO) and reduced graphene oxide (rGO) are presented in figure 14. Graphite has an intense peak at 26.3° corresponding to the (002) plane. On the conversion to graphene oxide (GO), this peak gradually shifts to a lower angle (2θ= 9.1°). Wide peak between 15° and 35° might be related to the formation of reduced graphene oxide since methanol has shown a reducing capability towards GO. After reduction of GO, the (002) plane shifted towards a higher angle value (2θ= 24.5°) due to removal of some oxygen functional groups. A representative transmission electron microscopy image of rGO is shown in figure 15. The observed fragmented thin film feature might be a result of an excessive centrifugation and ultrasonic treatment used along washing and exfoliation steps.

Eletroceramics

In the 2014-2016 period, research work has been devoted to two main areas: the development of ceramic solid electrolytes and intermetallics for solid oxide fuel cells and basic research on electric field assisted pressureless sintering of electroceramics. The solid electrolytes that were studied were yttria, scandia and scandia-ceria stabilized zirconia, strontium and manganese-doped lanthanum gallate, yttrium-doped barium zirconate. The synthesis techniques for preparing all these electroceramics were solid state reaction, peroxo-oxidant, spray pyrolysis and polymeric precursor. The ceramic powders that were obtained were characterized by nitrogen adsorption, X-ray fluorescence, X-ray diffraction, scanning and transmission electron microscopy and scanning probe microscopy. The pressed powders were sintered either by conventional heating dwelling-cooling profiles, spark plasma, or by two-step sintering. The facilities for carrying out research work on sintered ceramic pieces are X-ray diffraction, FEG scanning electron microscopy, impedance spectroscopy over a wide range of temperature (RT-1500K), frequency (0.01 Hz-140 MHz) and

oxygen partial pressures (10 ppm-1 atm). The highlight of the research carried out was the application of the flash sintering technique to several new electroceramics and composites like Silicon Nitride, Zirconium Diboride, SDC-CNT, 8YSZ-graphite, and others. Figure 16 shows SEM micrographs of (top) high density sintered BZY proton conductor prepared with particle surface clean powders synthesized using facilities at the University of California in Davis, and (bottom) of surfaces of SS446 steel oxidized at 800°C/250 h in air (a) and under oxygen (b) developed in collaboration with the University Rhone-Alpes, Grenoble, France.

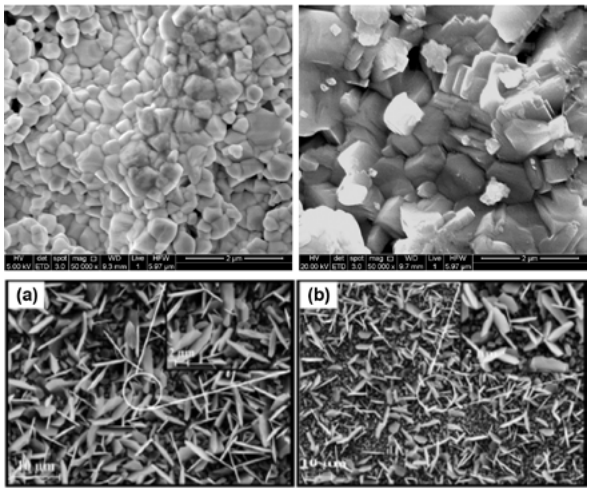

Figure 16: SEM micrographs. Top: yttrium-doped barium zirconate sintered at 1500°C using powders calcined under nitrogen at 900°C (left) and 1200°C (right). Bottom: SS446 steel intermetallic for SOFCs oxidized at 800°C/250 h in air (a) and under oxygen (b).

Ceramic spheres and microspheres prepared by Snowballing technique

The development of porous ceramic spheres is an alternative towards the use of granules as grafts, the application as a biomaterial can be as injectable bone grafts, filling defects and drug delivery system. Also, the application of the structural ceramics as filtering and adsorbing elements can be applied to numerous process. There are several routes to obtain calcium phosphates spheres, using different types of additives and process, nevertheless here is presented a novel process, without use of additives, no residues and low cost called "Snowballing technique".

Using the novel process, porous spheres and microspheres of HAp and β-TCP, Alumina and Zirconia were produced using the snowballing technique, which consists of taking the natural feature of aggregation of ceramic powders together with a continuous rolling process inside a cylinder container.

The values for open porosity of sintered HAp and Alumina microspheres were 47% and 39% respectively, obtained by hydrostatic density, and close porosity of 1.5% and 1.6% respectively, obtained by helium pycnometer.

The microspheres were evaluated by SEM, which presents their unique shape and microstructure. Figure 17 and 18 show HAp microspheres with the asteroid shape obtained in different sizes. Figures 19 to 22 show the detail of the surface aspect of the microsphere.

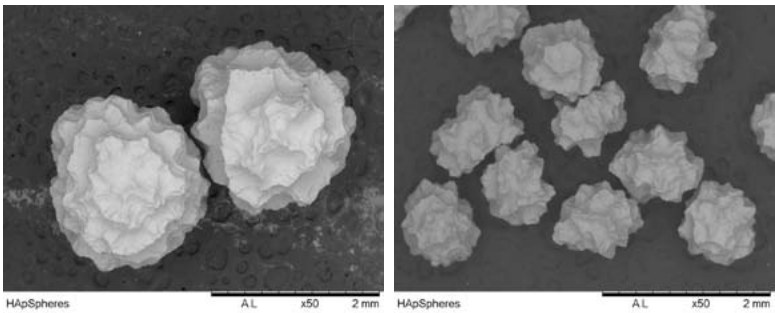

Figure 17: SEM of sintered HAp microspheres, diameter of >2mm and >710µm, respectively.

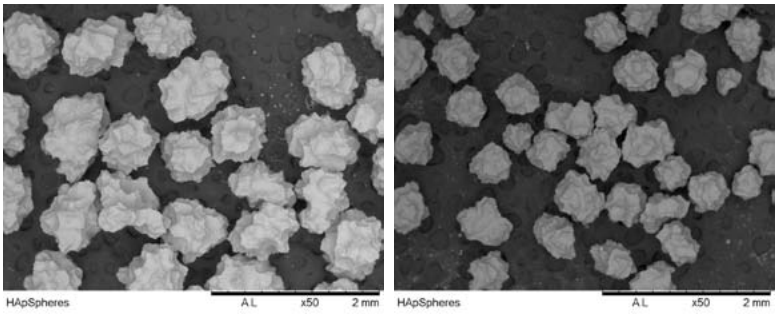

Figure 18: SEM of sintered HAp microspheres, diameter of >500µm and >250µm, respectively.

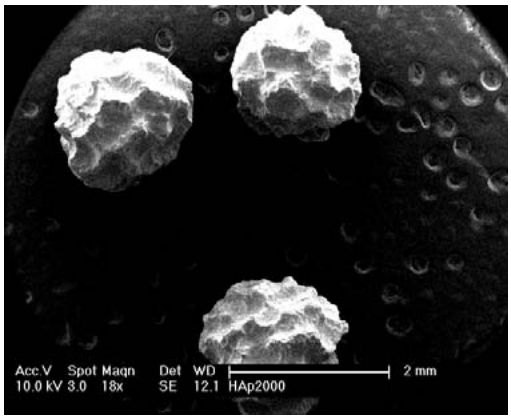

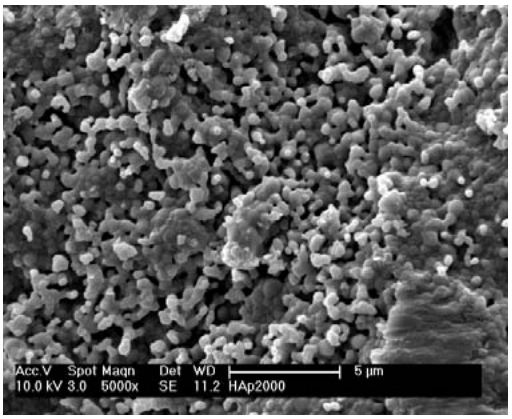

Figure 19: SEM of sintered HAp microspheres diameter of >2mm, magnification of 18x and 5000x.

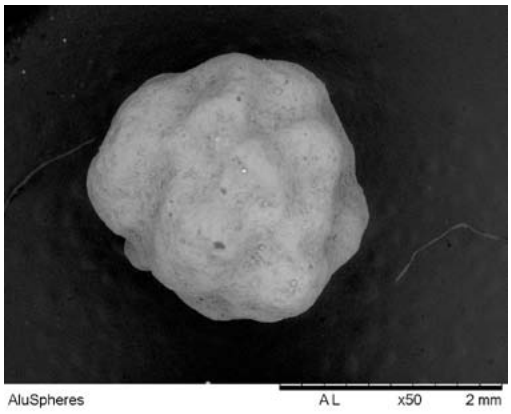

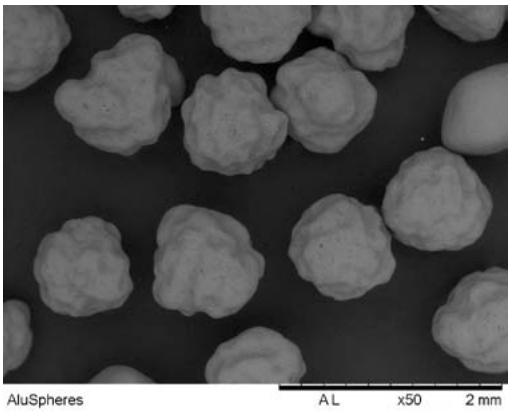

Figure 20: SEM of sintered Alumina microspheres, diameter of >2mm and >710µm, respectively

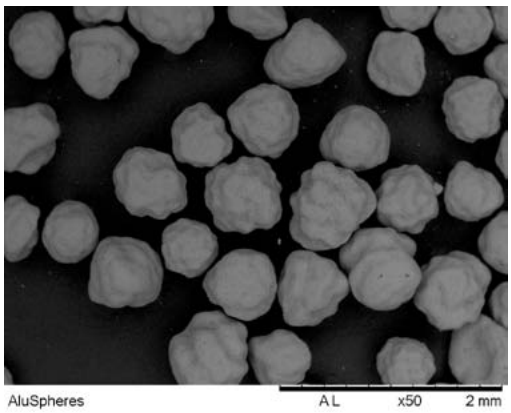

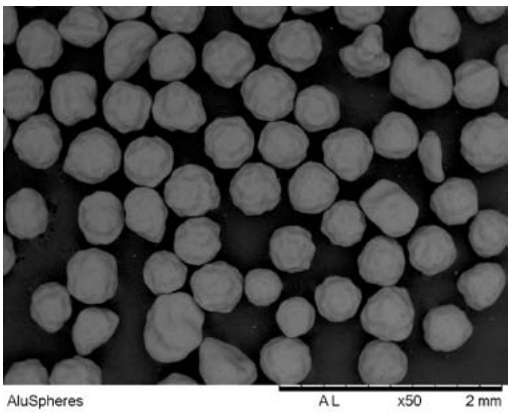

Figure 21: SEM of sintered Alumina microspheres, diameter of >500µm and >250µm, respectively.

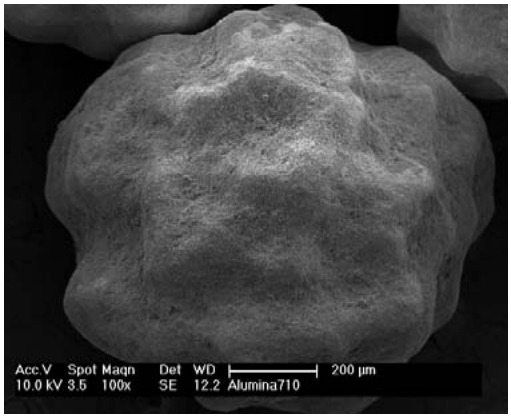

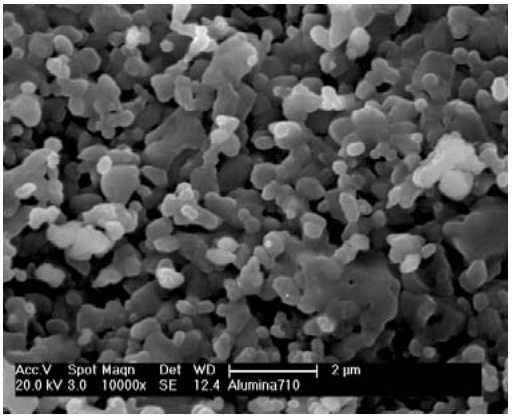

Figure 22: SEM of sintered Alumina microsphere diameter of >710µm, magnification of 100x and 10000x.

Mullite-based coating on silicon carbide refractory

Silicon carbide (SiC) presents low thermal expansion, high strength and thermal conductivity. For this reason, it is used as kiln furniture for materials sintering. On the other hand, SiC degrades at high temperature under aggressive atmosphere. The use of protective coatings can avoid the right exposition of SiC surface to the furnace atmosphere. Mullite can be a suitable material as protective coating because of its high corrosion resistance and thermal expansion coefficient matching that of SiC (4,7 x10-6/°C e 5,3 x10-6/°C, respectively). In the present work, a mullite coating obtained from ceramic precursor polymer and aluminium powder was studied to be applied over SiC refractories. Compositions were prepared with 10, 20, 30 and 50% (vol.) of aluminium powder added to the polymer. Aluminium powders were used with different distributions sizes. These compositions were heat treated at different thermal cycles to determine a suitable condition to obtain a high mullite content. The composition with 20% of the smaller particle size Al powder was selected and used to be applied as a suspension over SiC refractory. The applied suspension, after dried, crosslinked and heat treated, formed a mullite coating over SiC refractory. Cycles of thermal shock were performed in coated and uncoated SiC samples(Figure 23) to compare each other. They were carried out 26 cycles of thermal shock, in the following conditions: 600°C/30 min. and air cooling to room temperature. After each thermal shock, samples were analyzed by mean of optical and electron microscopy (Figure 24), elastic modulus was also determined. After thermal shock cycles, the coating presented good adhesion and no significant damage were observed.

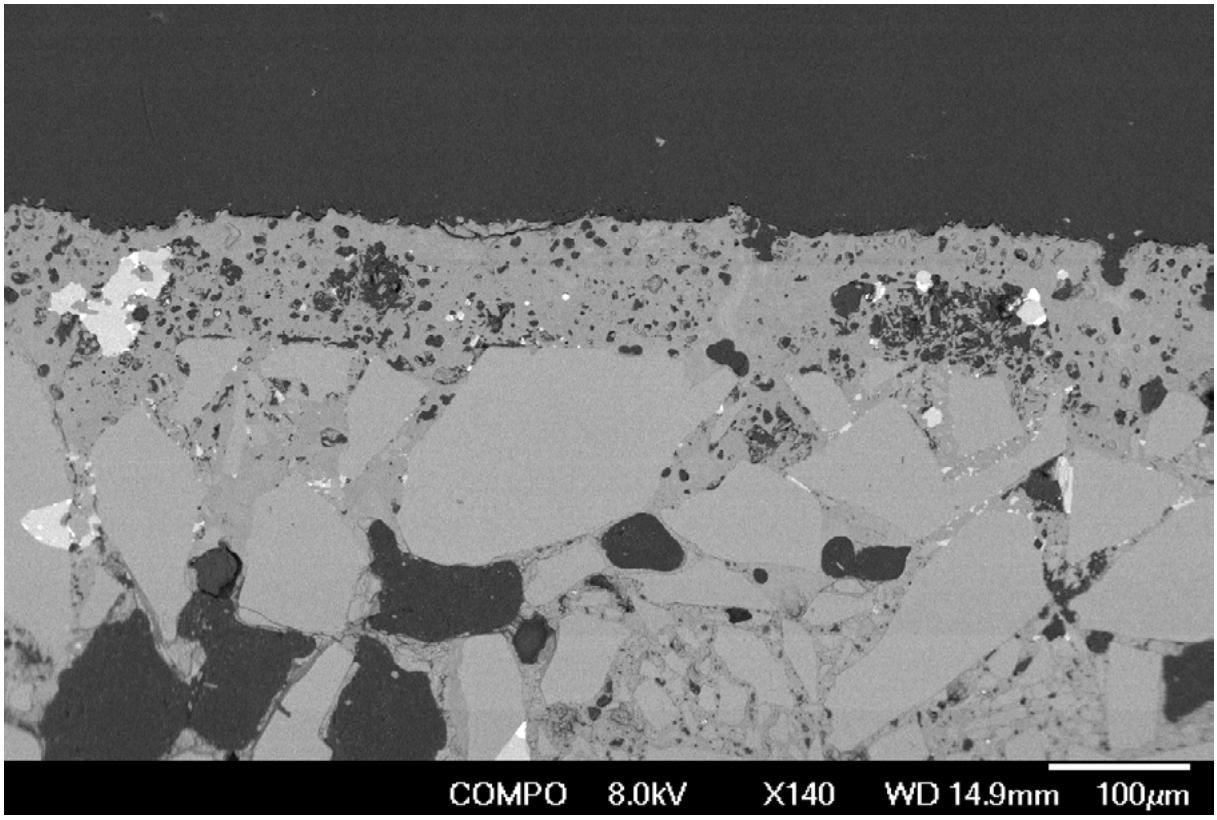

Figure 23: Coated (a) and uncoated (b) SiC refractory bars.

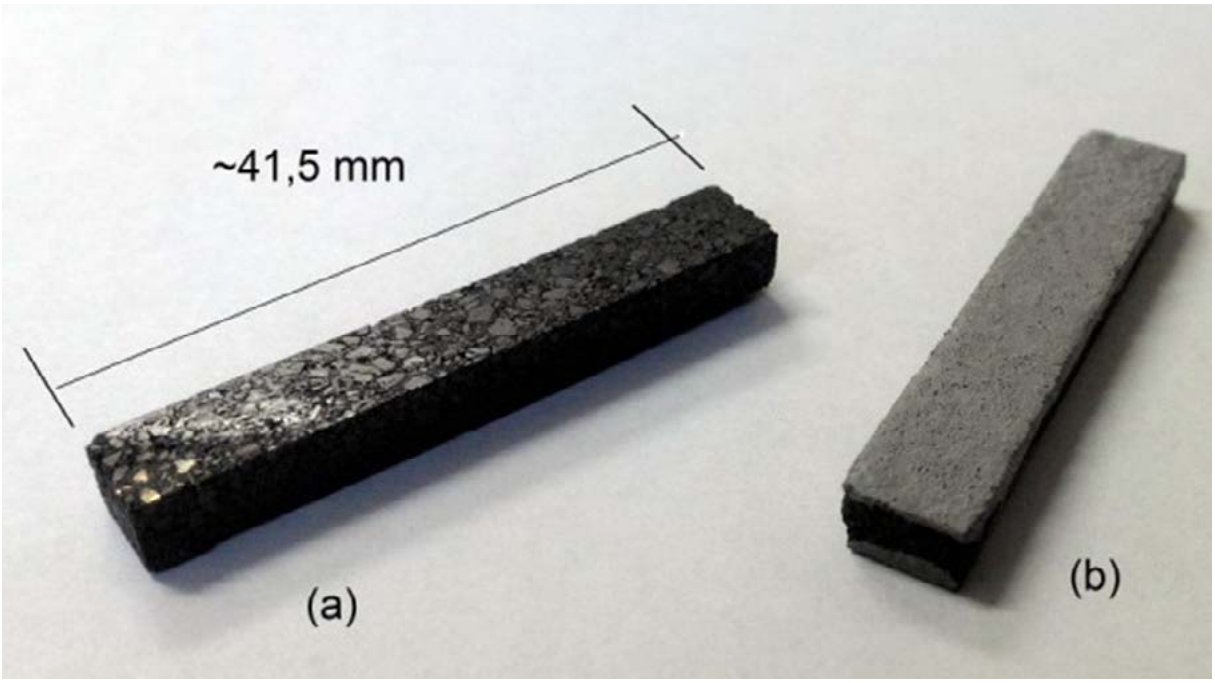

Figure 24: SEM image of longitudinal section polished surface of coated SiC refractory sample.

Materials and Technologies for a Self-Sustained Environment

Materials for Hydrogen Storage

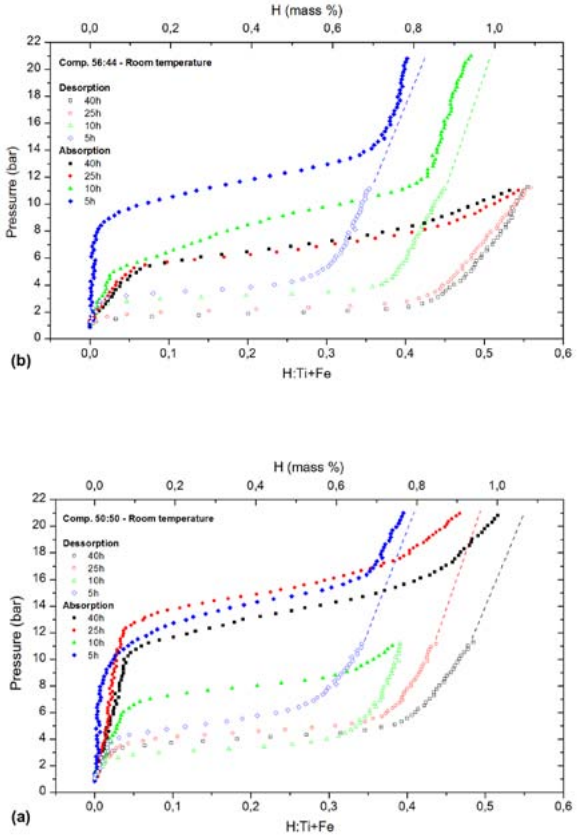

Figure 25: P-C isotherms at room temperature of (a) stoichiometric and (b) non-stoichiometric TiFe.

Among the various hydrogen storage methods, storing in the form of metal hydride holds a volumetric advantage over compressed and liquid hydrogen states and hence becomes the most popular development. Metal hydrides are very known by its good properties as a hydrogen storage material, i.e. reversible solid-state storage at low pressures with high volumetric capacity. In the laboratory of intermetallic materials, the activities on this matter have been focused on TiFe alloys and Mg-TiFe composites processed by high-energy ball milling. The research of the composites is a joint research effort with Federal University of São Carlos (UFSCar). We verified that non-stoichiometric TiFe can be prepared by appropriated change of the relative quantities of titanium and iron powders for milling. Non-stoichiometric TiFe could absorb and desorb hydrogen at lower pressures and higher rates compared to the stoichiometric compound, as shown on figure 25 (a and b).

Regarding Mg-TiFe, the strategy of using composites is based on the mixture of dissimilar materials, seeking to take advantage of what is best from each component. In this case, the purpose was to combine TiFe, which absorbs and desorbs hydrogen at or very near room temperature, with Mg, which has higher hydrogen storage capacity (7.6 wt.%). Figure 26 shows the results of absorption kinetics measurements of as-milled composites (Mg+40wt%TiFe) milled for 36 h (planetary mill) and 2 h (shaker mill). Planetary milled sample has faster kinetics at the start of experiment than shaker sample, attaining 3 wt.% of hydrogen after 1 h at room temperature. Higher hydrogen capacity was however attained by shaker milled sample after 5 h of absorption reaching almost 4 wt.% after 13 h, against 3.7 wt.% from planetary milled sample.

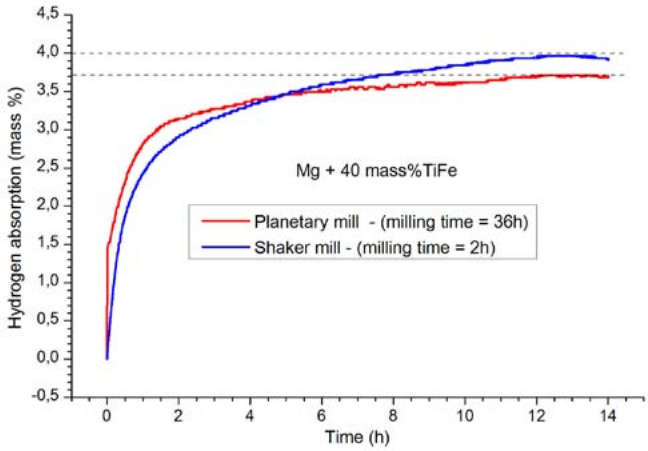

Figure 26: Absorption kinetics measurements at room temperature of as-milled composite samples

Mechanical Properties

Fracture mechanics and mechanical properties of metals, alloys and composites

An elastic-plastic fracture mechanics study of the application of Leak-Before-Break (LBB) concept in a relatively small-diameter (273 mm diameter) high-energy nuclear reactor coolant line was done, where it is proposed AISI 316LN type stainless steel to be used as base material welded with AISI 316L coated electrode. Results show a well-defined mechanical behavior where base material has a high toughness, weld region has a low toughness, and HAZ shows intermediate properties. For the load limit analysis, the lowest critical crack size was found for base material presenting circumferential cracks. For J-integral analysis, it was demonstrated that tearing instability leading to failure would not occur.

A preliminary draft version of a surveillance program for the materials presented in the nucleus of Brazilian Multipurpose Reactor (RMB) was developed. The surveillance program is needed to confirm and determine the effects of radiation on the mechanical properties of the core reactor materials: its effects on the tensile properties (strength and ductility), fracture toughness, radiation-induced growth and corrosion.

The mechanical behavior of high strength aluminum alloys of the 7075 series is under investigation, to study the occurrence of dynamic strain aging (DSA: Portevin-Le Chatellier effect) on tensile specimens, submitted to different heat-treatment conditions: (a) solution heat treated then artificially aged, T6, (b) T6 then solution heat treated at 485°C for 5 hours, (c) T6 then solution heat treated at 300°C for 5 h. Preliminary results show the occurrence of DSA in the (b) and (c) conditions.

A fracture mechanics analysis of flaws in grinding balls mills for mining plants was undertaken and the theoretical values of growth rate of those defects were compared with actual values obtained through periodic inspections performed in this component. The cracks nucleation was caused by lack of lubrication in the trunnion bearings, generating circumferential thermal stresses and the estimated temperature of the trunnion and bushing contact reached 150°C. During the analyzed period, the results obtained by the BS7910 standard proved to be closer to the actual values than the ASME Section XI standard.

A study of the influence of solution heat treatment temperature on the hardness response in incoloy 945 was done. Incoloy 945 is a hybrid Ni-Fe-Cr based superalloy with a mechanical strength and corrosion resistance comparable to those of Inconel 718 and Incoloy 925, respectively, with minimum yield strength reaching 860 MPa. The heat treatment at 1000°C causes a hardness reduction around 61%, reaching 63% at the temperature of 1020°C. The reasons for the reductions are the dissolution of the gamma prime hardening phase and a slight grain growth (ASTM 7). Above this temperature, the hardness loss is negligible, however, grain growth is more pronounced reaching a ASTM 2 grain size in the specimens treated at 1050°C.

Aluminum alloys for automotive applications

Automobile parts made of steel/cast iron have been replaced with those made with aluminum alloys to not only reduce weight, but also to reduce fuel consumption the emission of pollutants. Structural materials require not only high strength/weight ratio, besides rea-

sonable cost, but also high fatigue resistance. Moreover, the Al alloy parts have a rather high residual value, because the aluminum is fully recyclable at the end of the useful life of the part. Automotive cylinder liners are mechanical components with the function of being an internal coating of automotive engine cylinders. Among the different foundry casting methods, the centrifugal casting technique relies on a tubular die with a high rotational speed during pouring (1,700 rpm). The dynamic effect of the high rotational speed promotes high centrifugal acceleration, reduces porosity and promotes some density segregation effect that cannot be achieved in static foundry processes. The centrifugal casting process using the Al-Si alloys for cylinder liners can induce some reduction in the silicon content, mainly with low hypereutectic compositions compared to the materials used in static processes. The high centrifugal acceleration prompts silicon to run mainly in the inner diameter direction, due to its lower density compared to that of the aluminum alloy, even in the liquid state. Thus, with low silicon content on the outer side, it becomes easier to guarantee wear resistance in the cylinder/piston and ring working surfaces, as well as the mechanical properties requirements. The aluminum alloys studied are Al-19%Si with additions of up to 5%Mg and 5%Cu.

Extruded aluminum alloys find applications as automotive components. For automotive components, adequate mechanical strength/weight ratio at a reasonable cost is essential. Moreover, these materials should be resistant to fatigue when used as components exposed to cyclic loads. Precipitation hardening is an important method used to increase the strength of some aluminum alloys. Shot peening is a process to cold work the surface and is used to increase the fatigue life. This can be evaluated by residual stress measurements. The aluminum alloys studied are from the Al-Mg-Si and Al-Zn-Mg types (6005A, 6082 and 7108).

Ti-6Al-4V and γ-TiAl alloys

Ti-6Al-4V alloy has found applications at elevated temperatures and as biomaterial. The alloy Ti-6Al-4V is one of the most widely used titanium alloy because of an excellent combination of properties like strength, toughness, corrosion resistance and chemical stability. Surface modification of the Ti-6Al-4V alloy has been carried out to improve mechanical properties at elevated temperatures and fatigue resistance. The surface modification that was carried out was plasma nitriding. The nitriding was performed by varying parameters as time, temperature and gas mixture in the atmosphere. The gas mixture of Ar: N_2: H_2 (0.49: 0.49: 0.03) at 700°C for 4 hours was the chosen condiction. Creep and hot tensile tests were performed to evaluate the mechanical properties at elevated temperatures and fatigue test at room temperature. The phases of the nitrided sample detected by XRD were the ε-Ti_2N and δ-TiN, in addition to the α-Ti and β-Ti matrix phases. The layer thickness of this sample was about 1 μm. Hot tensile tests were performed in a temperature range from 500°C to 700°C in nitrided and no nitrided material and show an increase in the strength of the nitrided alloy. The creep tests were also performed in a temperature between 500°C and 700°C and stress range from 125 to 319 MPa. The result was an increase in creep resistance of the nitrided sample. This was evidenced by both the decrease in secondary creep rate and an increase in final creep time. Fracture of the tensile tested specimens was predominantly ductile with microcavities. The selected alloy after ion implantation by plasma immersion was submitted to creep tests at

600°C, in constant load mode at 250 and 319 MPa. The techniques used in this study were optical microscopy and scanning electron microscopy. Fractographic analysis of the creep tested samples showed necking and microcavities. The creep results revealed a significant increase in material strength.

Aiming at applications such as biomaterial, the effect of plasma nitriding on the Ti-6Al-4V alloy in fatigue behavior has be studied. The studies are being performed in the Ti-6Al-4V alloy will be comparative in the alloy with and without nitriding.

Ti-Al intermetallic alloyss with an Al content between 35 and 65 (atomic%) are usually divided into two categories: single-phase or two-phase alloys. The first group consists exclusively of the γ-TiAl phase, and the second, by the union of the γ-TiAl and α2-Ti3Al phases. Single-phase alloys do not have a balanced set of properties. The dual phase alloys allow the desired characteristics to be systematized by means of different microstructures, which can be classified into several groups: (a) partially lamellar, (b) near-γ, (c) duplex and D) completely lamellar. The study has focused on the microstructural characterization of Ti-Al-type alloys (Ti-44Al-4Nb-1Mo-B and Ti-48Al-2Cr-2Nb-B).

Nickel based superalloys

Inconel is a nickel-chromium-molybdenum superalloy with high corrosion resistance and strength at elevated temperatures. Surface modification of Inconel 625 has been carried out to improve mechanical properties at elevated temperatures. Creep and hot tensile tests were performed to evaluate the mechanical properties at elevated temperatures. The surface modification that was carried out was plasma nitriding. The microstructural characterization of the nitride layer was performed with the aid of optical microscopy (OM) and X-ray diffraction (XRD). Tensile tests were performed between 600 and 1000°C and deformation rates between 0.0002 and 0.002 s^{-1}. The results have shown that nitrided sample present expanded fcc phase and chromium nitride (CrN) phases. Tensile tests showed that there was no significant difference in the yield strength and elongation between non-nitrided and plasma-nitrided samples at the same temperatures. Serrated stress–strain behavior was observed in the curves obtained at 600 and 700°C, which was associated with the dynamic strain aging effect. At 600°C, the increase in strain rate promoted an increase of the amplitude and oscillation frequency of the stress.

Evaluation of adaptation and removal resistance of impacted abutment in small diameter conical dental implant

Dental implants of alloy Ti6Al4V (grade V) of narrow diameter came to solve a constant situation in the current implantology, which would be the installation of implants in reduced mesiodistal spaces, mainly to allow a final prosthesis with appropriate aesthetic requirement. Because it is a 2-part system, the installation of the abutment, made in the same alloy, is performed by impaction because its stabilization through a screw becomes inconsistent due to difficulties in machining such tiny components. The abutment after impaction in various ways in the implants were sectioned at 2 mm from the implant platform and the two halves were observed in a scanning electron microscope (SEM)(Figure 27), in order to measure the gap or the space between the implant/ abutment. Similarly, after the abutments were impacted in the implants, they were subjected to tensile test to evaluate their required removal force. This

study aimed to evaluate the accuracy, the juxtaposition of these parts in the conical connection and the force required to remove the abutment in order to check whether they were greater than the force of chewing.

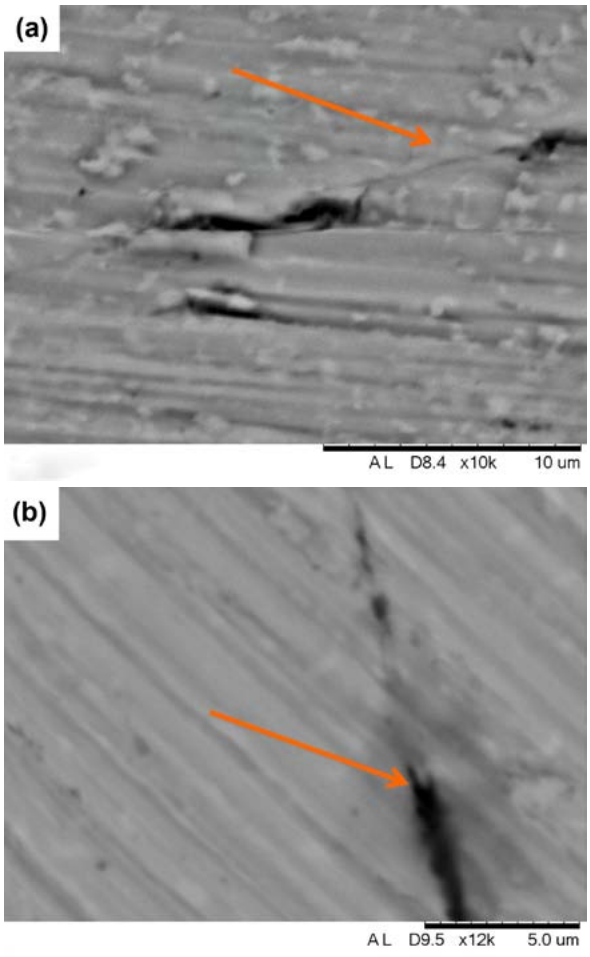

Figure 27: (a) Scanning electron microscopy image with back-scattered electrons showing the implant / abutment adjustment without maladjustment, see detail indicated by red arrows. (b) Gap of 0.5 µm in the part of the neck of the implant.

Grade 91 welded joints

Grade 91 steels have been widely used in components to work at high temperatures in power generation plants, petrochemicals and oil refineries due to their excellent creep and corrosion resistance. Despite these remarkable properties, some difficulties in welding Grade 91steels have been encountered, as they may exhibit hardness values outside the specified

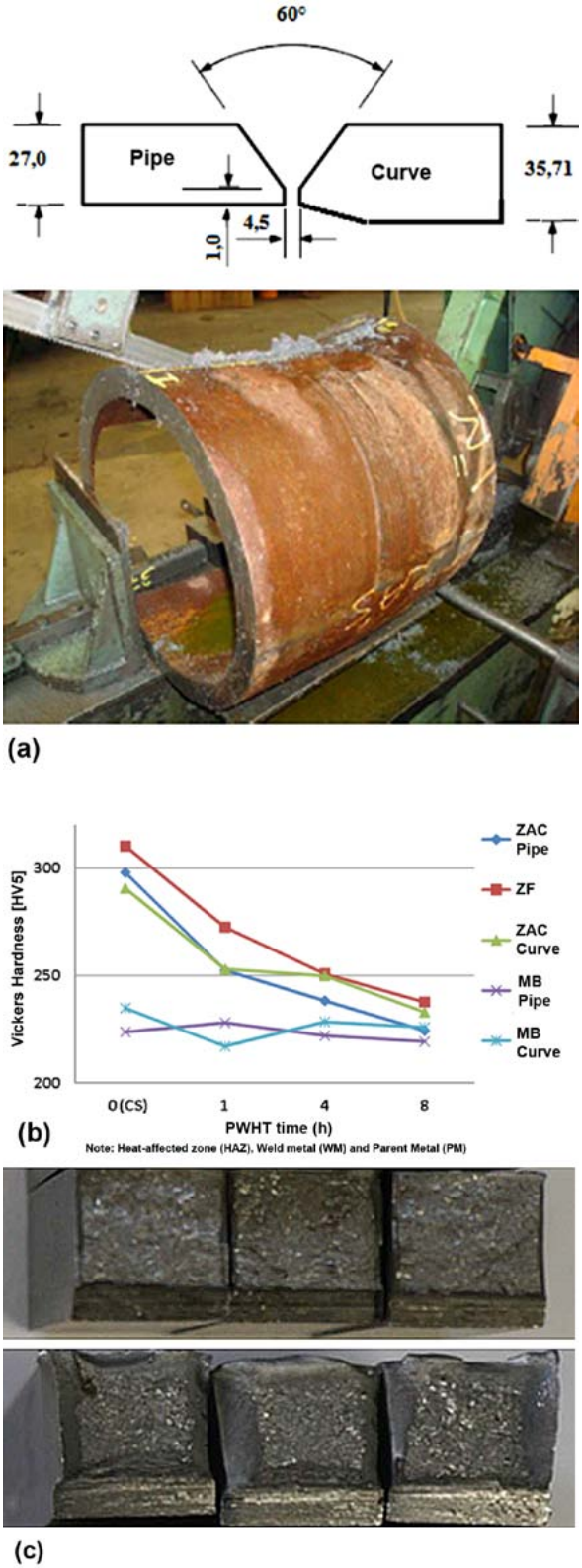

Figure 28: (a) Welded joint between tube and curve - Dimensions in millimeters (b) Influence of the tempering time in the various welding regions (c) Surface of the fracture region, the top sample without lateral expansion of the weld metal (WM-CS) and the bottom samples with lateral expansion of the weld metal (WM-8h) (d) Energy absorbed in the impact test x welded joint regions and (e) Lateral expansion in WM in the top and in the root.

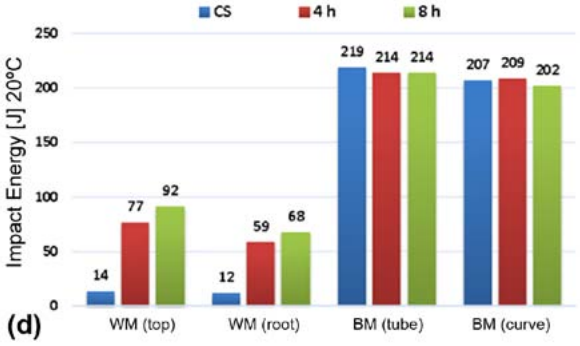

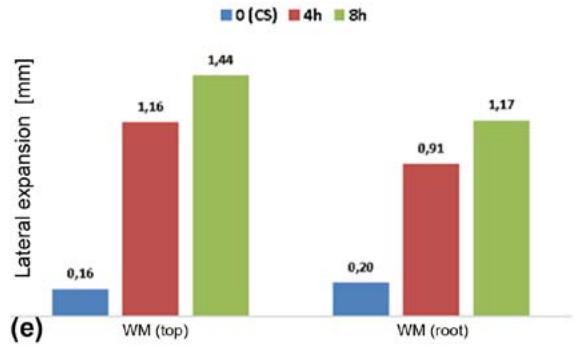

limits leading to a reduction of some mechanical properties. In this study, Grade 91 tubular joints were made through welding by using the GTAW process at the root and the SMAW process in the subsequent welding layers. The welded joints were subjected to PWHT with different tempering times (1h, 4h e 8h) and their mechanical properties were evaluated by performing conventional tensile, elevated-temperature tensile (540°C), Charpy V-notch impact toughness, Vickers hardness testing and microstructural characterization (Figure 28). Results indicated that mechanical properties of Grade 91 steel change with increasing tempering time, and a better combination of strength and toughness can be reached with more than 4 hours of PWHT, under certain conditions.

Study of the strain gage signals for the control of a micro torque meter

The controls of the stresses on the bone-implant and implant-abutment interfaces are crucial for the performance of an implant. Dental implants are a class in itself due to its size, chemical and biological environment. This paper presents a study on the electric signals from a strain gage used in a custom-made laboratory micro torque meter specially developed to evaluate the influence of the bone-implant and implant-abutment screwed interfaces on the micro torque signals. The original electric signals were acquired via National Instruments (NI) hardware and real time processed with the Labview® software for the evaluation of noise and its relation to the physical values of interest and equipment precision (Figure 29). The results indicate the need of careful attention to the noise pickup, noise source controls and mechanical amplification of the original signal in order to obtain higher accuracy of the equipment and automated control on the equipment (Figure 30).

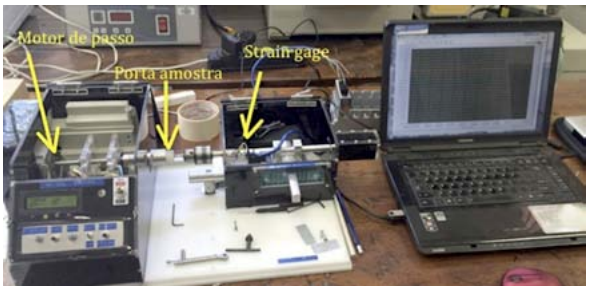

Figure 29: Image showing the inner and main parts of a prototype micro torquemeter.

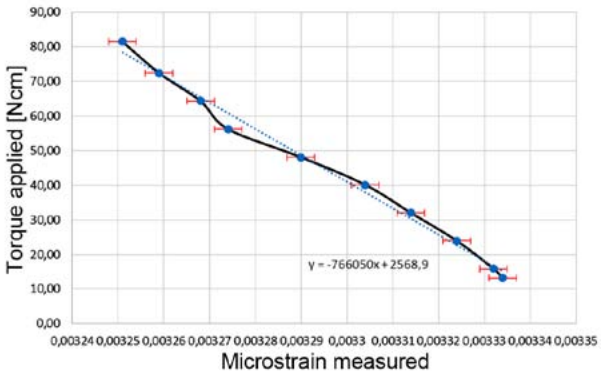

Figure 30: Experimental torque against microstrain calibration curve for the torquemeter.

Mechanical and metallurgical properties of sintered steels for valve seat inserts application

The aim of this work was to study the valve seat insert (VSI) obtained with three different alloys (mainly modified from the original AISI M3/2, M2 and D2 high-speed steels) from the mechanical and metallurgical point of view. These alloys modifications were intended as an alternative to replace cobalt and lead used in the original alloy due to their high cost and toxicological effect, respectively. Such alloys have been developed for internal combustion engines VSI manufacture. The VSI studied in this work was previously produced by powder metallurgy (P/M) route. The VSI production was performed by using a uniaxial hydraulic press and a belt conveyor furnace. The VSI was submitted to metallic infiltration during the sintering process using copper as filler (Figure 31). The studies were performed according to standardized apparent density (ASTM C 373-88), apparent hardness (ASTM E 92-82) and radial crush strength (MPIF Standard 35) tests. The VSI produced with M3/2 alloy proved to be more advantageous considering the highest values obtained in the apparent hardness and radial crush strength tests. The microstructure example was presented in figure 32.

Figure 31: Copper rings (left) and inserts (right) before sintering process, respectively.

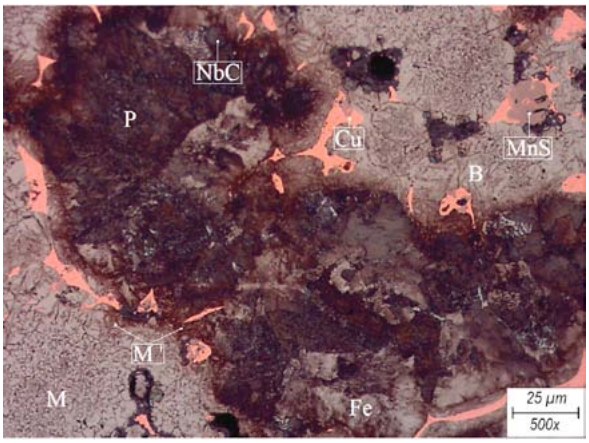

Figure 32: Micrograph obtained by optical microscopy of Alloy 1 (AISI D2 mixture) air quenched and double tempered at 500 °C.

Selective laser melting and precision casting of the Cobalt-Chromium-Molybdenum alloy

The mechanical properties and microstructural characterization of specimens of the Co-Cr-Mo alloy obtained by additive manufacturing - selective laser melting (SLM) and precision casting (PC) (Figure 33 a and b)- aiming at the manufacture of dental prosthesis were evaluated. The following steps were carried out on Co-Cr-Mo gas-atomized powders: 1) investigation of the physical, chemical and thermal properties of atomized powders in different grain sizes (denominated: D1 <15 µm, D2 20-50 µm and D3 > 75 µm); 2) the consolidation of standard specimens via consolidation techniques; 3) characterization of consolidated by analysis of: cytotoxicity, porosity, X ray diffraction and dilatometry; 4) mechanical characterization of tensile, 3 point bending, hardness (macro and micro Vickers) tests and microstructural characterization (OM and SEM-EDS). In general, the results observed were: the grain size D2 (20-50 µm) is the one that best fits in the analysis of packaging, for the consolidation by SLM; the biocompatibility of the samples obtained a positive result for both processing techniques; the mechanical evaluation of the specimens

shows that the SLM technique provides superior mechanical properties (yield stress, rupture stress, maximum stress, elongation and hardness), compared to those obtained by the precision casting technique; the microstructure obtained by the SLM process results in an ultrafine grains with high chemical homogeneity, differentiated by the gross dendritic microstructure in the casting process (Figure 33 c and d) . In this way, the development of the present study evidenced superior quality in manufacturing customized dental components (copings) by SLM technique compared to precision casting.

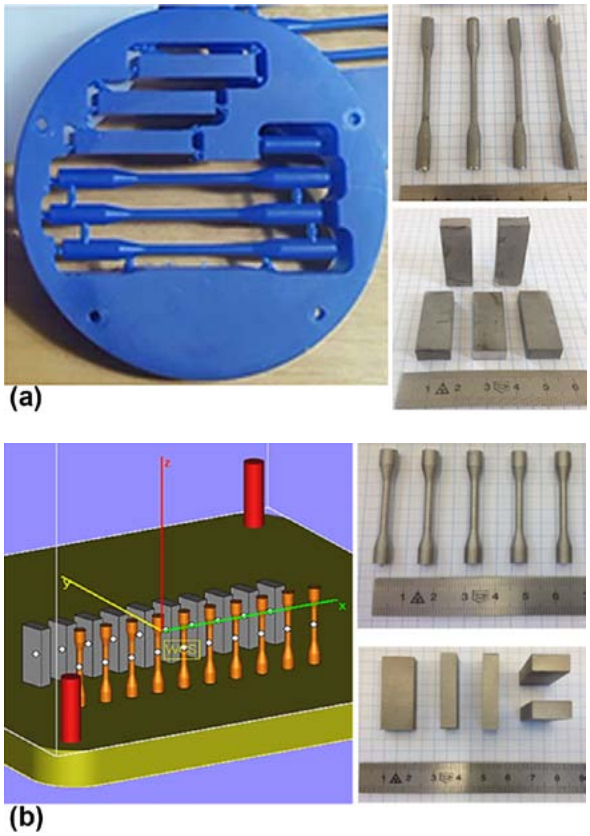

Figure 33: (a) Wax models machined in the standard dimensions – precision casting (PC), (b) Orientation in selective laser melting (SLM) consolidation of the standard samples and SEM micrographies of CoCrMo (c) PC (d) SLM

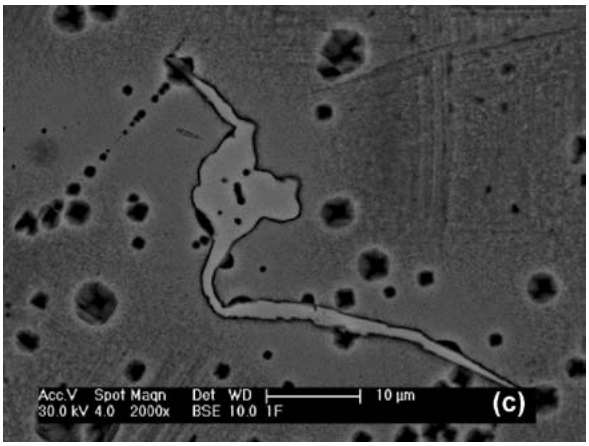

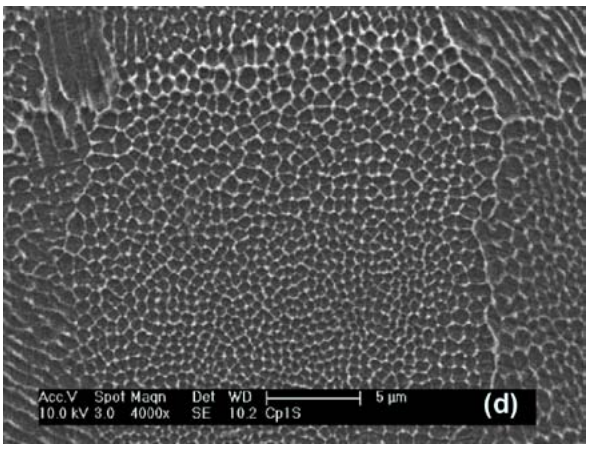

Coatings and Corrosion Protection

Hydrotalcite coatings to protect spent Al-clad fuels during wet storage

An all-room temperature process was developed to coat Al alloy surfaces with hydrotalcite (HTC). This process consists of pre-treatment, coating with HTC and post-treatment of the Al alloys. Field tests were carried out in which dummy MTR type fuel elements containing uncoated, HTC coated and HTC + Ce coated plates were exposed for periods of up to 2 years to the spent fuel basin of the IEA-R1 reactor. The HTC + Ce coated plates were free from any form of corrosion compared with the other plates, revealing marked potential for its use to protect spent Al-clad fuel elements against corrosion during extended wet storage. Figure 34 shows HTC coating on an aluminum alloy surface.

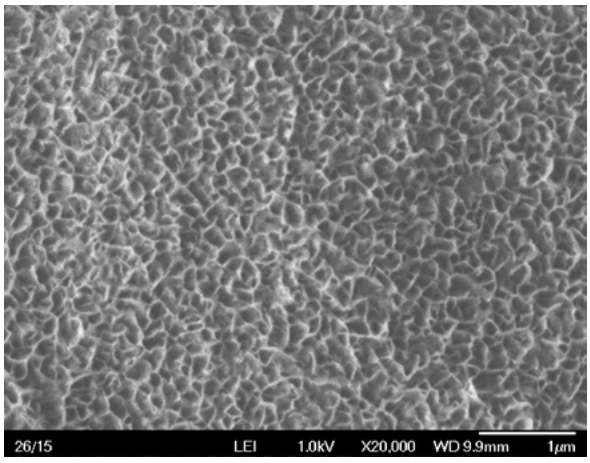

Figure 34: Scanning electron micrographs of RT-HTC coatings

Nanocrystalline rare earth oxide coatings for increased high temperature oxidation resistance of chromia forming alloys

Optimization of the use of different rare earth (RE) oxides as coatings to further enhancement of the high temperature oxidation resistance of chromium dioxide forming Fe-Cr alloys was studied. This optimization took into consideration the nature of the RE, RE oxide crystallite size, RE oxide morphology, ionic radius of the RE and the RE oxide coating coverage. In this study, the oxidation behavior of three ferritic stainless steels with varying amounts of Cr and coated with individual and mixtures of nanocrystalline oxides of Ce, La, Nd and Pr in air at 1000 °C was determined. The main criterion for optimization was the extent of addition of a trivalent RE oxide to bivalent cerium oxide. Figure 35 shows a mixed RE oxide coating on AISI 409 surface. The CeO_2 + 10% Pr_2O_3 mixture imparted maximum oxidation resistance to the steel surface at 1000 °C.

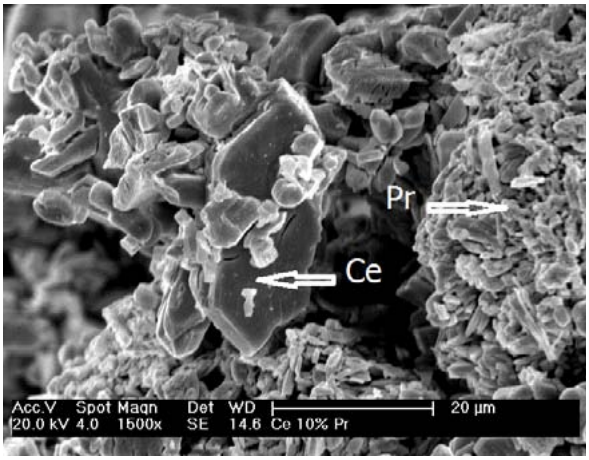

Figure 35: Scanning electron micrograph of CeO_2 + 10% Pr_2O_3 mixture on AISI 409 surface.

Localized electrochemical study of welded Al alloy joined by friction stir welding

Friction stir welding (FSW) is an efficient way to join high strength aluminium alloys. However, FSW generates different microstructural areas in contact that may give rise to galvanic couplings and affect the corrosion resistance of the assembly. In the present work, a localized electrochemical study of the AA7475-T651 and AA2024-T3 alloys butt-joined by FSW was carried out. Much lower impedances were associated to the FSW affected zones

comparatively to the two aluminium base metals tested individually. Corrosion of the welded system resulted in the establishment of a galvanic coupling, clearly shown by local electrochemical impedance measurements, at which the AA7475 alloy behaves anodically with respect to the AA2024 alloy. A Zn deposit was observed on the intermetallic particles of the AA2024 alloy after 24 h of immersion in the electrolyte resulting from the galvanic coupling. Such a behaviour in combination with LEIS results allowed to describe the development of the galvanic coupling between two different aluminium alloys (AA2024-T3 and AA7475-T761) butt-welded by FSW as a function of time from the early stage of immersion.

Friction stir welding effects on microstructure and localized corrosion resistance of S82441 lean duplex stainless steel

Friction stir welding (FSW) has been considered an alternative to replace fusion welding processes of stainless steels. In this study, the UNS S82441 lean duplex stainless steel (LDSS), a recently developed alloy, was FSWed and the effect of this welding process on the microstructure and localized corrosion resistance of the steel was investigated by assessment of phase volumetric fraction in each zone resulting from FSW, either affected or unaffected zones of the steel by X-ray diffraction (XRD), scanning electron microscopy, transmission electron microscopy and electrochemical tests. The pitting resistance of each zone was investigated by polarization tests and by determination of the pitting critical temperature. The results indicated that microstructural changes promoted by FSW did not affect the pitting resistance of the LDSS studied at room temperature. However, the critical pitting temperature at the thermomechanically affected zones of the LDSS slightly decreased comparatively to the stir zone (nugget) or to the zones unaffected by FSW.

Corrosion resistance investigation of Al-Cu-Li alloys

Aluminum-copper-lithium alloys are widely used in the aircraft industry due to their advantageous properties of low weight and high mechanical resistance. Precipitation hardening is one of the mechanisms to increase their resistance caused by second phase particles precipitates in the aluminum alloy matrix. These particles are formed during solidification or thermomechanical treatments. Addition of Cu and Mg leads to increased mechanical resistance of Al-Li alloys in solid solution condition and to homogeneous precipitation of coherent phases, such as $\delta'(Al_3Li)$ in the matrix with spherical morphology, besides other phases, such as Θ '(Al_2Cu), S (Al_2LiMg) or T1 (Al_2CuLi). It is important to note that hardening by precipitation of particles with Li involves the formation of metastable precipitates, which are phase precursors, such as T1. The aim of this study is to investigate the localized corrosion resistance of aluminum-copper-lithium alloys. This study has been carried out by surface observation as a function of exposure to various corrosion environments and by electrochemical techniques. The microstructure of Al-Cu-Li alloys is also under evaluation.

The effect of cerium in the sealing of anodized aluminum alloys

Aluminum alloys for application in the aircraft industry are highly susceptible to localized corrosion. Consequently, it is usually protected by anodizing and sealing treatments. In this study, Al-Cu-Li alloys were anodized in tartaric sulfuric acid solution, simulating

the industrial process adopted by the aircraft industry, and subsequently sealed, either in boiling water or in a solution with cerium ions. The aim of this study is to investigate the effect of sealing treatments with Cerium ions on the corrosion protection of anodized aluminum alloys. The surface of the anodized and sealed samples has been evaluated by Scanning Electron Microscopy and X-ray energy dispersive analysis. The corrosion resistance of the alloys has been monitored as a function of time by electrochemical impedance spectroscopy. The results indicate that sealing in cerium ions containing solution increases corrosion resistance and the long duration of the resistance with time of immersion is related to repair of corroded areas by formation of corrosion products that heal the defective sites indicating a healing process.

Protective coatings against corrosion for innovative automotive chassis: studies in situ by time-resolved synchrotron radiation

The Brazilian automotive industries are targeted to meet the program called Inovar-Auto. This Incentive Program for Technological Innovation and Intensification of Production Chain for Motor Vehicles (Inovar-Auto) is an action taken by the Brazilian Federal Government in order to encourage investment in the domestic auto industry. Companies, from 2016, are required to meet targets for reducing fuel consumption and CO_2 emission to obtain tax reductions, as well as to continue being competitive in the national and international markets. The assumptions of this project are to study by time-resolved X-ray diffraction, using synchrotron radiation, steel plates meant for hot stamping. It is important that a new coating with specific properties be developed to enable hot stamping and further application of automotive paint. This is the aim of the present work, which proposes the development, and characterization of coatings for application to the 22MnB5 steel in replacement of aluminum silicon coatings (Figure 36). The low use of high strength steels in Brazil is due to the high cost of the plates, today imported. The preparation of these new materials has as fundamental step, the necessity of use of advanced X-ray diffraction at grazing incidence, available in the National Synchrotron Light Laboratory - LNLS in Campinas - SP (Figure 37). The objective of this study is to shed light on what occurs during the processing of plates coated with zinc and nickel during hot stamping.

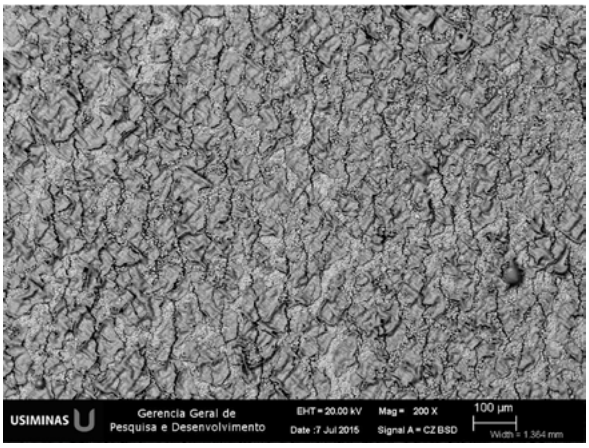

Figure 36: Hot stamped steel coated with zinc-nickel.

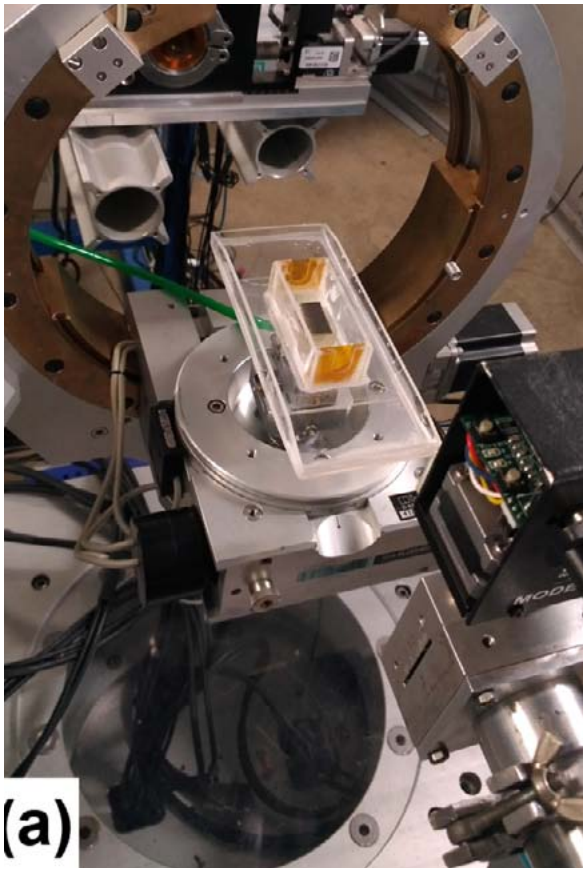

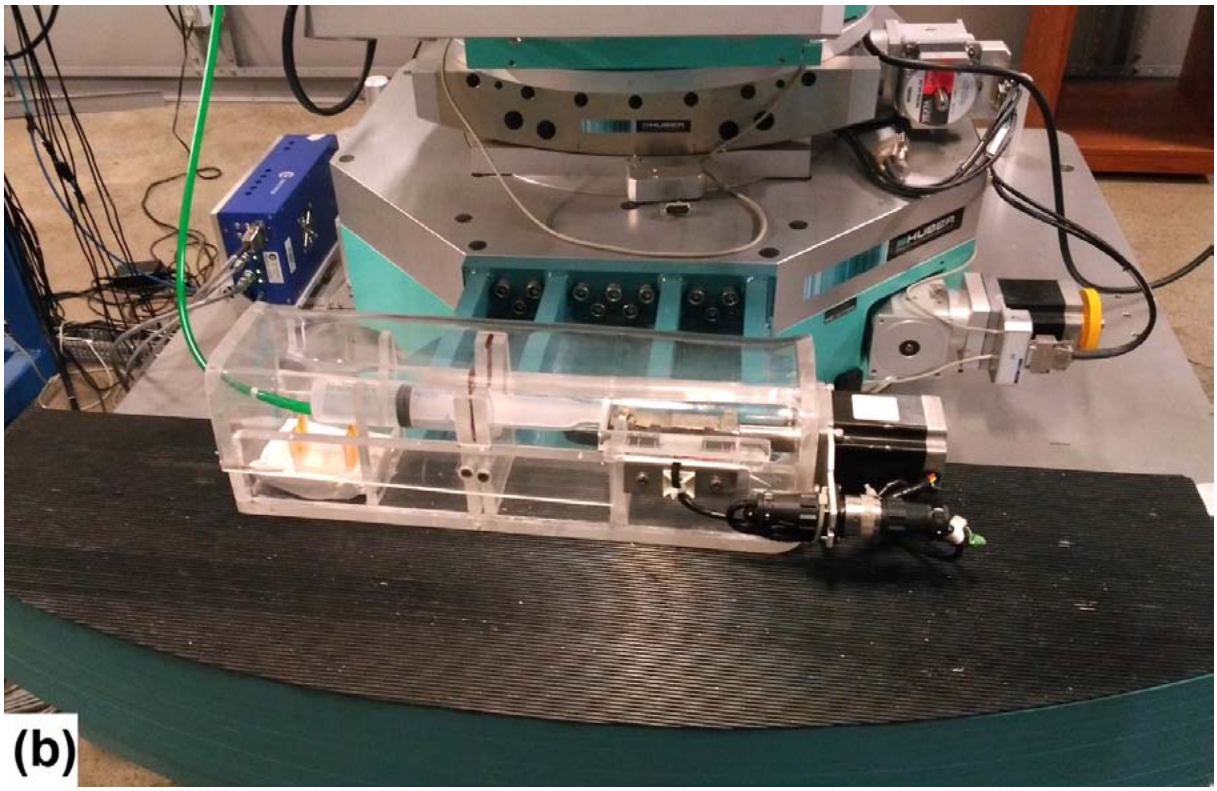

Figure 37: (a) Corrosion cell for X-ray diffraction using synchrotron radiation.

(b) Infuser.

Magnetic, Electric and Nuclear Materials

Supercapacitors – Photoelectric cells - Batteries

The increasing demand on sustainable energy impelled the development of alternative energy sources with high power and energy densities. Supercapacitors, batteries and fuel cells are typical non-conventional energy storage devices which are based on chemical to electrical energy conversion. These devices find extensive applications in consumer electronics ranging from mobile phones, laptops, digital cameras, emergency doors and hybrid vehicles etc. In all these devices, the chemical energy is converted into electrical energy by means of electrochemical reactions. In fuel cells, as long as the fuel is fed, the electrical energy will be obtained and in batteries, the stored energy would be drawn on demand, requiring a recharging time afterwards. Electrochemical supercapacitor is a typical storage device which possesses high specific capacitance, high power density and long cycle life and can be used in combination with batteries or fuel cells to meet the start-up at high power density.

Electrical double layer capacitors, pseudo-capacitors and asymmetric supercapacitors are the three types of supercapacitors, classified on the electrochemical responses and electrodes design. Double layer devices use high surface area materials such as activated carbons or derivatives for providing high electrostatic double-layer capacitance. The separation of charge obtained in the Helmholtz double-layer device occurs at the interface between the conductive electrode and the electrolyte. The advantages of these electrochemical devices include high power density and good cycling life while low energy density and low cell voltage are the common shortcomings. With this perspective, supercapacitors have been acknowledged as one of the promising devices in the energy storage industry and fast progress has been made in the development of fundamental and applied aspects of these energy devices.

In this brief progress report, we describe our recent research investigation on the preparation of various nanostructured graphene and zinc oxide electrode materials and the performances of symmetric supercapacitors. Vacuum thermal reduction of graphene oxide has been carried out in the group of Supercapacitors, Batteries and Photovoltaic cells. Graphene oxide nanocomposites have also been successfully used to prepare electrical double layer supercapacitors. Internal series resistance has been diminished with the thermal reduction procedure. A post-doctorate research project has been carried out on this subject, which resulted in the publication of papers and a patent deposit. A master degree on this subject has been finalized and another patent is being written. A doctorate project has also been implemented in the promising area of palladium incorporation on graphene nanomaterials and also three master degree investigation studies in carbon supercapacitors. Measurements techniques have been applied to estimate the specific capacitance of the electrode nanomaterials. Cyclic voltammetry and galvanostatic cycling have been employed with success for this purpose. Efforts have also been made to increase the specific capacitance of the electrode nanomaterials. In the field of batteries, a doctorate has been approved and another is being finalized. Progress has also been made in the field of photovoltaic cell with the implementation of an automatic research facility for preparing zinc oxide nanomaterial for energy conversion devices. Zinc oxide thin films have been deposited using a Successive Ionic Layer Adsorption and Reaction (SILAR)

technique. Zinc oxide nanorods prepared in this SILAR facility are also being employed to produce supercapacitors for energy storage and several undergraduate students are engaged in these investigations.

Copper based composites for electrical application

Copper and its alloys have been used in function of the high thermal and electrical conductivity, good mechanical properties, resistance to corrosion, ease of fabrication and by the high value of scrap. Metal alloys can also be combined with other classes of materials to obtain new properties, superior to the original alloy, this union of two or more materials forms a composite.

In this project copper alloys were developed by powder metallurgy for use in electrical application, including fuel cell. The studied composite has a ternary metal alloy (copper, chromium and silver) as a matrix and a ceramic oxide (alumina or ceria) as the reinforcing phase. The addition of chromium, silver and tin amounts of finely dispersed metal oxides in copper improves their mechanical properties and increases the operating temperature, causing little loss of conductivity. A possible application of these composites is as anodes in Solid Oxide Fuel Cells (SOFC) (Figure 38).

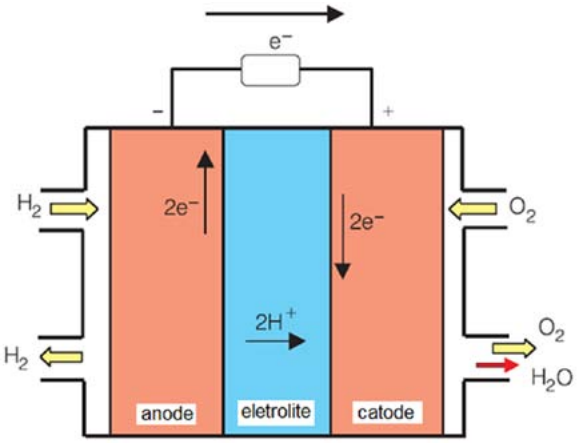

Figure 38: Chemical-electric energy conversion device.

Cermets based on rare earth oxides and metals such as copper, silver and chromium) have been studied (80% Cu – 20% CeO_2; 80% Cu – 8% Cr – 4% Ag – 8% CeO_2; 80% Cu – 20% Al_2O_3; 80% Cu – 8% Cr – 4% Ag – 8% Al_2O_3). The aim of this study involves microstructural characterization (optical microscopy, scanning electron microscopy, and X ray diffraction of composite processed by powder metallurgy. The samples used were fabricated in laboratory scale of 25 mm diameter, 3.5 mm ≥ h ≥ 4.0 mm of height and 6.5 g of mass.

To obtain the samples, the powders were weighed on a precision balance (according to each composition), mixed manually and cold-compacted in uniaxial press with 450 MPa pressure and sintered in an EDG furnace under 10-3 torr of mechanical vacuum and 650°C in

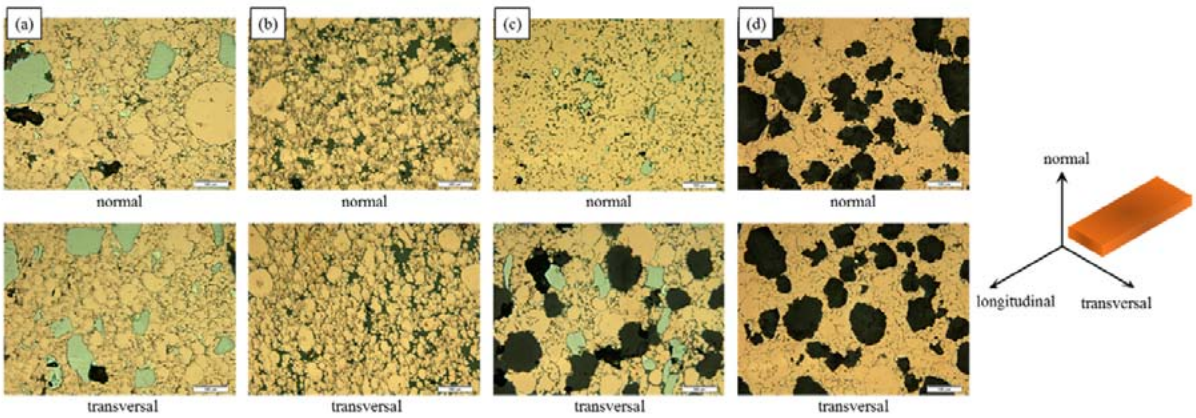

Figure 39: Optical micrographs of the composites Cu-Cr-Ag-(CeO_2, Al_2O_3) in normal and transversal directions, as polished (100 µm scale).

6 h. The samples were prepared metallographically and observed in an optical microscope, the micrographs indicated coalescing of the copper particles and other metallic elements and formation of porosity.

Optical micrographs indicated presence of porosity inside the structure and partial homogeneity, due to the non-dissolution of the elements involved in the metal alloy (Figure 39).

Control rod plates for the IEA-R1 reactor

An innovative program to develop new control rods for the IEA-R1 Research Reactor at IPEN was undertaken. Four rectangular Ag-In-Cd plates were inserted and sealed in stainless steel envelopes using a laser welding process (Figure 40). The sealed steel envelopes were then laser welded to stainless steel plates to form one of two forks of a control rod.

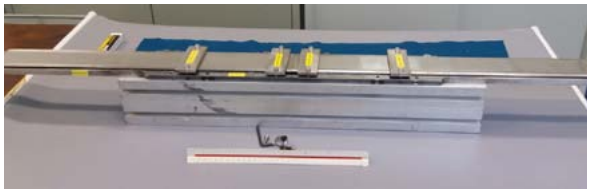

Figure 40: IEA-R1 reactor's control rod plate assembled for laser welding.

Hydrogen induced degradation of zircaloy-4

Delayed Hydride Cracking (DHC) has been responsible for cracking in zirconium alloy pressure tubes and fuel cladding and is a concern for spent fuel storage. A flaw in a loaded component may extend by DHC because hydrogen diffuses up the tensile stress gradient at the flaw tip. Sufficient hydrogen must be present for hydride to form at the flaw tip and the local tensile stress must be sufficiently large to crack the hydride. A crack will not extend if the threshold in stress intensity factor, KIH, is not exceeded. Hence, the threshold stress intensity factor KIH at 227 °C and 250 °C of zircaloy-4 tubes charged with 125 ppm of hydrogen was determined. This study, carried out in CCTM, was part of a global round-robin test involving 10 countries with PWR reactors and coordinated by the IAEA. The objective was to determine whether zircaloy-4 clad spent in nuclear fuel is immune from Delayed Hydride Cracking during Dry Storage. The overall results of this Coordinated Research Project suggested that unirradiated Zircaloy-4 fuel cladding is immune from DHC above about 320°C and this temperature increases to 360°C by irradiation.

Options for the Back-End of the Nuclear Fuel Cycle of research reactors

Research reactors (RR) are used worldwide for education of nuclear scientist and engineers, to produce medical and industrial radioisotopes, for Silicon doping, to perform advanced fuel and material testing to support life extension of operating nuclear power plants, to qualify new fuels (including studies on fuel behaviour in incidental and accidental conditions), etc. Presently, there are over 400 RRs worldwide and of these 230 are operating and the rest are either in a stand by situation, decommissioned or under decommissioning. A common problem related to all RR is management of the Back End of the Nuclear Fuel Cycle. To help address this problem, the IAEA initiated in 2015 a Coordinated Research Project (CRP) to develop a comprehensive set of options for the back end of the fuel cycle. The options included the means and methods for storage, transport, security, and disposal. In addition, the CRP is creating a tool to analyse scenarios comprised of these options with a focus on their economic aspects. In this context, CCTM has been participating to provide an additional option to safely store spent nuclear fuel for extended periods in wet basins.

Establishment of Material Properties Database for Irradiated Core Structural Components of aging Research Reactors

Today, more than 50% of operating research reactors (RR) are over 45 years old, and more than 30% are over 50 years of operation. Continued safe and efficient operation depends amongst others on the predictability of structural materials behaviour of major components such as reactor vessel and core support structures, many of which are difficult to replace. Management of the ageing process requires predictions of the behaviour of materials subjected to irradiation. In many instances, data for the radiation-induced changes of research reactor core materials resulting from exposure to very high neutron fluences are not generally available because the materials and operating conditions are diverse and specific. Therefore, effective sharing of experimental results related to the core-structural materials is needed in order to evaluate the reliability of ageing reactor core components. To address this issue, the IAEA initiated in 2013 a Coordinated Research Project (CRP) to collect, review and assess existing data of the relevant materials properties and operating experience with research reactors from over 14 Member States. Brazil participates in the CRP with CCTM contributing data for inclusion in a Research Reactor Components and Material Properties Database that can be used by research reactor community to help predict aging related degradation, and to promote safe and reliable operation and lifetime extension.

Materials Characterization and Visualization

Scientific Visualization in Materials

The Research Group for Scientific Visualization in Materials (GVCM) is part of the Materials Science and Technology Center (CCTM). It was formed in 2009 responding to a need for a multidisciplinary space for sharing research and ideas related to Scientific Visualization, Virtual Reality, Computational Simulation and advanced teaching methodologies for the study of Materials Science. Although detailed ongoing initiatives are available online at (http://gvcm.ipen.br/), from 2014 to 2016, GVCM has been focused mainly on two key research projects: CrystalWalk (CW) and GrainCrawler (GC).

CW is a web-based 3D interactive crystal editor and visualization software designed for teaching materials science and engineering aiming to provide an easy to use and accessible platform to students, professors and researchers. Aligned with the material sciences and engineering curricula, CW introduces a new simplified approach that creates crystal structures by combining a lattice with a motif using solely translational symmetry. Although very restrictive from the crystallographic point of view, CW makes it simple for students to experiment, reproduce and visualize, in an interactive manner, most of the crystal structures that are commonly introduced in materials science and engineering curricula, like fluorite structure shown in figure 41. CW is open-source and accessible, integrating state-of-the-art technologies for interactive web applications, such as HTML5/WebGL, service oriented architecture (SOA) and responsive, resilient and elastic distributed systems and support to advanced interaction and virtual reality interfaces as Oculus Rift, Google Cardboard, LEAP Motion, multi-touch devices and 3D printing technologies (Figure 42). CW can be accessed online at http://cw.gl from desktop, mobile and tablet devices and video demos and its source code is available at the project website at http://gvcm.co/CrystalWalk.

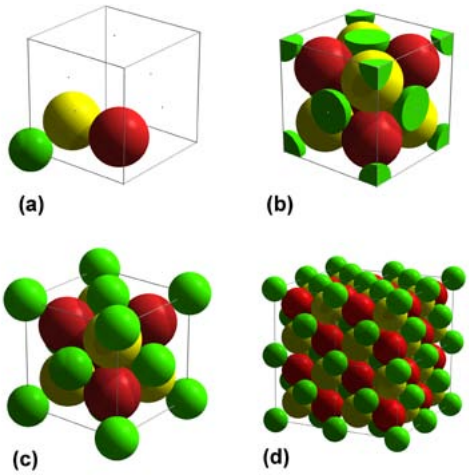

Figure 41: Fluorite (CaF_2) structure in different mode views: (a) motif formed by one calcium atom (green) and two Fluorine atoms (yellow and red); (b) Cropped unit cell (c) full unit cell; (d) crystal.

Figure 42: Advanced Interaction Support using Oculus Rift (head mounted display) and Razer Hydra (tracked joysticks).

Leveraging CW's technological premises, GC is a web-based 3D interactive visualization software sought to improve spatial understanding of grain structures. Based on solid cognitive and learning research, GC introduces novel domain-specific tools that support capturing fun-

damental characteristics, such as grain size and shape, number of neighbors, local heterogeneities, extreme values and distribution patterns. GC allows seamless exploration of virtual grain samples through first-person fly navigation (Figure 43) on a grain-by-grain basis, evaluating individual sizes and shapes, but also allowing capturing structural information such as neighborhoods and heterogeneities. Interactive real-time sectioning allows infinite sections to be visualized continuously in a brief period and designed rendering techniques improve depth perception either on 2D scenarios (Figure 44) or in full-fledged stereoscopic visualization, presenting superior visualization value compared to earlier attempts. GC can be accessed online at http://gvcm.co/GrainCrawler/ from desktop, mobile and tablet devices and video demos and its source code is available at the project website at http://gvcm.co/en-graincrawler/.

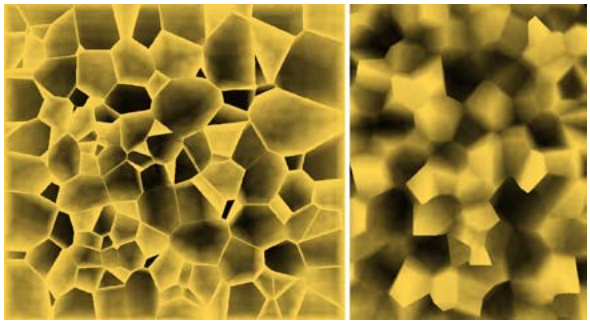

Figure 44: GrainCrawler screenshots demonstrating a real-time rendering technique that enhances depth perception on 2D visualization. (Left) section plane of a virtual 3D polycrystalline material. (Right) grains intercepted by the section plane were removed.

Development of x-ray diffraction methodologies of materials characterization

X-ray diffraction is a fundamental phenomenon resulting from the interaction of the photons and the atoms revealing the crystal structure of the materials. This technique is widely used to study the microstructure evolution that takes place during various processes including thermomechanical processing of materials. The continuous evolution of materials development, in the scientific aspect as well as for industrial applications, also implies in a continuous evolution of the methodologies of materials characterization. The following application was performed in the CCTM´s x-ray diffraction laboratory.

Nanomaterials:

Nanostructured coatings have been used to protect components exposed to severe service conditions. High energy milling is widely used to produce nanocrystalline feedstock of coating materials such as chromium carbide and tungsten carbide. During the high energy milling of Cr^3C^2–25(Ni20Cr) powder, severe plastic deformation takes place. A small part of the energy spent in this process is stored in the crystal lattice as deformation energy. The crystallite size and microstrain in nano-

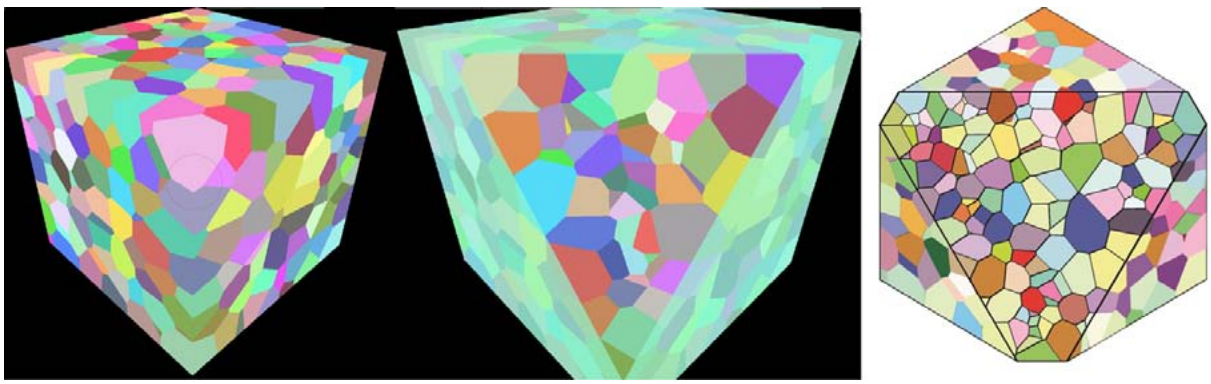

Figure 43: GC screenshots, showing: (left) perspective view of a cubic grain sample in first person navigation; (center) real-time interactive sectioning; (right) boundary enhancement rendering.

crystalline Cr^3C^2–25(Ni20Cr) powders milled for different times were determined by X-ray diffraction measurements.

Calcium phosphates, including hydroxyapatite [HA, $Ca_{10}(PO_4)_6(OH)_2$] and beta-tricalcium phosphate [β-TCP, $Ca_3(PO_4)_2$], are the main mineral component of bone tissue and teeth. The synthetic calcium phosphates are of special interest in medicine because of their biocompatibility, bioactivity and non-toxicity. Europium-doped hydroxyapatite (HA), beta-tricalcium phosphate (β-TCP) and biphasic phosphate nanopowders were synthesized by co-precipitation method and their crystal structures and fluorescence properties were investigated depending on the pH of the starting solution. In the range of pH 6–10, HA and β-TCP phases coexist. The β-TCP proportion increased as the pH of the solution decreased, while HA yields decreased. At pH below 6, monophasic β-TCP powder was obtained after thermal treatment. In particular, HA and β-TCP can be used as luminescent materials when activated by Eu^{3+}ions in substitution of Ca^{2+} ions. Herein, the Eu^{3+} ions doped HA and β-TCP phase composition were analyzed in order to investigate the fluorescence emission of the HA, β-TCP and biphasic compounds. Eu-doped HA exhibited a red-orange emission at 575 nm with several minor peaks at 610–640 nm, while Eu-doped β-TCP had an unexpected strong red emission at 610–620 nm and a secondary band at 590–600 nm. In fact, the Eu:β-TCP integrated emission area is almost 20-fold higher than Eu:HA for the same europium ion concentration. These results demonstrate the potential of Eu:β-TCP as biomarker for medical applications, as drug release and targeting based on their luminescent properties.

A nanosized magnesium-substituted beta-tricalcium phosphate (Mg:β-TCP) was synthesized by an aqueous precipitation method, at room temperature, in one single step. The novel and stable Mg:β-TCP resulted in a crystalline and spherical nanoparticles (diameter of approximately 20nm), with mesoporous structures and a high specific surface area (about 574m^2/g). These special characteristics make this novel crystalline mesoporous Mg:β-TCP nanoparticles ideal candidates for drug delivery system and a promising non-viral vector for gene therapy.

Texture

We studied the influence of particle size from powders and addition of sintering additives Al_2O_3 (0.25 to 1 wt.%), H_3BO_3 (0.25 and 0.50 wt.%) and SiO_2 (1 wt.%) on strontium ferrite permanent magnets magnetic properties. The milling step was carried out in a planetary ball mill with milling time between 30 and 360 minutes using 30 ml and 12 ml of deionized water as grinding media with and without sintering additives. After this process, powders were characterized through average particle size using Fisher Sub Sieve Sizer equipment and laser granulometry method, average crystallite size through x-ray diffraction, and morphology using scanning electron microscopy images. These powders were aligned to a 6 T magnetic field, isostatically pressed and sintered at 1220°C during 25 minutes and 60 minutes. The sintered magnets were characterized by its density, pole figures, alignment degree and magnetic properties through demagnetization curves.

The aluminum alloy 3104, H19 temper, is commonly used in the production of two-pieces beverage cans. The objective of the present study is to compare three different rolled sheets of this alloy. All three of them are routinely used in production lines dedicated to can manufacturing. The yield strength for all three was found around 265 MPa, the ultimate

tensile strength 281 MPa, and the average elongation 4.19%. The strain hardening exponent (n) was similar for all three sheets, averaging 0.078. The plastic strain ratios for planar anisotropy (ΔR) and for normal anisotropy were found to be near zero and 0.4, respectively. Values of ΔR near zero indicate there is no earing tendency. The crystallographic texture analysis yielded four dominating components: Brass ({110}<112>) and Copper ({112}<111>), which are typical of strain hardened aluminum, Cube ({001}<100>), usually associated with recrystallization, and Goss ({110}<001>). Such a texture would be conducive to balanced earing. The metallographic images for all three sheets were alike, with constituents not homogeneously distributed and with similar size and chemical compositions in addition to dispersoids finely spread throughout the aluminum matrix. The Erichsen tests also showed alike results with an average of 4.6 mm before failure.

Titanium alloys offer high specific strength and excellent corrosion resistance. These characteristics make titanium alloys an excellent choice for the aerospace sector and medical engineering. One of the main problems with using metallic implants for bone replacement is their relatively high Young's modulus. The higher stiffness of a prosthesis reduces the stress applied on the bone. We study the effects of cold deformation and recrystallization on the microstructure, texture evolution, and mechanical properties of Ti–30Nb–4Sn alloy. The samples are cold rolled to reduce their thickness by up to 85%. The most deformed sample is subjected to recrystallization treatment. The crystallographic texture is determined by X-ray pole figures. The 51% deformed sample shows a {203}<010> texture. The 85% deformed sample shows two texture components: {203}<010> and {130}<-310>, while the recrystallized sample shows a fiber texture with the {130} plane parallel to the sample surface. Hardness increases and Young's modulus tends to decrease in response to increasing deformation. The recrystallized sample shows low hardness and Young's modulus.

The effect of texturing Al_2O_3 and Al_2O_3/ZrO2 surfaces using femtosecond laser has been evaluated in terms of the roughness, wettability and microstructure of the substrate to increase growth efficiency and adhesion of hydroxyapatite. Femtosecond laser treatment of these materials causes phase transformation from alpha-alumina to gamma-alumina. Heat effects during femtosecond laser treatment causes the grains to be in the nanometer scale. Without heat effects, the grains are in the micrometer scale. The use of femtosecond laser permits control of the surface roughness of the alumina specimens. The higher the femtosecond laser energy, the higher is the wettability of the specimen and the total surface energy. Specimens with laser textured surfaces upon immersion in 1.5 SBF for 6 and 15 days revealed apatite layers well bonded to the substrate and without detachment. The adhesion of apatite to surfaces of specimens that were not textured with femtosecond laser was inadequate.

The production of tribological nanoscale multilayer CrN/NbN coatings up to 6 μm thick by Sputtering/HIPIMS has been reported in literature. However, high demanding applications, such as internal combustion engine parts, need thicker coatings (>30 μm). The production of such parts by sputtering would be economically restrictive due to low deposition rates. In this work, nanoscale multilayer CrN/NbN coatings were produced in a high-deposition rate, industrial-size, Cathodic Arc Physical Vapor Deposition (ARC-PVD) chamber, containing three cathodes in alternate positions (Cr/Nb/Cr). Four 30 μm thick NbN/CrN multilayer

coatings with different periodicities (20, 10, 7.5 and 4 nm) were produced. The coatings were characterized by X-Ray Diffraction (XRD) and Transmission Electron Microscopy (TEM). The multilayer coating system was composed of alternate cubic rock-salt CrN and NbN layers, coherently strained due to lattice mismatch. The film grew with columnar morphology through the entire stratified structure. The periodicities adopted were maintained throughout the entire coating. The 20 nm periodicity coating showed separate NbN and CrN peaks in the XRD patterns, while for the lower periodicity (≤10nm) coatings, just one intermediate lattice (d-spacing) was detected. An almost linear increase of hardness with decreasing bilayer period indicates that interfacial effects can dominate the hardening mechanisms.

Rietveld´s method

The aim of this study was to evaluate the aging behavior of a dental Y-TZP submitted to an accelerated hydrothermal aging (HA). Specifically: a) determine the kinetic curve of tetragonal to monoclinic phase transformation (t-m); b) calculate the speed of the front of phase transformation zone growth during the HA; c) evaluate the relationship between percentage of monoclinic phase and depth of phase transformation with the biaxial flexural strength (BF); d) evaluate the effect of the association of HA and fatigue at the BF. Sintered discs of dental Y-TZP (YZ- Vita YZ, LP- Lava Plus) were submitted to HA at 120°C, 130°C and 150°C and analyzed by X-ray diffraction analysis (XRD). One specimen of each group was submitted to scanning electron microscopy (SEM) and optical coherence tomography (OCT) to calculate the phase transformation depth and the speed of the front transformation zone. Groups (YZ, LP and LA-Lava) were divided according to the aging time (n=10): 0, 5, 25, 70 and 140 hours (150°C/3.01 bar). After the HA, the YZ group was divided once again (n=10): with and without mechanical cycling, all ceramics were submitted to biaxial flexural strength test (ISO 6872) and one way analysis of variance (ANOVA) (α=0.05) to compare the results. XRD results indicated that YTZP presented a sigmoidal behavior due to the limited depth of XRD penetration (~6.3 μm). SEM and OCT analysis confirmed a linear growth of the front as function of the time to all temperatures One way ANOVA showed a decrease in mechanical strength (10-19%) after 140 hours of HA (150°C) for all ceramics. Extrapolating the depth of the transformed zone results to 37°C, it was calculated that the front of the transformed zone would take around 1053 and 2104 years to reach 62.67μm and 85.55μm, depth that decreased the mechanical strength of the YZ and LP, respectively. The association of HA and mechanical cycling did not present a deleterious effect for the YZ. The OCT was validated as a precise, easy and fast method to evaluate the depth of the transformed zone and for kinetics studies.

Residual stress

Some effects caused by shot peening on Cr-Si-V steel have been studied, a process that aims to increase fatigue resistance. For this study, he variation of parameters in the process are tools to better understand the mechanisms that influence this property. The parameters used in this work were the variation of the grit and the pre-tensioning of the samples applied in leafs used in automotive springs of chrome silicon vanadium alloy steel (SAE 9254 + V).

The evaluation of the residual stress profile was performed by x-ray diffraction using the sen2Ψ method along the thickness in the region where the stress is compressive. The results show an anomalous effect in relation to the characteristic profile of the residual stress

distribution with the decrease of compression in the initial layers in relation to the blasted surface. With the use of scanning electron microscopy, the region affected by grit blasting was observed, noting that the plastically deformed regions are located in the same regions where the compressive residual stress decrease.

The profile obtained by X-ray diffraction provides necessary information with the aim of combining the effects of microstress (microstrain) on macrostress (residual stress). This relationship was confirmed by the overlap of the results found in the distribution of the microstrain of the crystalline lattice with the residual stress along the thickness in the plastically deformed region.

The results of the x-ray diffraction tests show an existence of tensile anisotropy between the planes generated by stacking faults and the dislocations density. Therefore, to obtain the values of the microstress, the factors of the elastic constants and the crystallographic planes must be considered. The method applied was the modified Williamson-Hall.

In addition, the study of the distribution of the mean crystallite size along the thickness of the X-ray diffraction profile was provided and the results showed that this distribution varies inversely with microstrain. The relationship between the mean crystallite size and the variation of the interplanar distances corresponds directly to changes in the densities of dislocations occurring in the material, which in turn are linked to the microstrain of the crystalline lattice.

Nanotechnology

Novel fluorescent, crystalline and mesoporous beta tricalcium phosphate nanoparticles

Synthetic calcium phosphates, especially hydroxyapatite ($Ca_{10}(PO_4)_6(OH)_2$) and beta-tricalcium phosphate ($Ca_3(PO_4)_2$), are of special interest in medicine because of their biVompatibility, bioactivity, non-cytotoxicity and their similarity with human bone and teeth. Due to their excellent biological functions and responses in physiological environments, particular attention has been placed to β–tricalcium phosphate, which has being widely used in a number of biomedical applications such as orthopedics, dentistry, tissue engineering, and drug, gene and protein delivery.

A novel and stable nanosized magnesium-substituted beta-tricalcium phosphate (Mg:β-TCP) was synthesized by an aqueous precipitation method, at room temperature, in one single step, for the first time, resulting in a crystalline and spherical nanoparticles (diameter of approximately 20nm), with mesoporous structures and a high specific surface area (about 574m^2/g) (Figure 45).

These special nanoparticles become fluorescent when doped with Europium ions. The Eu/Mg:β-TCP has an efficient visible luminescence and constitutes a new nanoprobe that can be used as optical contrast agents, affording

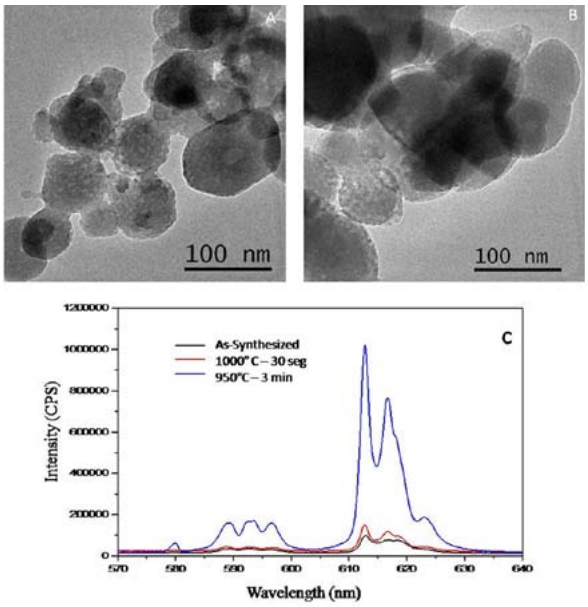

Figura 46: Eu and Mg doped β-TCP nanopowders after thermal treatment at (A) 1000°C for 30 seconds and (B) 950°C for 3 minutes. And (C) shows the emission spectrum of Eu/Mg:β-TCP before (as-synthesized) and after thermal treatments, under excitation at 394nm.

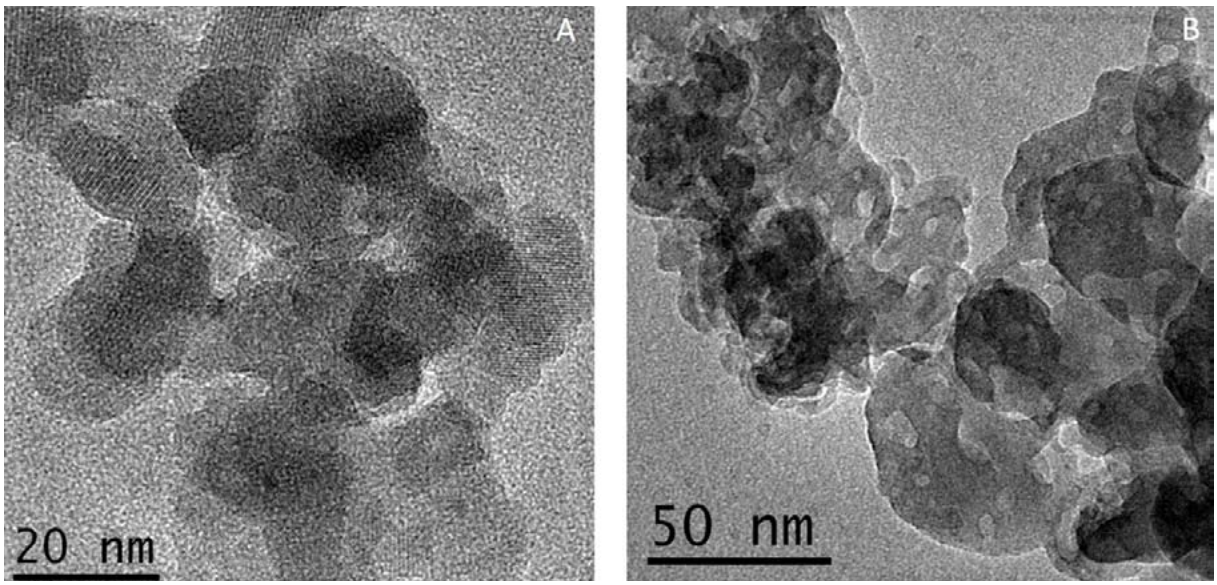

Figure 45: TEM micrographies of Mg:β-TCP (A) as-synthesized and (B) after thermal treatment at 1000°C for 30 seconds.

high resolution and sensitivity for biomedical applications.

The results showed new luminescent calcium phosphate presenting the ideal characteristics for drug delivery and gene therapy, as a non-viral vector for gene therapy: small particle size, spherical shape, mesoporous structures, high crystallinity, high specific surface area, high positive surface charge and efficient red luminescence (Figure 46).

Development of a ONE POT radiation process for the production of an advanced wound dressings with Silver Nanoparticles based on hydrogels

Ideal advanced dressings should meet various requirements, such as: retaining of the wound moisture to accelerate healing, transparency to facilitate inspection; non-adhesion to the wound bed to avoid injury and difficulty of exchanging dressings associated with intense pain; adherence to the health skin to facilitate manipulation; softness, complacency and flexibility for pain relief, good absorption of exudate, microbiocidal and anti-inflammatory properties. These desirable properties should be attained at the lowest possible cost to make it compatible with the Brazilian public health system (SUS). Our research group on polymeric biomaterials developed a process that combine in only one step (irradiation with ionizing radiation) the complete sterilization of the dressing already in its final packaging, combined with the formation of the gelled network, in a simultaneous operation. This step provides crosslinking for adequate mechanical properties to the use as dressing and provides reduction and stabilization of silver nanoparticles which in turn adds microbiocidal and anti-inflammatory properties to the dressing. Clinical trials have already been carried out in several institutions, with emphasis on the Tocantis ITPAC, the National Reference Center on Sanitary Dermatology and Leprosy of the University of Uberlandia CREDESH / UFU and at the wound management group of the University of the Southwestern of Bahia (Figure 47).

Figure 47. Polymeric biomaterials- hydrogels & silver nanoparticles.

Development of Gold 198 nanoparticles for cancer therapy and theranostic applications

Nanoparticles, in particular gold nanoparticles, have a wide range of applications in areas such as cosmetic, industrial catalysis and medicine. The broad application in medicine is mainly explained by the low toxicity, low reactivity and easy modification with biomolecules, and can thus be used to transport drugs and other species that are capable of increasing cell incorporation.

According to the National Cancer Institute, it is estimated in Brazil that around 500,000 people will be diagnosed with any type of cancer in 2017. Breast and prostate cancers are the highest incidences, and there are already numerous effective treatments for cancers with early diagnosis in both cases. However, the treatment is always very aggressive, charging a high price on the quality of life of the patient, so the search for increasingly effective,

more specific and less harmful methods to patients are always being developed. At this point, nanoparticulate systems have played an important role.

The use of gold nanoparticles from 198Au is already a reality. The ability of this metal to be used both as a contrast agent for diagnosis and as a therapeutic agent classifies it in the class of agent for "theranostic". Katti and colleagues have demonstrated that nanoparticles formed from 198Au are highly effective in the treatment of prostate cancer, a method proposed by him to prepare these nanoparticles using molecules obtained directly from natural products such as green tea (epigallocatechin- 3-gallate), drawing even more attention to these materials, however little was presented on the yield and stability of this method, besides forming nanoparticles with great dispersion of size.

We have recently developed a method capable of generating gold nanoparticles with sizes around 14 nm, very stable (zeta potential greater than -30 mV) and with a yield greater than 99.7% using a gold leaf (Figure48). It is therefore intended to apply such materials in vitro and in vivo tests for the treatment of both prostate cancer and bladder cancer.

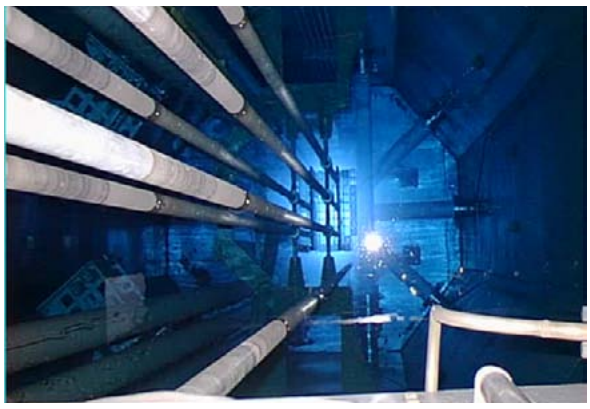

Figure 48

To this end, the 198AuNps will be prepared and, in collaboration with the Laboratory of Nuclear Medicine of the University of São Paulo, together with Dr. Fabio Luiz Navarro Marques, will be tested both as diagnostic agents and for treatment in cultured cells or in animals with induced tumors.

Development of Gold nanoparticles as radiation sensitizers in cancer therapy and as internal nanodosimeter

Every year, many millions of people worldwide are diagnosed with cancer and there are a high percentage of deaths from the disease. Even the survivors of the cancer treatment have serious deleterious heath effect due to chemotherapy and radiotherapy. Radiation therapy is very aggressive, but it is an increasing important tool to fight cancer. It is still a great challenge in radiation therapy to Deliver the proper curative dose of radiation to tumor while sparing normal tissues from radiation. We have recently developed a method capable of generating gold nanoparticles with sizes around 14 nm, very stable (zeta potential greater than -30 mV) and with a yield greater than 99.7% using a gold leaf. It is therefore intended to apply such materials in vitro and in vivo tests for the treatment of both prostate cancer and bladder cancer.

To this end, the 198AuNps were prepared and encapsulated with Albumin, by direct physio absorption effect and with the use of coupling agents (3-MPA) (Figure 49). Gold nanoparticles were also conjugated with a new peptide

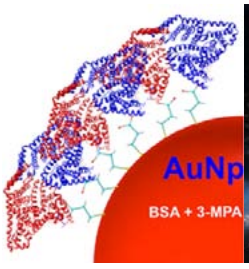

Figure 49. 198AuNps encapsulated with Albumin by coupling with3-MPA

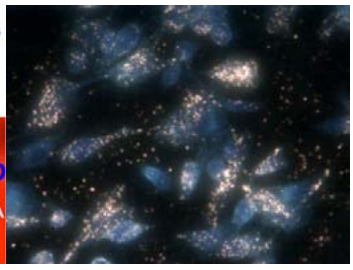

Figure 50. Internalization in PC-e cells of Au nanoparticles conjugated with CD-163 mimic.

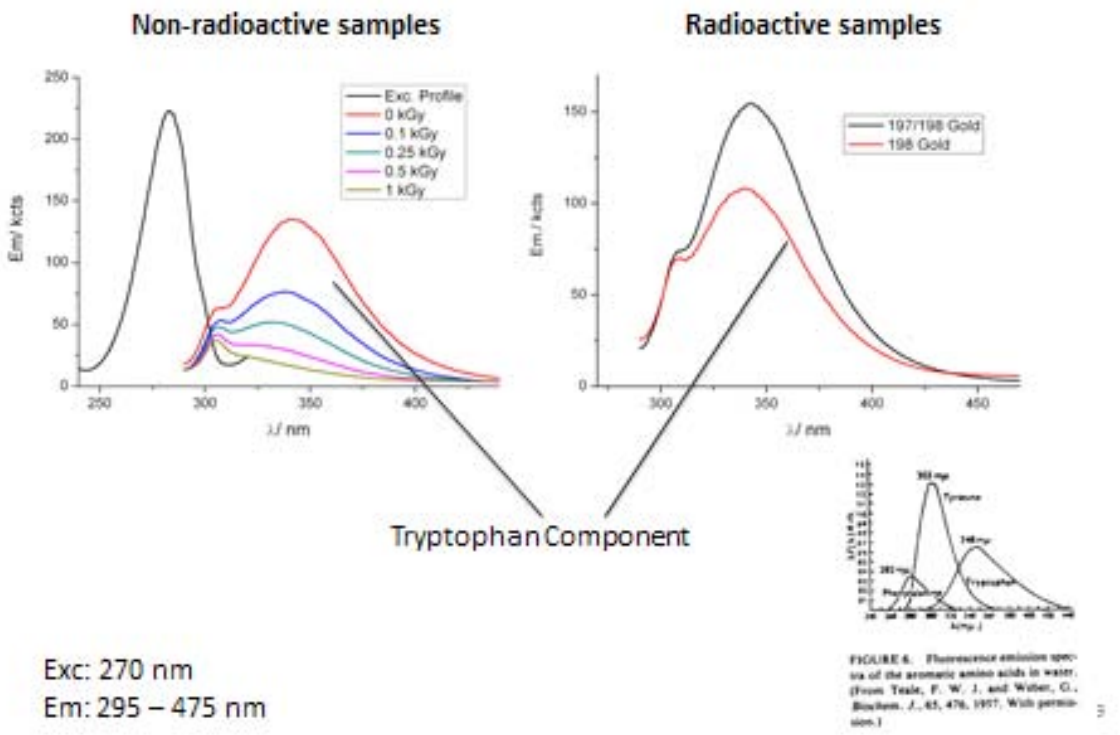

Figure 51. Fluorescence spectroscopy of bovine serum albumin biding to gold nanoparticles

(CD163 mimic) developed by Dr. Rosemeire Silva for internalization studies in prostate cancer cells and pancreatic cancer cells (Figure 50). We have also explored the chromophores of Albumin as a possible internal dosimeter for radiation therapy as follow bellow (Figure 51).

Development of protein based nanocarriers for the delivery of radiopharmaceuticals

Nanoparticles and nanoparticulate systems are considered a breakthrough in several fields as novel applications and features of commonly used materials were brought to light as a result of the nanostructuration. Biopharmaceutical and biomedical advantages, including site specific delivery are good examples of advantages that are offered by nanotechnology over conventional systems. At the same pace, concerns regarding toxicity emerge as most molecules or nanoparticles have no biological affinity, thus adverse reactions may take place including non-specific toxicity. Within this context, the seek for biologically-friendly materials are of highlighted role. Proteins are biocompatible by nature and hold strong biological affinity with a considerable lack of toxicity when administered to humans. Within this context, several studies have been performed using proteins as nanocarriers. In this work, we developed protein based nanocarriers, using bovine serum albumin or papain as model protein and enzyme respectively, by the use of radiation. Unlike conventional pathways, radiation allows the sterilization and simultaneous crosslinking of the protein in a single step, without the need for toxic monomers or crosslinkers that commonly lead to undesirable reactions when administered to biological systems. The nanocarriers are being radiolabeled with 99mTc by the direct and indirect method, in order to achieve an alternative system for the delivery of this and other radioisotopes for diagnose and treatment of a variety of disorders. High radiolabeling yields with good radiochemical stability have been identified throughout the experiments

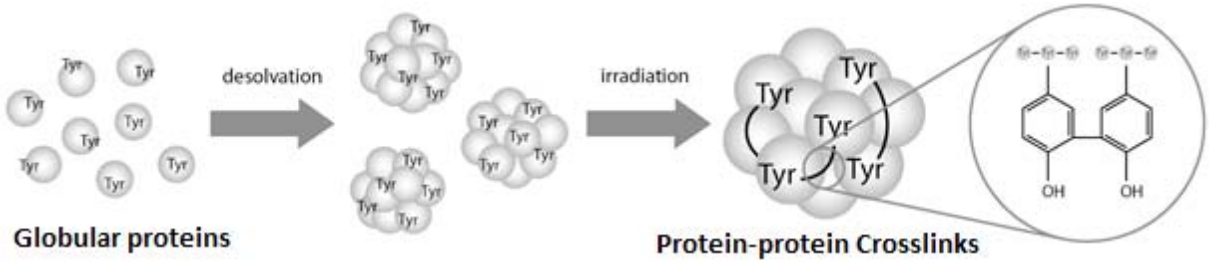

Figure 52. Nanocarriers.

and further steps concern the assessment of ex vivo and in vivo biodistribution of the developed systems.

In addition to that, we are developing a technique for the capping of inorganic nanoparticles of biomedical and clinical relevance with crosslinked proteins, without the need of toxic reagents and solvents, to improve the bioavailability, provide site specific delivery and possibly reduce allergenic reactions (Figure 52).

Recovering/recycling of butyl and halobutyl rubbers compounds by ionizing radiation

Polymeric materials (plastics and rubbers) attain a continuously and increasing proportion of litter discarded in landfills; their impact in environment are more and more concerning. The implementation of new technologies toward polymeric residues reduction, acceptable under environmental viewpoint and at an effective cost, proved to be a great problem, due to inhering complexities for polymers re-use. Ionizing radiation is capable to change structure and properties of polymeric materials; it is an expectation for problem solving of polymeric residues management. Butyl and halobutyl rubbers are used in a comprehensive scale, in a great variety of applications such as tires spare-parts and various artifacts. Rubbers are provided with a very low natural decomposition, due to their chemical structure weather resistant and to enzymatic degradation and microorganisms. Rubber recovering is difficult by its insolubility due to very cross-linked structures. Besides, this tridimensional structure shows a lot of problems for material recovering and reprocessing. In spite of various processes already developed and applied toward rubber recycling, the viability of these processes presents many challenges, either technical or referring to material quality. The major effect of high energy photon, as gamma rays in butyl and halogenated butyl rubbers is the generation of free radicals, along changes in mechanical properties. The addition of halogen atoms in the butyl rubber promotes a molecular rearrangement on the dehydrohalogenation of halobutyl rubber to form a double bond in secondary and tertiary carbon in bromobutyl and chlorobutyl rubbers, respectively, which facilitates the formation of cross-links when exposed to radiation high energy. It was developed a controlled degradation process (de-vulcanization) in butyl and halobutyl rubbers (chlorine and bromine), in order to characterize their availability for changing their properties. The rubber devulcanized induced by high energy degradation was tested for reuse in the original formulation of the mixture of rubber and can replace some parts of the pistine in the manufacture of final products. Butyl and halobutyl rubbers compounds were subjected to gamma radiation, in air, at 5 kGy, 15 kGy, 25 kGy, 50 kGy, 100 kGy, 150 kGy and 200 kGy, in a gamma radiator, Co60. Mechanical essays of tension and elongation at break showed chain-scission at doses up to 25 kGy; for doses higher than 50 kGy, it was observed an intense degradation.

Especially butyl rubber, halogenated rubbers are a little more radiation resistant. Irradiated butyl, bromobutyl and chlorobutyl rubber compounds and sheared at 25 kGy doses presented compatible results between scission and crosslinking and, so, they were selected for the mixtures between pristine and recovered rubber. The assessment of physical-chemical properties of compounds comprising recovered rubber showed that the addition of recovered rubber via irradiation and shearing favors a slight decreasing in tensile and elongation at break. Nevertheless, results indicate a compatibility of this incorporation. In summary, it was possible to conclude that, in spite of further adjustments in formulations, containing recovering of butyl and halobutyl rubbers, the strategy of a previous irradiation and a further shearing showed a great potential in recycling scenery.

Development of sulfonates multifunctionals fluoroelastomers based on nanocomposites

Polymer nanocomposite is a material formed by a polymer matrix and, usually, an inorganic compound. This inorganic material has nanometers with size of 100nm and is dispersed in the matrix. These nanocomposites have been studied in Universities and industries because of the final properties presented by this kind of material. The combination of properties of organic and inorganic materials revealed an improvement of mechanical, thermal, electrical and optical properties. In the case of nanocomposites, the same behavior was noticed due to the incorporation of inorganic nanoparticles in the polymer chain. In this work, the effect of incorporation of inorganic nanoparticle in the fluoroelastomer matrix has been studying. The selection of materials is very important because the mixture process and quality of final product.

The fluoroelastomer has been selected as the matrix polymer because of its properties, such as: solubility; chemical resistant to aliphatic and aromatic hydrocarbons; physical resistant to high temperature; low gas permeability; and others. The inorganic nanoparticles are clay and a silsesquioxane polymer (POSS). The objectives of the use of these particles are improving the mechanical property, reducing the swelling of the elastomer and maintaining the dimensional stability. The incorporation was carried out by mixture process in a two roll cylinder at room temperature. After the incorporation, the samples were pressed in order to vulcanize and to obtain films with 0,2mm thickness. The films will be submitted to gamma radiation to induce graft polymerization by simultaneous method. After irradiation, the films will be immerse) in the sulfonation solution to complete the experimental part.

Issues on hydrogels for drug delivery

Hydrogels for wound dressings are usually developed for contact surfaces where mechanical properties are conveniently required. In this sense, nanocomposite hydrogels based on poly(vinyl alcohol) (PVAl) and poly(N-2-vinil-pirrolidone) (PVP), containing 0.5 - 1.5 wt% of the synthetic laponite RD clay, were prepared by gamma radiation process and compared with similar membranes composed separately of PVP or PVAl. This study aimed to evaluate the effect of clay on the properties and the differences of the polymer binary system instead of a one polymer nanocomposite hydrogel. The morphology of the hydrogels was evaluated by spectrometric techniques using X-Ray Diffraction, scanning electron microscopy (SEM), swelling, and Infrared Spectroscopy (FTIR). Swelling kinetics at 22 °C and mechanical properties by tensile test evaluated the structural properties. The results showed PVA/PVP network depends directly of

the clay concentration in the nanocomposite hydrogels. The blend PVP/PVAl proved to have mechanical properties of stress tensile modulus higher than PVAl nanocomposite and higher elongation compared to PVP nanocomposites. Hydrogels of PVP were formulated with neomycin followed by radiation in gamma source for crosslink and sterilization. The antibiotic neomycin released from the hydrogel crosslinked membranes was determined by Liquid Chromatography – Mass Spectrometry. The drug is released in the 20h of essay. Hydrogel/neomycin exhibited antibacterial

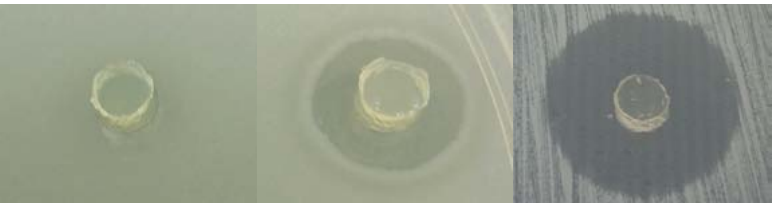

activity effects against Stephylococus aureus and Pseudomonas aeruginosa, Figure 53.

Figure 53. (A/B/C). Antibacterial results of activity against: control(A), P aeruginsa (B); S. aureus (C), after 24 h of incubation at 37°C.

Polymeric films for antibacterial activity

Polyethylene is widely used for packing applications. Different grades of polyethylene, LLDPE and LDPE play a major role in the film blowing industry. The use of nanoclay in polymer matrices (non-polar) requires the use of a compatibilizer agent, ethylene graft maleic anhydride copolymer (PE-g-MA), which acts as a bridge for nanoclay-matrix-interaction. In our study, blown films of LLDPE, LDPE, and their blends were produced using a twin screw extruder. The combination of PEs as matrix, montmorillonite (MMT) and silver nanoparticles (AgNPs) intended to improve mechanical and thermal properties. Nanocomposites films with 1 wt% of montmorillonite and 0.5–1.0 wt% silver nanoparticles were prepared by blow extrusion and evaluated. Nanoclay intercalation/exfoliation degree was investigated by X-ray diffraction spectroscopy (XRD) and scanning electron microscopy (SEM). Mechanical and thermal properties were evaluated. The results showed optimum dispersion at intercalation/exfoliation levels for polyethylene nanocomposite (PENC), slight increasing in mechanical and especially improvement in thermal properties. Polyethylene is widely used for packing applications. Different grades of polyethylene, LLDPE and LDPE play a major role in the film blowing industry. The use of nanoclay in polymer matrices (non-polar) requires the use of a compatibilizer agent, ethylene graft maleic anhydride copolymer (PE-g-MA), which acts as a bridge for nanoclay-matrix-interaction. In our study, blown films of LLDPE, LDPE, and their blends were produced using a twin screw extruder. The combination of PEs as matrix, montmorillonite (MMT) and silver nanoparticles (AgNPs) intended to improve mechanical and thermal properties. Nanocomposites films with 1 wt% of montmorillonite and 0.5–1.0 wt% silver nanoparticles were prepared by blow extrusion and evaluated. Nanoclay intercalation/exfoliation degree was investigated by X-ray diffraction spectroscopy (XRD) and scanning electron microscopy (SEM). Mechanical and thermal properties were evaluated. The results showed optimum dispersion at intercalation/exfoliation levels for polyethylene nanocomposite (PENC), slight increasing in mechanical and especially improvement in thermal properties.

X-ray diffraction spectroscopy of sample PENC/AgNP1.0% showed intercalated morphology. The results with MMT indicated the formation of microstructures predominantly exfoliated in film PENC1. In SEM/EDS microscopy the morphology of the silver/clay particles with homogeneous distribution. The film PENC/

AgNP0.5% showed increase of elongation at break above 1000%, which suggests the ap Processing starch biodegradable nanocomposites.

Polymer-clay nanocomposites (PCN) based on cassava starch, synthetic hectorite clay and inverted sugar cane syrup (plasticizer) were prepared by solvent-assisted (casting) process producing transparent and homogeneous films. Small amounts of clay (5-15 wt.%) resulted mainly in exfoliated nanocomposites while large amounts (30 wt.%) promote the intercalated nanocomposites formation. FT-Raman bands sensitive to hydrogen bonding in starch granules are progressively shifted to lower wavenumbers as the clay content is raised. Nanocomposites show a similar thermal behavior up to 320°C while the biomolecule decomposition at about 500°C is dependent on the clay content. CO_2 release at about 300°C (non-oxidative decomposition of polymeric chains) decreases if compared to the gas delivery at ca. 500°C, as the clay content is increased. Films with clay content higher than 10 wt.% show no substantial benefit for either elongation or resistance properties, FIG. 54.

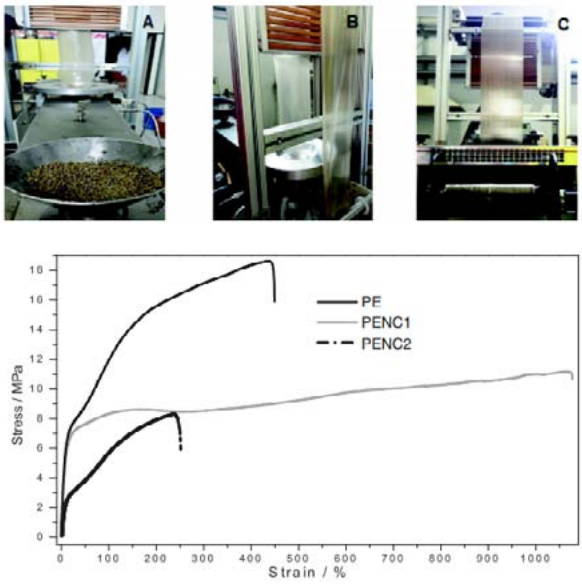

Figure 54. (a/b) . Film process (a) and stress X strain curves (b) for nanocomposites films.

Processing starch biodegradable nanocomposites

Polymer-clay nanocomposites (PCN) based on cassava starch, synthetic hectorite clay and inverted sugar cane syrup (plasticizer) were prepared by solvent-assisted (casting) process producing transparent and homogeneous films. Small amounts of clay (5-15 wt.%) resulted mainly in exfoliated nanocomposites while large amounts (30 wt.%) promote the intercalated nanocomposites formation. FT-Raman bands sensitive to hydrogen bonding in starch granules are progressively shifted to lower wavenumbers as the clay content is raised. Nanocomposites show a similar thermal behavior up to 320°C while the biomolecule decomposition at about 500°C is dependent on the clay content. CO_2 release at about 300°C (non-oxidative decomposition of polymeric chains) decreases if compared to the gas delivery at ca. 500°C, as the clay content is increased. Films with clay content higher than 10 wt.% show no substantial benefit for either elongation or resistance properties.

PCN materials based on synthetic hectorite clay and cassava starch were prepared. When small amounts of clay are added, the XRD data indicate the formation of mostly exfoliated nanocomposites, in which individual or few stacked inorganic layers are dispersed in the polymer matrix. However, when amounts of clay higher 10% are added, intercalated nanocomposites are formed. FT-Raman spectra indicate that crystallinity of starch in the hybrid films decreases as the amount of Laponite is increased, corroborating with XRD data. Prepared films are transparent and homogeneous. According to TGA analysis, the different steps of thermal decomposition are dependent on the amount of clay in the hybrid material. The good dispersion of Laponite

particles in the biodegradable starch polymer is attractive to develop functional materials for nanomedicine applications, Fig.55.

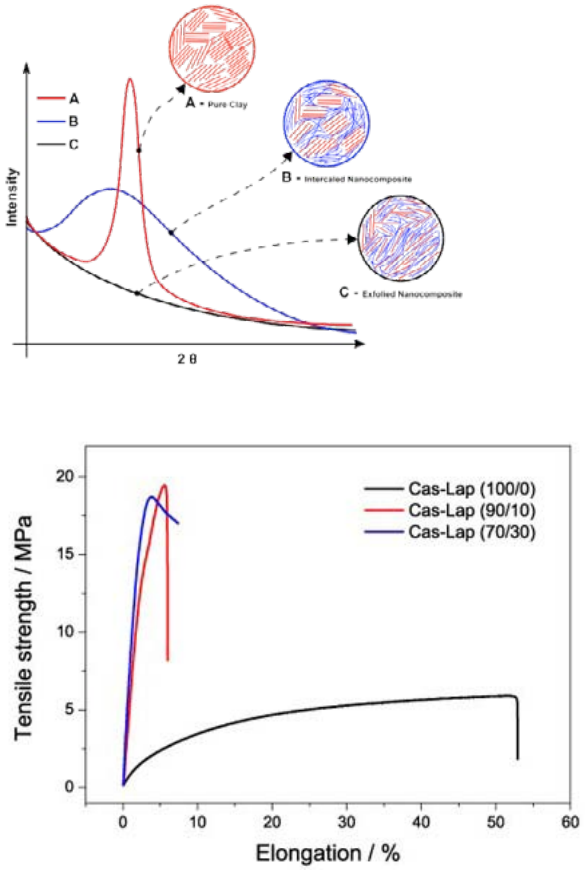

Figure 55. (a/b). DRX Differences in diffractograms of nanocomposites (A) and differences in elongation % for nanocomposites (B).

Polymer composites reinforced with micro and nanoparticle from natural resources

The interest in polymer composites that enable the use of products with less environmental impact, such as vegetable fibers, agroindustry residues, clays and other natural resources have rapidly grown in the last two decades worldwide. However, there is still a long way to go in research to obtain ideal polymeric composites and nanocomposites from natural resources.

The focus of this research is to explore Brazil`s enormous natural resources for the production of biobased and conventional polymer composite and nanocomposite materials and to avoid the huge amount of waste produced by its agroindustry, thus contributing to a sustainable development and, consequently, helping to improve the life standard of people, who can live off the exploitation of these resources. Based on the previous important questions, the present research focuses the preparation of micro and nanoparticle from natural resource and development of advanced polymer composite materials for several applications. Micro and nanoparticle preparation: Bio-$CaCO_3$ was obtained from white chicken eggshells; green silica was obtained by keeping sugarcane bagasse or rice husk ashes in an air insufflating oven at 450°C, then ball-milled and classified granulometrically (particle sizes ≤ 125 µm). Coffee parchment husk, Brazil nut shell, sugarcane bagasse, piassava, and rice husk fiber residues were scraped, washed, dried and reduced to fine powder, with particle sizes ≤ 250 µm by using ball mills. Bio-$CaCO_3$ and green silica nanoparticles were synthesized using sonochemical methods, by irradiation with high intensity ultrasonic (20 kHz, 450 W/cm^2). Cellulose nanowhiskers were produced from commercial microcrystalline cellulose (MCC, Avicel PH- 101, FMC BioPolymer, USA) and from sugarcane bagasse using acid hydrolysis and irradiated with a high intensity ultrasonic (20 kHz, and 450W/cm^2). Brazilian clays were modified by the addition of a quaternary salt and sodium carbonate Graphene oxide (GO) was prepared from purified conventional flake graphite and irradiated with a high intensity ultrasonic (20 kHz, and 450W/cm^2) to obtain GO nanosheets (Figure 56).

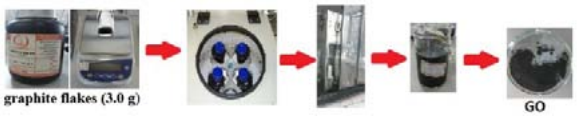

Figure 56. Graphene Oxide preparation.

Development of flexible packaging material based on biodegradable polymer reinfoced with micro and nanoparticle from natural resources

Flexible film based on biodegradable blend prepared from of poli(butileno adipato-co-tereftalato) "PBAT" and Poly Lactic Acid "PLA", (PBAT/PLA Blend) and reinforced with micro and nanofillers from natural resources were prepared by melting extrusion process, using a twin-screw extruder Haake Rheomex P332, L/D 25 and blow extrusion (laboratory line). The flexible films were characterized by mechanical tests, Oxygen transmission rate (OTR), Water vapor transmission rate (WVTR), XRD, SEM, SEM-FEG, TG and DSC analysis (Figure. 57).

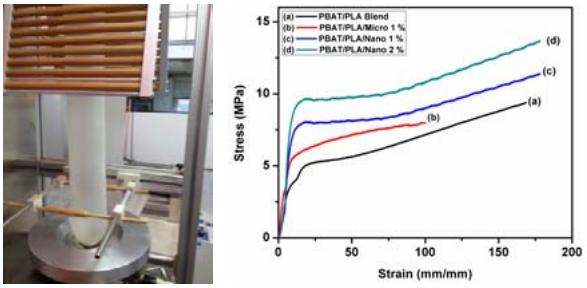

Figure 57 (a/b). Flexible Films based on PBAT/PLA/iPLA blend and PBAT/PLA/iPLA reinforced with microcrystalline cellulose and nanowhiskers.

The results showed an important gain in tensile strength at break, elongation at break and Young modulus properties of blend due to addition of bio-$CaCO_3$ micro and nanoparticles, Brazilian clay, green silica nanoparticles and cellulose nanowhiskers. However, based on test results, it may be claimed that the produced PBAT/PLA/iPLA/Nanowiskers flexible films presented superior mechanical properties than commercial LDPE/PA/LDPE structure and with mechanical properties close to commercial PE/PP structures, both used as dry food packaging materials. However, the vapor transmission rate (MVTR) characteristics still needs to be improved in order to extend the shelf life of packaged dry food. In conclusion, it may be claimed that PBAT/PLA/iPLA Flexible Films reinforced with nanowhiskers produced according to the methodology developed in this research are suitable materials for dry food packaging application, when compared with packaging material commercially used for this purpose, but has the advantage of being produced from biodegradable polymers and reinforced with micro and nanoparticles obtained from renewable waste.

Development flexible packaging materials based on conventional polymer (polymer petroleum-derived) with addition of Brazilian clay, graphene and also ionizing radiation treatment

Flexible film based on Ethylene–vinyl alcohol copolymer (EVOH) and Poly [(ethylene)-co-(vinyl acetate)] (EVA) with Brazilian Clay addition (1-3 wt.%) were prepared by melting extrusion process, using a twin-screw extruder Haake Rheomex P332, L/D 25 and blow extrusion (laboratory line). The flexible films were characterized by mechanical tests, Oxygen transmission rate (OTR), Water vapor transmission rate (WVTR), XRD, SEM, SEM-FEG, TG and DSC analysis (Figure 58).

The results showed that incorporation of 1- 3 % (wt.%) of Brazilian clay in the EVOH, or EVA matrix, resulted in a gain of mechanical properties

Figure 58. Flexible Films based on EVOH and EVA reinforced with Brazilian Clay.

of the film and caused structural changes in the EVOH, or EVA component, and leads to obtain a flexible film with major melting enthalpy and, consequently, major crystallinity percentage. However, when EVOH and EVA flexible film content only 1 % Clay addition (falta conector??) were irradiated at 150 and 200 kGy a significant gain of up to 30 % in tensile strength and elongation at break was observed when compared with non-irradiated samples. It may be claimed that the incorporation of modified Brazilian Clay in the EVA or EVOH followed by electron-beam irradiation effectively improved the mechanical properties of neat EVA and neat EVOH led to obtaining films materials with superior properties suitable for packaging development, concerning mechanical properties. The superior mechanical properties of EVOH/CLAY and EVA/CLAY nanocomposites observed in this study can be attributed to the stiffness of Brazilian clay, reinforcing effects, to the degree of the intercalation and good dispersion of the clay layers in the matrix.

Flexible films based on Ethylene–vinyl alcohol copolymer (EVOH) with graphene oxide addition (0.1-0.5 wt. %) were prepared by melting extrusion process, using a twin-screw extruder Haake Rheomex P332, L/D 25 and blow extrusion (laboratory line). The flexible films were characterized by mechanical tests, Oxygen transmission rate (OTR), Water vapor transmission rate (WVTR), UV/VIS, XRD, SEM, SEM-FEG, TG and DSC analysis (Figure. 59).

The results of XRD diffraction patterns provide clear evidence that for EVOH/GO films with 0.1; 0.3 and 0.5 wt. % of GO nanosheets content some GO with stacked layers remained but a large part of GO nanosheets are intercalated or exfoliated by EVOH chain molecules. The incorporation of GO in EVOH matrix led to obtain transparent EVOH/GO flexible films with improved oxygen barrier in high RH

Figure 59. EVOH/GO (0.1 wt. % GO nanosheets Flexible Films.

conditions with a gain of about 160 wt. % in tensile strength at break of neat EVOH and ca. of 40% in elongation at break.

Projects: IAEA-CRP # 17760 - Application of Radiation Technology in Development of Advanced Packaging Materials for Food Products, March 2014 to February 2017. CAPES - Programa Pesquisador Visitante Especial (PVE) - Use of Ionizing Radiation in Modification and Compatibilization of Polymer Matrix Composite Materials, 02/2015 to 01/ 2018.

Synthesis and characterization of SnO_2@ TiO_2 nanoparticles doped with lanthanide for biological labeling.

Fluoroimmunoassay is an ultrasensitive technique for investigation of enzymes, antibodies, cells, hormones and others. The demand for highly sensitive systems brought the nanomaterials for biomedical and biotechnological field. Semiconductor nanocrystals (quantum dots) doped with lanthanide ions, when functionalized with biomolecules, can be used as luminescent biomarkers. Aiming this application, we have been synthesized and characterized nanoparticles of titanium and tin mixed oxide doped with europium, terbium and neodymium. The synthesis was

done by the co-precipitation and hydrothermal methods characterized by SEM, IR, XRD, TGA and luminescence spectroscopy. These particles were functionalized by silica using two different methods, that are, the microwave and Stöber, facilitating the conjugation with biological entities (Figure 60).

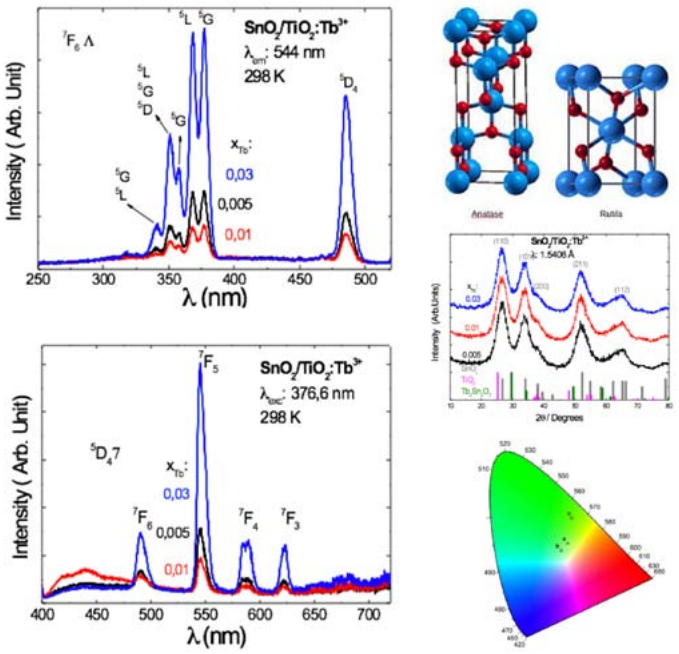

Figure 60. Excitation and Emission spectra of $SnO_2/TiO_2:Eu^{3+}$ nanoparticles (left up and down) and structures of SnO_2 (right -upper) X-ray powder diffraction (right -middle) chromaticity diagram (right -down).

Figure 60. Excitation and Emission spectra of $SnO_2/TiO_2:Eu^{3+}$ nanoparticles (left up and down) and structures of SnO_2 (right -upper) X-ray powder diffraction (right -middle) chromaticity diagram (right -down).

Synthesis and characterization of $TR_2(MoO_4)_3@SiO_2$ nanoparticles doped with Eu^{3+}, Tb^{3+} and Nd^{3+} for biological labeling

The interest in using rare earths to investigate the properties and functions of biochemical systems as well as to determinate biological substances has increased in several fields, including biomarkers as a tool for immunology (fluoroimmunoassays). Nowadays, the use of lanthanides in the diagnosis of various diseases has become more important through the development of commercial diagnostic kits. As main feature, these rare earths can show a long lifetime, photostability and emission bands of atomic like behavior and well defined, in the visible region, demonstrating unique advantages when compared to other luminescent species. The present research synthesize rare earth molybdates by the co-precipitation method as well as characterize these materials by X-ray diffraction, near infrared spectroscopy, thermogravimetric analysis, scanning electronic microscopy, transmission electronic microscopy and luminescent studies. This research focuses three different studies as followed :the influence of the vortex speed variation during co-precipitation in the structure of the final product, morphology and luminescence properties; the influence of the annealing temperature also in the structure, morphology and luminescence properties; and the influence of concentration of the doping in the luminescence properties. Another important step of this research is the functionalization of nanoparticles using an organosilane (APTES) to coat and establish points for binding the particles to biological species. It was proved that this process was very efficient by the char-

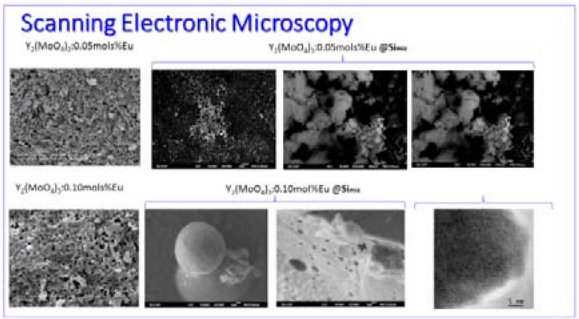

Figure 61. Ilustration of $Eu:Y_2(MoO_4)_3$ under excitation of UV lamp, SEM of the $Eu:Y_2(MoO_4)_3$ and $Eu:Y_2(MoO_4)_3@Si$ Microwave and $Eu:Y_2(MoO_4)_3@Si$ Stöber and emission spectra of the $Y_2(MoO_4)_3$.

acterization results and the silica incorporation was well succeeded. Specific prostatic cancer (PSA) was then linked to the functionalized nanoparticles to diagnostic prostatic cancer by fluoroimmunoassay and levels for detection were established. Figure 61.

Europium βetha- diketonate complexes with tetracycline (TC), fluoxetine (FL) and piroxican (PX) as ancillary ligands. bloloGIC and solar convention application

Luminescent materials containing trivalent rare earth (RE^{3+}) complexes with β-diketonate ligands have been intensively studied in recent years. The RE^{3+} compounds present some characteristics such as narrow emission bands in the UV-Vis region, large Stokes shift and the antenna effect that enhance the overall quantum efficiency. As a result, these complexes have found wide applications as luminescent markers, photoluminescent sensors, electroluminescent devices and multicolor display. In the field of biomarker, these compounds linked with biological parts. At this time, it was synthesized new complexes of europium β-diketonate with tetracycline,piroxican and fluoxetine as ligand. IR spectra of the Eu(III) complexes show two strong absorption bands at ~1597 and ~1566 cm^{-1} attributed to ν_s(C=O) and ν_{as}(C=O) vibrational stretching modes, suggesting that the β-diketonate ligand acts as chelate ligand. SEM image showed particles rounded with grain size lower than 10 nm (Fig. 62). The emission spectrum of europium complexes, in the solid state, recorded in the range of 520 to 720 nm at liquid nitrogen temperature, under excitation at β-diketonate transitions (~350 nm) is shown in Fig. 62. This emission spectrum exhibits some characteristics such as narrow emission bands that are assigned to the 4f6-4f6 transitions of Eu(III) ion, attributed to the emitting $^5D_0$ level to the ^7F_J (J = 0, 1, 2, or 4) levels, where the most intense

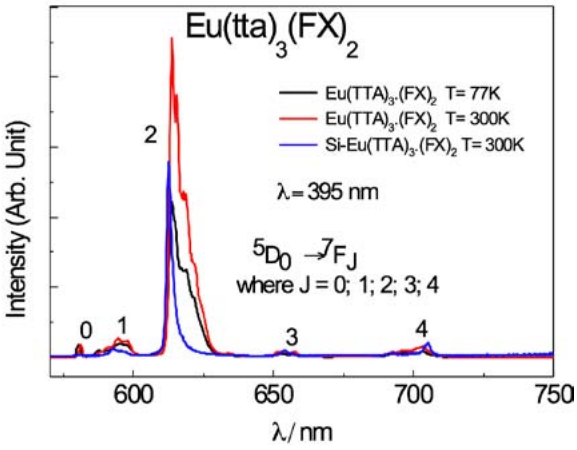

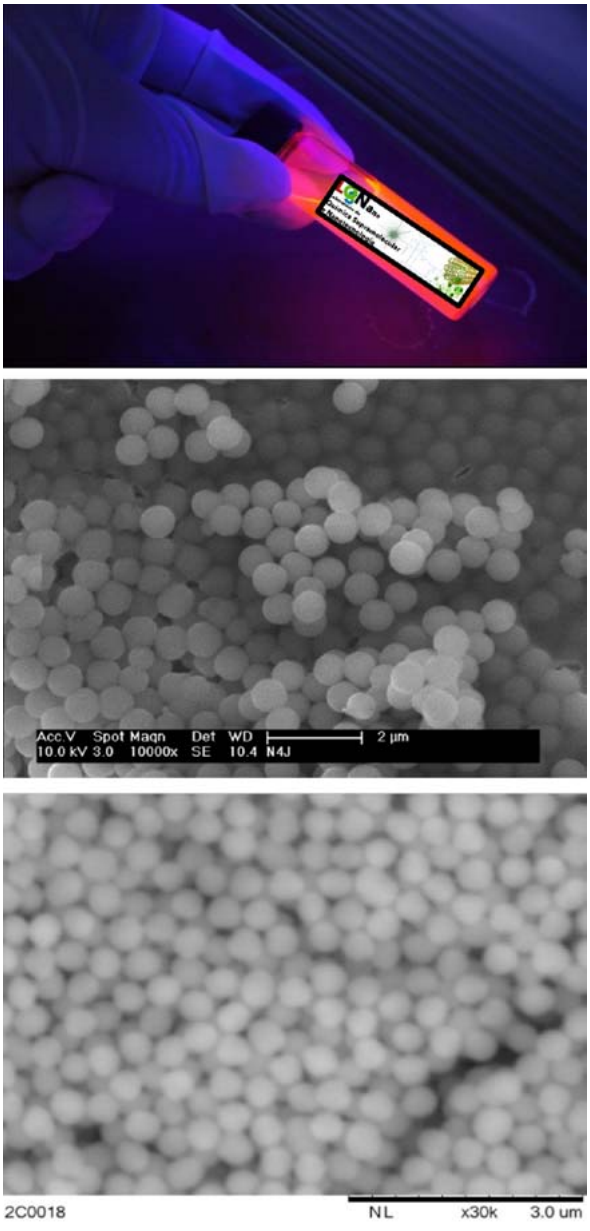

Figure 62. Luminescent biomarkers for chemicals detection in biologic fluids.

corresponds to $^5D_0 \rightarrow {}^7F_2$ transition taking place around 613 nm. An important feature to be observed is the nonexistence of broaden bands arising from the β-diketonate centered transitions, indicating that intramolecular energy transfer from the β-diketonate ligands to the Eu(III) ion is operative.

Development of a low cost diagnostic kit that use luminescent Nanobiomarkers for use in sickle cell anemia

Luminescent materials, such as the rare earth's complex, can be used as markers in cytology and immunology, being also used as luminescent biomarkers, once the development of these nanomaterials create new possibilities in many fields, particularly in diagnostic medicine. Besides, it establishes one kind of fluorescent probes, for which there are no equivalent organic molecules. Due to its potential in market's application, the objective of this work was to develop luminescent materials, allowing the use of these supermolecules of lanthanides as markers for the detection of Sickle Cell Disease (HbS). Six luminescent markers were developed based on rare earth compounds. The main methodology used for the detection of HbS was fluoroimunoassay, which is already used in investigation of enzymes, antibodies, cells, hormones, and so on. The studied methods were applied for the diagnosis of this disease, which has genetic origin, very typical of the hemoglobin-pathology group and considered to be a public health problem in Brazil (ANVISA). When is early detected, Sickle Cell Disease (SCD)

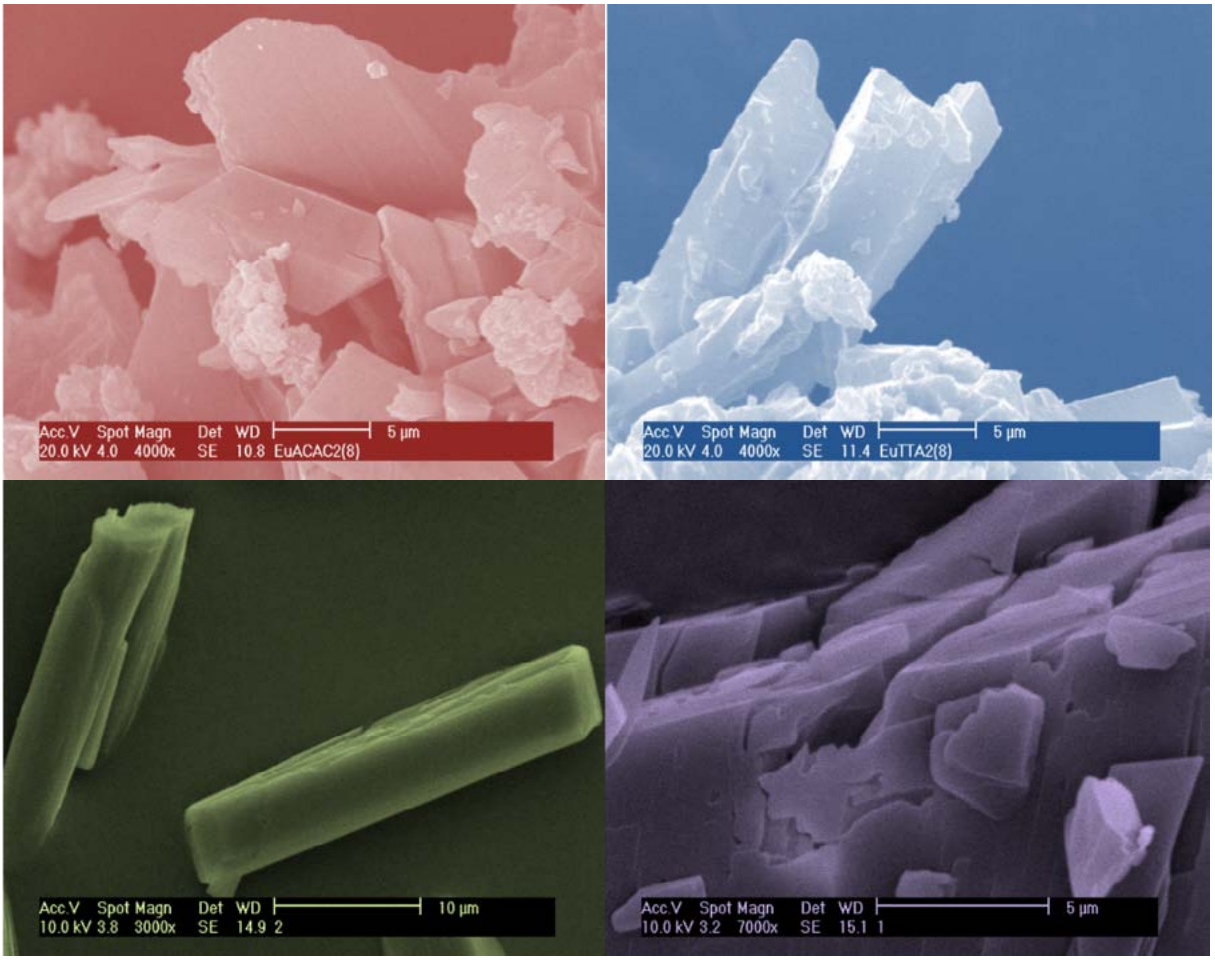

Figure 63. SEM of the Europium and terbium supermolecules.

has a significant decrease in morbidity and mortality. Comparing the obtained results to the already known methodologies, it was possible to conclude that they are viable methods to detect HbS. Besides, when totally developed, these methods will contribute to the production of Sickle Cell Anemia's diagnostic, and they will have impact in São Paulo state's public measures, as well as in Brazil's ones. An prototype kit is in the validation phase for use as a simple way to detection (Figure 63).

Luminescent polymeric nanoparticles (LUMPNP) for biological labeling.

A major difficulty in biomarker process is related to the solubility of the nanoparticles in the biological media. This fact limits the process of bioconjugation and consequently the signaling. Developing markers based on Chitosan, PMMA and cachew-gun resin (CG) markers that are easier to be functionalized with biocompatible chemical group for reactions with biological entities is the goal. In this context two methods of synthesis for implementation of the project were chosen: the first method synthesizes the nanoparticle by cryogenics technique and the second method is the microemulsion technology. Figure 64 shows the SEMs images of these particles and it can be seen that the particles are more dispersible than the particles used previously. It can also be noted that the polymer nanoparticles incorporating the complexes [TR(β-diketone)$_3$ (Ligand)$_x$] showed emission quantum efficiencies close to 100% . The PMMA polymer nanoparticles doped with 0.5 to 5% by weight of the europium complex were functionalized with a diamine to act as a spacer in bioconjugation (Figure 64).

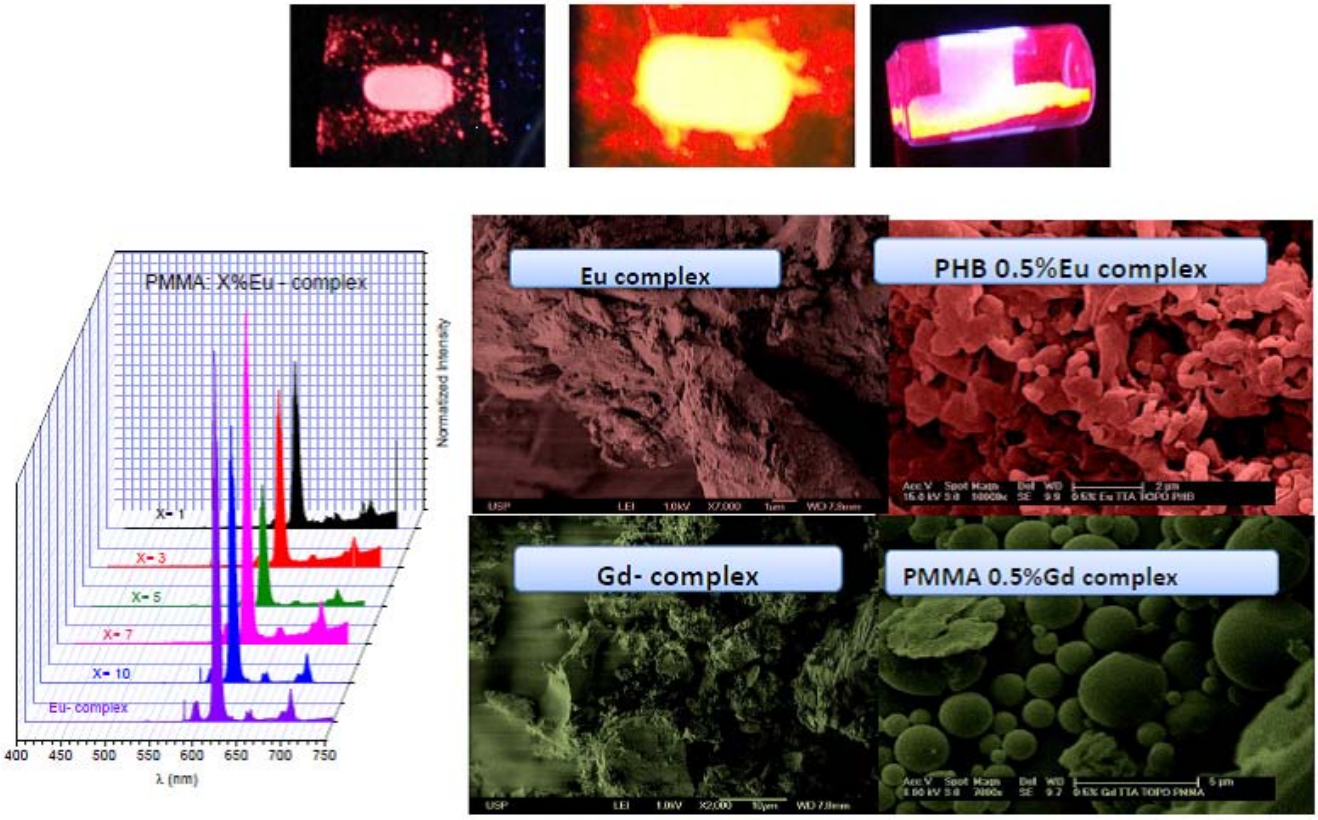

Figure 64. Luminescent polymeric nanoparticles (LUMPNP) for biological labeling– cryogenics Europium nanoparticles under UV excitation (upper); Emission spectra of NPPLUM (down-left); SEM of precursor and NPPLUM (down-right).

Bifunctional magnetic and luminescent nanoparticles for diagnostic and theranostic.

The design of bifunctional luminescent magnetic nanomaterials containing MFe_2O_4 (where M=Fe and Mn) doped with rare earth and functionalized with rare earth ions inclusion complexes of calixarene and phosphine oxide and also β-diketonate ligands or chitosan natural polymer and quantum dots have been investigated. These novel kind of luminescent magnetic nanomaterials (MFe_2O_4 @QD,Ln) complexes/compound present very interesting superparamagnetic and photonic properties. The magnetic properties were explored at 5 and 300K temperature and showed that extent of coating and crystallinity affect the saturation magnetization values of nanoparticles. Although ferrite is a strong luminescence quencher, the coating of the MFe_2O_4 nanoparticles has overcome this difficulty. The intramolecular energy transfer in the nanomaterials from the T1 excited triplet states of TTA and ACAC ligands to the $^5D_0(Eu^{3+})$ and $^5D_4(Tb^{3+})$ emitting levels has been determined. In addition to the superparamagnetic behavior, these nanophosphors may act as emitting layer of red and green light converting molecular devices (LCMDs) and are responsible for new ways in the diagnostic and teranostic field. This research has been developed in collaboration with the LNLS, Chemistry institute of University of São Paulo and Campinas University (Figure. 65).

Luminescent material associated to a metal nanoparticles and Plasmon effect

The use of these metallic nanostructures to favorably modify the optical properties of fluorophores in order to increase the intensity of fluorescence emission. The project aims to synthesize metallic nanoparticles using green chemistry and use these nanoparticles in photonic materials. Particles of Ag^0, Au^0 and Cu^0 are produced using green chemistry protocols and then are associated to luminescent materials based on lanthanides to improve the efficiency of the materials luminescence. They are now being targeted

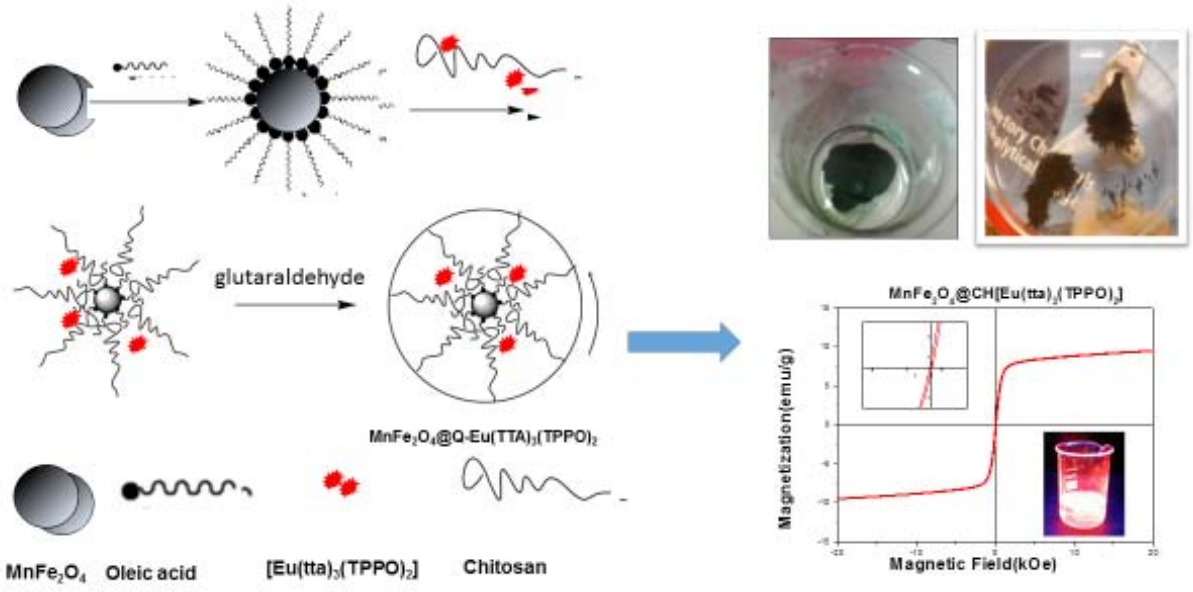

Figure 65. Synthesis protocol of $MnFe_2O_4$@CH-Eu(TTA)$_3$(TPPO)$_2$(left); $MnFe_2O_4$@CH-Eu(TTA)$_3$(TPPO)$_2$ composite, and the composite under effect of magnetic field(upper -right); Magnetization curve of $MnFe_2O_4$@CH-Eu(TTA)$_3$(TPPO)$_2$ inserted fig solution of chitosan and complex under 366nm excitation (down-right).

for biological applications of nanoplasmonic as flow cytometry, immunoassays, cell imaging and bioassays where it can improve fluorescence signatures (Figure. 66)

Figure 66. Plasmonic effect in some materials produced in IPEN.

Materials For Security And Solar Cell Storage:

Luminescence - tuneable multicolor PMMA films doped with lanthanide β-diketonate complexes for lighting

Interest in luminescent materials containing trivalent lanthanide ions (Ln^{3+}) as emitting centers has grown significantly in recent years. However, the Ln^{3+}-complexes generally present low thermal stability, limited photostability and poor mechanical properties. Another parallel challenge is that most of these compounds are usually achieved as hydrates, consequently the luminescence intensity is suppressed due to the activation of non-radiative channels. In order to overcome simultaneously these deficiencies and improve the characteristics of light emission (e.g. quantum yield, lifetimes), Ln^{3+}-complexes have been incorporated into organic polymers, liquid crystals and sol-gel derived organic-inorganic hybrids. Polymers offer several advantages for the development of materials, such as flexibility, versatility, optical quality and moderate processing conditions. By incorporating luminescent Ln^{3+}-complexes within the polymer matrix, the resulting product represents not only the sum of individual contributions of both organic and inorganic phases, but also novel properties for a new class of materials.

Work has been developed with bases on the complexes diaquatris(thenoyltrifluoroacetonate)-europium(III), $[Eu(tta)_3(H_2O)_2]$, ditriphenylphosphine oxide(thenoyltrifluoroacetonate)-europium(III), $[Eu(tta)_3(TPPO)_2]$, triaquatris(acetyl-acetonate)Terbium(III), $[Tb(acac)_3(H_2O)_3]$ and triphenylphosphine oxide (acetyl-acetonate)Terbium(III), $[Tb(acac)_3(TPPO)_2]$, $[Tb(acac)_3(n\text{-}picNO)_2]$, $[Eu(tta)_3(n\text{-}picNO)_2]$, (n=2,3,4) complexes were co-doped into polymers in order to obtain multicolor light-emitting devices controlling concentration and excitation energy lines. These materials are of great interest due to their strong luminescence and relatively simple and no expensive preparation (Figure. 67).

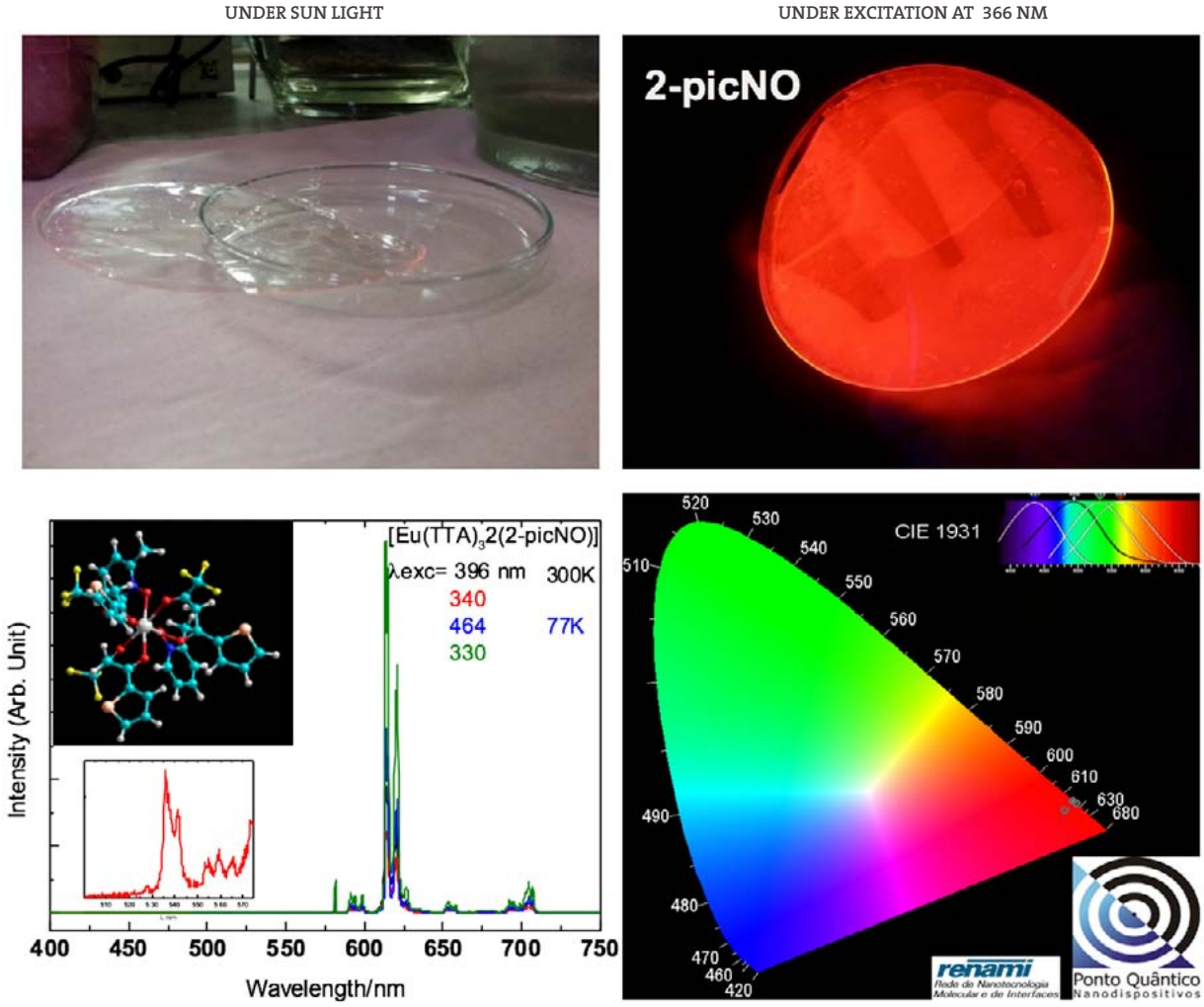

Figure 67. PMMA Films doped with Eu(tta)3 (2-picNO)2 (upper) and Emission spectra of the complex under various excitation (down-left) and CIE diagram of the 3 differing methyl group in the ligand.

Persistent luminescence materials: Thermoluminescence and synchrotron radiation studies on the persistent luminescent materials

Since 1995, the research on persistent luminescence materials has increased substantially .This is due to the progress in the properties of these materials: they can emit nowadays in visible for many, up to 24+ hours, after ceasing the irradiation. Because of the long emitting time, these phosphors can be exploited commercially in emergency signs, road signalization, wall painting, watches, micro defect sensing, optoelectronics for image storage and detectors of high energy radiation. According to the literature, the $BaAl_2O_4(:Eu^{2+},TR^{3+})$ materials are prepared via a solid state route, usually by heating $BaCO_3$ with Al_2O_3 (or their precursors) at elevated temperatures. However, low temperature routes as combustion and sol-gel syntheses are not uncommon. In the actual research $BaAl_2O_4$ materials were prepared: Eu^{2+} , TR^{3+} through the ceramic methods and combustion, and $CdSiO_3$: TR^{3+} (TR : Y, La, Ce, Pr, Nd, Sm, Eu, Gd, Tb, Dy, Ho, Er, Tm, Yb, Lu) , by ceramic method, showing persistent luminescence property. As usual, the combustion synthesis produces crystals with smaller size, evidently due to higher local temperature during the spontaneous explosion. Since the thermoluminescence analyses suggested the presence

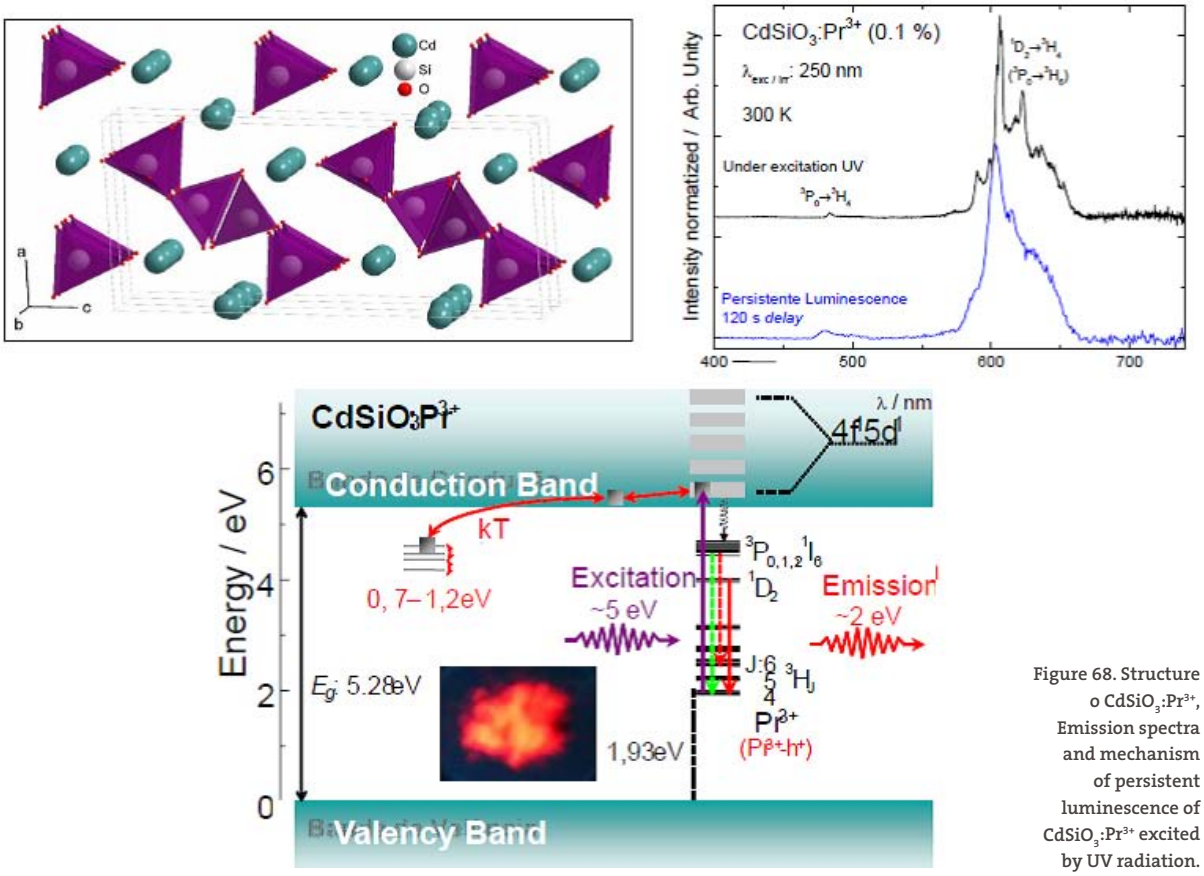

Figure 68. Structure o $CdSiO_3:Pr^{3+}$, Emission spectra and mechanism of persistent luminescence of $CdSiO_3:Pr^{3+}$ excited by UV radiation.

of one and three traps for the combustion and solid state prepared materials, respectively, the method of preparation has a significant influence on the defect structure of the materials. $BaAl_2O_4 : Eu^{2+}$, TR^{3+} and $CdSiO_3$: TR^{3+} materials were investigated by absorption spectroscopy in the infrared, scanning electron microscopy , absorption spectroscopy, X-ray structure were studied by absorption of X-rays near the edge-XANES absorption fine structure and X-ray extended - EXAFS other than electron excitation and emission spectroscopy in the regions of UV and vacuum - UV- vis and thermoluminescence. It was also investigate the photoluminescence properties of their excitation and emission spectra, the lifetime of excited states and the positions of the ground states of the ions $TR^{2+/3+}$ in the Band Gap. Mechanisms were discussed for the persistent luminescence phenomenon of Eu^{2+} ion doped in $BaAl_2O_4$ matrix and TR^{3+} ions doped in $CdSiO_3$ matrix. The mismatch between the band gap (Eg) value obtained from the synchrotron radiation excitation spectra and the DFT calculation was deduced to results from the covalent bonding in the $BaAl_2O_4$ host. The XANES spectroscopy showed a predominance of Eu^{3+} which can be present as a result of the in situ conditions of persistent luminescence during the X-ray irradiation (Figure 68).

Multiferroic properties in rare earth doped oxide thin films

For the last few decades, the consumption of electronic devices and the high demand for data storage have shown great opportunities to create modern technologies that assure the worldwide needs in computing development. Some multiferroic materials have been extensively studied. The $BiFeO_3$ is considered the only one that has at least two ferroic at room temperature, so that it has received special

attention as a candidate to produce logic and memory devices. The use of growth techniques such as pulsed laser deposition allowed the production of thin films with high quality control. Multiferroic thin film heterostructures of $BiFeO_3$ and $LaBiFeO_3$ were grown to evaluate and test their electrical and magnetic properties. The multiferroic project was developed at the University of California - Berkeley covered by the Everton Bonturim doctoral project and his supervisor Professor R. Ramesh, looking to improve the state-of-the-art in devices technologies through the pure and applied nanoscience (Figure. 69).

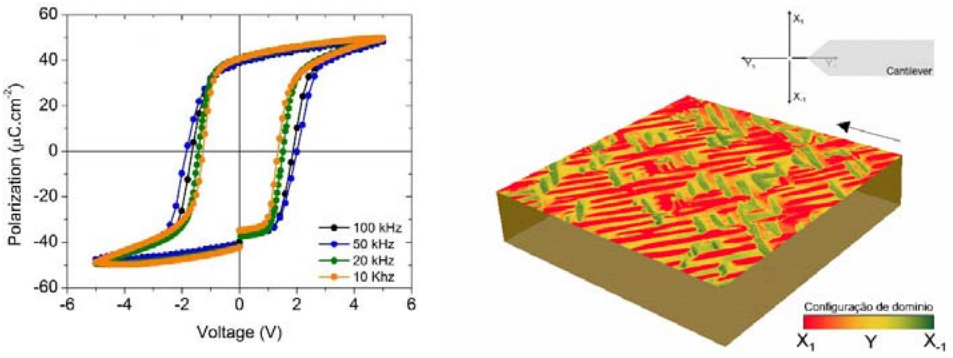

Figure 69 – In-plane PFM image with its vector component of the domain structure (a) and the electrical hysteresis loops at different frequencies (b) of a ferroelectric thin film heterostructures grown via physical deposition technique.

Program Team

Research Staff

Dr. Ana Helena de Almeida Bressiani; Dr. Ana Lúcia E. Godoy; Dr. Antonio Augusto Couto; Dr. Arnaldo H. Paes de Andrade; Dr. Carlos Alberto da Silva Queiroz; Dr. Cecilia Chaves Guedes e Silva; Dr. Chieko Yamagata; Dr. Claudio J. da Rocha; Dr. Cristiano S. Mucsi; Dr. Dolores Ribeiro R. Lazar; Dr. Eguiberto Galego; Dr. Eliana Navarro dos S. Muccillo; Dr. Emília Satoshi M. Seo; Dr. Flávia Rodrigues de O. Silva; Dr. Hidetoshi Takiishi; Dr. Isolda Costa; Dr. Ivana Conte Cosentino; Dr. Jesualdo Rossi; Dr. José Carlos Bressiani; Dr. José Roberto Martinelli; Dr. Lalgudi V. Ramanathan; Dr. Larissa Otubo; Dr. Luis Antonio Genova; Dr. Luis Gallego Martinez; Dr. Luzinete P. Barbosa; Dr. Maria Claudia F. C. Felinto; Dr. Marilene M. Serna; Dr. Marina Fuser Pillis; Dr. Maurício D. M. das Neves; Dr. Nelson Batista de Lima; Dr. Raquel de Moraes Lobo; Dr. Reginaldo Muccillo; Dr. Ricardo Mendes Leal Neto; Dr. Rodolfo Politano; Dr. Rubens Nunes de Faria Jr; Dr. Sonia Regina H. M. Castanho; Dr. Valter Ussui; Dr. Walter K. Yoshito; MSc. Edson Pereira Soares; MSc. Francisco J. Breda; MSc. Fredner Leitão; MSc. Glauson A. F. Machado; MSc. Lia Maria C. Zarpelon; MSc. Luis Carlos E. Silva; MSc. Mariano Castagnet; MSc. Rene Ramos de Oliveira; MSc. Yone V. França; Bel. Sandra M. Cunha.; Tech. Celso Vieira de Moraes; Tech. Dileusa A. S. Galissi; Tech. Marcelo A. de Oliveira; Tech. Marco Andreoli; Tech. Nildemar A. M. Ferreira; Tech. Olandir V. Correa; Tech. Pedro P. Freitas; Tech. Reinaldo A. da Costa; Tech. Thiago dos Santos Ferreira; Elizabete dos Santos; Marlene de Fátima P. Marcelino.

Postdoctoral Fellows

Dra. Ana Lígia Piza Micelli; Dr. Armando Cirilo de Souza; Dr. Frederico Nigro; Dr. Julio César Serafim Casini; Dr. Kalan Bastos Violin; Dr. Leandro da Conceição; Dr. Luiz Alberto Tavares Pereira; Dr. Márcio W.D. Mendes.

Graduate Students

Ana Carolina Gugliotti; André Ventura Piaggio dos Santos;Anelyse Arata; Antonio Paulo Rodrigues Fernandez;Arnaldo Augusto Ciquielo Borges; Bruno Pizol; Camila Pucci Couto; Carlos Eduardo; Carolina Sayuri Hattori Neto; Chester Contatori; Clóvis de Oliveira Junior; Daniel de Resende Leme; Daniel Nagano da Silva; Daniela Maria Cerqueira Leite; Diogo Rodrigo de Oliveira; Douglas dos Santos Leite; Elaine Farneze de Camargo; Eliana Ionara de Oliveira Pesqueira; Emanuelle Zangerolame Santos; Eurico Felix Pieretti; Evandro Giuseppe Betini Felippe Eduardo de Oliveira Bartalo; Fernando Bardella; Fernando dos Santos Silva; Fernando Gabriel Benitez Jara; Francisco Carlos Cione; Gabriel Giannini de Cunto; Gabriel Souza Galdino; Gisele Fabiane Costa Almeida; Givanildo Alves dos Santos; Gleicy Xavier; Graziele Cristiane Seco Coutinho; Guilherme Luis Cordeiro; Henrique Duarte Lopes; Igor Colado P. Martins; Janine Nemeh Nogueira; Jeferson Matsuji Matsui; Jefferson Malavazi; Lígia Silvéria Vieira da Silva; Lucas di Pretto; Luciana Crepaldi Yazawa Pistarini; Luis Augusto Mendes dos Reis; Maicon Cavalieri de Alencar;

Marcello Ferrari; Marcello Vertamatti Mergulhão; Marcos Antonio Teixeira; Marilia Fernandes Bolsanello; Maurilio Pereira Gomes; Mauro Machado de Oliveira; Mayra Dancini Gonçalves; Michele Cristina Biondo de Castro; Narayanna Marques Ferreira Mendes; Pedro Vitor Duarte da Cruz; Priscilla Danielle de Oliveira Lopes Cost; Quézia de Aguiar Cardoso; Rafaela Cerqueira Batista de Oliveira; Railson Bolsoni Falcão; Renato Baldan; Renato Paulo Rezende; Ribas de Morais; Roberta M. de Mello; Robson L. Grosso; Rodrigo Ramos Barbosa; Sabrina Macedo Gonçalves Carvalho; Sérgio do Nascimento; Shirley L. Reis; Tatiane C. Porfírio; Vanessa Galvão Rodrigues; Wilson Carlos da Silva Junior

Undergraduate Students

Beatryz Gonsalez de Oliveira; Bruna Gonçalves Duca de Souza; Bruna Rodrigues de Lima; Daniel Vieira da Silva; Déborah Y. B. da Silva; Eduardo José Nogueira; Giovanna Lucchesi Maset; Guilherme Dias Moreno; Igor Bernardes Urias; Larissa Abade Marcelo; Letícia Soares; Lucas F. do Amaral; Luis Otávio de Oliveira; Marcos V. Surmani Martins; Mariana Ferreira Gutierrez da Silva; Mayara Cardoso de Araújo; Natali Nazare dos Santos James; Paula Cruz Mendes Silva; Rodiney Randello de Souza; Tatiane Yumi Tatei.

Collaborators

Dr. Almir Oliveira Neto; Dr. Álvaro A.A. Queiroz; Dra. Amanda Abati AGUIAR; Dra. Ana Maria D. C. Ferreira; Dr. Anderson Zanardi De Freitas; Dra. Andrea Cecilia Dorion Rodas; Dra. Andrea Cecília Dorion Rodas; Dr. Angelo Fernando Padilha; Dr. Antônio Jorge Abdalla; Dr. Aparecido E. Morcelli; Dr. Argemiro Soares da Silva; Dr. Carlos Angelo Nunes; Dr. Carlos de Moura Neto; Dra. Carola Gomez Ágreda; Dra. Christiane Ribeiro; Dra. Danieli Aparecida Pereira Reis; Dr. Edilson Rosa Barbosa de Jesus; Dra. Eleni Cristina Kairalla; Dra. Elisabeth Djurado; Dra. Elizabeth Ferreira Martinez; Dr. Fernando M. B. Marques; Dr. Flavio Machado de Souza Carvalho; Dra. Francesca Deganello; Dr. Garabed Kenchian; Dr. Gerson Marinucci; Dra. Grace Mendonça Dias de Souza; Dr. Guilherme De Siqueira Ferreira Anzaloni Saavedra; Dra. Ivone Mulako Sato; Dra. Izabel F. Machado; Dr. Jan Vatavuk; Dr. Jivaldo R. Matos; Dr. Jorge Otubo; Dr. Jose Roberto Berretta; Dra. Juliana Marchi; Dra. Kátia Cristiane Gandolpho Candioto; Dra. Lauralice de C.F. Canale; Dr. Laurent Dessemond; Dra. Mara Oliveira; Dr. Marcelo Yoshimoto; Dr. Marco Antônio Colosio; Dr. Marcos de Arruda; Dr. Marcos Massi; Dr. Marcos Tadeu D'Azeredo Orlando; Dra. Maria Margareth da Silva; Dr. Mario Ueda; Dra. Nancy Tiaki Maeda;Dra. Olga Zazuko Higa; Dr. Paulo Francisco Cesar; Dr. Renato Altobelli; Dr. Ronaldo Câmara Cozza; Dra. Rosa M. Rocha; Dr. Rubens Nisie Tango; Dr. Sebastião Ribeiro; Dr. Sérgio Allegrini-Jr; Dr. Sergio Delijaicov; Dra. Solange Kazumi Sakata; Dra. Stela M. C. Fernandes; Dra. Susana Zepka; Dra. Tamiye Simone Goia; Dra. Tarcila Sugahara; Dra. Thais Santos; Dra. Vânia Trombini; Dr. Wagner de Rossi; Dr. Waldemar Alfredo Monteiro; Dr. Xabier Turrillas;

Honor Mention and Awards

The Brazilian Ceramic Society honored the research "Synthesis study of nickel-alumina-lanthana catalysts for hydrogen production from ethanol" developed by G. L. Cordeiro, W. K. Yoshito,

V. Ussui, N. B. de Lima, F. B. Noronha, D. R. R. Lazar as the best post-graduate work of the 59th Brazilian Congress on Ceramics held in Barra dos Coqueiros (SE); 17-20 May, 2015.

The Academy of Dental Materials, during the annual meeting held in Chicago (USA), 12-15 october, 2016, awarded the second place of prize "Paffenbarger" to the research "Y-TZP low temperature degradation: a sigmoidal or a linear behaviour?" developed by A. Arata, L. R. de Pretto, V. Ussui, N. B. de Lima, A. Z. de Freitas , J. P. B. Machado, R. N. Tango, G. M. D. de Souza e D. R. R. Lazar.

Honorable Mention – 8th edition of the Brazilian Association of Automotive Engineering of Environment with the work - Morphology Coatings NbN / CrN nanoestrutured deposited by PVD - Juliano Avelar Araujo, Roberto Martins de Souza, Andre Paulo Tschiptschin e Nelson Batista de Lima

The 'Distinguished Alumnus Award' in 2014 from the Indian Institute of Technology, Madras, India, was conferred on Lalgudi V.Ramanathan for his Technological, Academic and Research contributions in the area of 'Corrosion of Materials'. The Indian Institute of Technology, Madras is the foremost Institute for engineering studies and has an acceptance rate of 0.01%. Up until 2014, from the 40.000 alumni, only 100 had been conferred this award.

An award was given to S. L. Reis and E. N. S. Muccillo for their research work "Improved Densification and Ionic Conductivity of of Sr- and G-doped Lanthanum Gallate", presented in the "11th International Symposium on Ceramic Materials and Components for Energy and Environmental Applications" in Vancouver, Canada (June 14-19, 2015).

Dr. E. N. S. Muccillo was selected to have her CV included in the book. Successful Women Ceramic and Glass Scientists and Engineers: 100 Inspirational Profiles, together with women from America, Europe, Asia and Oceania.